LOCAL DELIVERY OF THERAPEUTIC NANOPARTICLES FOR TREATMENT OF MALIGNANT GLIOMA

by
Clark Zhang

A dissertation submitted to the Johns Hopkins University in conformity with the requirements for the degree of Doctor of Philosophy

Baltimore, Maryland
November 17, 2015

Abstract

The treatment regimen for patients that present with glioblastoma (GBM) has improved over the years with the advent of the chemotherapeutic Temodar® and the inclusion of concurrent radiotherapy. However, the 5 year survival rate remains below 10% [1]. The current treatment regimen is unable to effectively eradicate all pathological tumor cells that can reside up to centimeters away from the tumor bulk. This leads to tumor recurrence, the main culprit behind the disease's low survival rate. In addition, currently developed conventional therapies fail to address this need for improved therapeutic distribution in order to achieve therapeutic outcome. In this thesis, we develop 3 different nanotechnology platforms that are engineered to distribute throughout the brain and tumor microenvironment upon intracranial administration using an optimized form of convection enhanced delivery (CED). It is my belief that this technology represents a promising start towards addressing the poor survival rates and quality of life of those patients suffering from GBM.

We began by tailoring the parameters that allow for effective administration of therapeutics using CED. Following the size and surface chemistry criteria established by our recent Science Translational Medicine publication (sub-100nm, near neutral surface charge) [2], we demonstrate that a probe, brain penetrating nanoparticle (NP) can achieve synergistically improved distribution in the brain of both mice and rats when delivered using CED. Furthermore, a mechanistic investigation of the parameters of CED reveals a combination strategy (i.e. hyperosmolar infusate solution + brain penetrating NP) that can enable more homogeneous therapeutic distribution in the brain, which is currently the main obstacle in successful translation of CED-based therapies to the clinic.

With the understanding gained from these probe NPs, we developed three therapeutic brain penetrating NP formulations with dense surface coatings of polyethylene glycol (PEG) that are capable of delivering chemotherapeutics or therapeutic gene sequences. When administered using CED, these therapeutic NPs similarly achieve widespread distribution in the brain. The first platform is a biodegradable poly(lactic-co-glycolic acid)(PLGA) polymer and we demonstrate its ability to rapidly penetrate and distribute in the brain tissue as compared to gold standard NPs that have been engineered to pass through the blood brain barrier (BBB). Secondly, we developed a non-viral brain penetrating gene vector platform derived from a highly efficient polyethylenimine (PEI) polymer. When administered using CED, they successfully deliver higher overall levels of widespread reporter gene expression. These NPs can be rapidly adopted to deliver therapeutic plasmids that can encode for p53 for anti-tumoral efficacy or glial derived neurotrophic factor (GDNF) for treatment of Parkinson's disease. Finally, we've engineered brain penetrating cisplatin NPs that, when administered using CED, leads to curative effects in a clinically relevant, orthotopic rodent model of human GBM.

Together, these three brain penetrating NP formulations, in conjunction with optimized CED administration, represent promising adjuvant therapies to be tested for treatment of GBM.

Advisor:
Justin Hanes, Ph.D.

Readers:
Justin Hanes, Ph.D.
Charles Eberhart, M.D., Ph.D.
Betty Tyler
Warren Grayson, Ph.D.

Preface/Acknowledgements

A successful Ph.D. is not a reflection on that individual's "intelligence" or "capabilities"; instead, it is the culmination of years of support, hard work, and dedication of a team that lifts that single individual to that career point. I have been blessed in being surrounded by the brightest and most supportive mentors, colleagues, and friends that have made all of this possible. Each individual that I list below (and even those unmentioned) has made immeasurable contributions to this finished thesis product and am indebted to each and every person that has made this result possible.

First of all, to my advisor, Dr. Justin Hanes, who had the open mind to take an unproven first year Ph.D. student into his lab and provide a supportive, nurturing environment that has enabled me to mature and flourish as an academic researcher. To the other academic mentors throughout the last 5 years: Dr. Rangaramanujam Kannan, Betty Tyler, Dr. Charles Eberhart, Dr. Seulki Lee, Dr. Honggang Cui, Dr. Haiquan Mao, Dr. Elizabeth Orwin – thank you for providing the mentorship and guidance throughout both the highs and lows of my Ph.D. experience. That impact truly cannot be quantified. To Laura Ensign-Hodges and Jung Soo Suk, I thank you both as crucial mentors throughout this process, but more importantly, I thank you both as good friends in making the academic experience here at the Center for Nanomedicine (CNM) so memorable and enjoyable.

To all members of the CNM that preceded me - thank you for the mentorship and close camaraderie in the work environment. This includes Elizabeth Nance, Jane Chisholm, Graeme Woodworth, Ting-Yu Shih, Craig Schneider, Qingguo Xu, Himat Patel, Katharina Maisel, Tao Yu, Benjamin Schuster, Anthony Kim, Nick Boylan, and anyone else who, in my unfortunate state, I have forgotten to mention. You all truly showed me what it was like to be in the ideal lab, and my hope is to provide this experience for the generations of new students to come. To other members of the CNM – including Panagiotis Mastorakos, Sneha Berry, Eric Song, Karina Nieves Torres, Michael Noback, Kunal Parikh, Shu Chattopadhyay, Joshua Kays, Taarika Babu, Thuy Hoang, Namho Kim, Gregg Duncan, Abhijit Date, Xinglu Huang, Fan Zhang, Siva Khambamphati, Manoj Mishra, Rajsekhar Reddy, Yumin Oh, Jongsung Park, and Maggie Swierczewska – I have continued to learn from each of you on a daily basis. I will cherish the whole gamut of emotions that we've encountered including celebration/triumph/despair (okay maybe not that much despair!).

To the "brain team", beginning with Elizabeth, Graeme, and Ting – continuing with Panos, Eric, and Sneha – and finally moving forward with Karina and Michael – you have all been the heart and soul of this journey for the last 5 years. This further includes all of our undergraduate students – James Verdone, Delia Cardona, Kevin Kuo, Miguel Sobral, Young Eun Kim, Hee Won Park, Paul Choi, and Michael Mudgett. In just the short 8 years since this team's inception, we've established ourselves and our research as a powerhouse worthy of consideration in both the lab and in the academic field – I can't be more proud of how far we've come and how fortunate I am to have been a part of that.

To all my mentors at Johns Hopkins Technology Ventures – including Vera Sampels, Ying-Li Chen, Nakisha Holder, Peter Ball, and Alevtina Zhelonkina – I feel blessed to have been able to work with each of you individually. These experiences have exposed me to the world of translational technology and have furthered my interest to the point that I look forward to transitioning and dedicating my career to invention commercialization.

To the friends I have made here at Johns Hopkins – my first roommates, Kyle Rupp, Geran Kostecki, Tashrik Ahmed – thank you for all the good times as we embarked on this journey. To all the individuals that I've met throughout Thread (Incentive Mentoring Program) – especially the Dunbar students (Devin, Dariz, Jamal, Equan, Tyriq, and Joe) thank you for making that experience so rewarding. To the original Yogurt Lane: Jean Suh, Kathy Jee, Tiffany Ho- I hope that our paths never cross in the professional setting because I will never imagine any of you as ever being medical professionals! To my closest friends and staunchest supporters inside and outside the lab – Elizabeth and Jane – you have both been true inspirations and I cannot begin to quantify my thanks and how much your continued friendship has meant over the years. Eager to continue hearing about each of your continued successes!

A big thanks to all my friends in California that have consistently asked about when I would finish school and come back– Wesley Cheung, JC Chang, Jackie Lam, Angus Ho, Michael Ho, Jessica Wen, your support and unquestioning friendships have kept me grounded and I do look forward to our continued get-togethers.

And of course, to my family. Truly my biggest supporters that have made all of this possible – I cannot begin to thank you enough. To my mom – Helen, who has sacrificed so much to raise two boys over 25 years to be successful to this day. To my dad - Shenghua, who to this day continues to provide the words of wisdom. To my brother – Powell, who I will always share an unquestionable bond with. And finally to my loving girlfriend – Janet, who has been with me through thick and thin and has stood unyieldingly in support by my side.

Table of Contents

List of Tables

List of Figures

1. INTRODUCTION

The diffuse nature of many neurological diseases necessitates the development of novel treatments (i.e. nanotechnology) that can similarly distribute throughout the central nervous system (CNS) to target pathological abnormalities. To do so, these therapies must be aptly engineered to enable their unhindered distribution throughout the brain interstitium upon administration. Using probe polystyrene nanoparticles (NP), our lab has previously shown that in order for NPs to rapidly penetrate and travel through the brain extracellular spaces, they must be designed to be small (sub-100 nm) and non-adhesive (dense surface layer of polyethylene glycol (PEG)). In this thesis, we build upon our prior findings by developing several therapeutic, brain penetrating NP platforms for the treatment of human glioblastoma (GBM) and intracranially administer them into the brain using convection enhanced delivery (CED), a common method of adminstration that has demonstrated promise in human clinical trials.

Chapter 2 of this thesis describes the current background and problems facing the acceptance and implementation of new nanotechnology treatments for GBM. Chapter 3 begins to address those shortcomings by establishing that a sub-100 nm, densely PEG shielded NP can safely achieve widespread distribution upon CED administration into the healthy rodent brain. We find that this improved distribution is observed completely independent of NP concentration. Furthermore, we demonstrate that the fate of the infused NPs remain distinct as non-adhesive NPs are likely uptaken and cleared through unactivated microglia whereas unmodified NPs remain entrapped within the brain interstitium near the point of administration.

Having conducted the majority of prior studies using probe, polystyrene NPs that are incapable of delivering therapeutic agents, we further engineered brain penetrating NPs derived from biodegradable poly(lactic-co-glycolic acid)(PLGA), an FDA approved polymer that has been widely utilized in drug delivery applications [3]. Chapter 4 focuses on testing PLGA NPs that possess a wide variety of surface-altering surfactants that have previously been shown to enable NP transcytosis across the BBB. We compare the ability of our NP formulations to diffuse throughout healthy brain tissue to the gold-standard human serum albumin NPs (HSA-NP) that are designed for passage through the BBB. Intriguingly, we find that surfactants that enable BBB passage are poor for NP diffusion within the brain interstitium. In fact, we confirm that cholic acid (CHA), is an ideal small molecule surfactant that enables densely PEGylated PLGA NPs to diffuse 2500 times faster in brain tissue than HSA-NP. When administered *in vivo* using CED, these PEG-PLGA NPs coated with CHA achieve widespread distribution in the rodent striatum, mirroring our findings in Chapter 3.

In Chapter 5, we focus on developing a non-viral, brain penetrating gene vector platform, given that the field of gene delivery has gained momentum as a promising approach for treatment of mutation-based diseases such as GBM. We utilize polyethylenimine, the gold-standard polymer choice for synthesis of non-viral gene vectors and highly PEGylate the linear chain to achieve a densely PEGylated NP upon its complexation with plasmid DNA. In comparison to conventionally PEGylated NPs (3-fold less PEG), our gene vectors are able to rapidly diffuse in brain tissue and achieve widespread distribution when administered using CED, similar to what we observed in Chapters 3 and 4. Most importantly, we find that improved NP distribution leads to 1) higher and 2) more widespread levels of transgene expression. Thus, this has set the groundwork for transitioning to delivering therapeutically relevant anti-tumor genes such as p53 or thymidine kinase.

Although gene therapy has demonstrated promise in preclinical studies, chemotherapeutics such as temozolomide (TMZ) remain the standard of care for GBM [4]. However, TMZ and many chemotherapeutics continue to suffer from lack of efficacy and increased toxicities. In Chapter 6, we develop a highly cytotoxic, cisplatin (CDDP) brain penetrating NP for the treatment of rodents bearing GBM tumors. We engineered sub-100 nm, CDDP NPs with a near neutral surface charge that widely distributes in brain tissue following CED. These NPs exhibit 24 hour controlled release of the CDDP payload, thereby significantly improving the therapeutic index as compared to freely administered CDDP. Most importantly, when rodents bearing malignant glioma are treated with this CED-administered CDDP NP, 80% of the animals are cured (i.e long term survival and no tumor regrowth). Thus, this CDDP platform represents a promising adjuvant therapy for human GBM following tumor resection.

Although our combination of CED + brain penetrating NPs in Chapters 3-6 have all demonstrated very promising preclinical results, many clinical trials utilizing CED as the main administration method have ultimately failed [5, 6]. The inability to meet primary and second endpoints have been attributed to nonhomogeneous distribution of the infused therapeutic; namely, therapeutic accumulation in perivascular spaces (PVS) has been shown to occur [7, 8] which ultimately prevents the therapeutic from targeting the pathological cells in the brain interstitium. Chapter 7 looks to address these shortcomings by delivering non-adhesive NPs in a hyperosmolar solution using CED, thereby modulating the tissue microenvironment to prevent therapeutic sequestration and enhance the distribution of NPs in the brain. Furthermore, we find that these NPs are able to travel through PVS to far distances (up to 1.5 mm) and escape back into the brain interstitium. We believe this combination delivery strategy may be a promising approach to addressing the current limitations of CED-based therapies in clinical trials.

Altogether, we have built upon our lab's previous findings by 1) developing three therapeutic brain penetrating NP formulations and 2) optimizing their intracranial delivery through a mechanistic investigation of CED as the administration strategy. These results corroborate our prior findings that a NP must be engineered with a dense PEG layer in order to achieve penetration and widespread distribution within the brain interstitium. Here, we've engineered multiple tailorable platforms capable of delivering therapeutic genes or chemotherapeutics. We believe that these NPs may be of the utmost interest, especially given the burgeoning field of gene delivery along with the ongoing interest in more effective delivery of chemotherapeutics for the treatment of GBM.

2. BACKGROUND

2.1. Glioblastoma and nanotechnology treatments

Central nervous system (CNS) diseases such as malignant brain gliomas remain very difficult to treat due to the infiltrative, malignant nature of the disease [9]. In the case of GBM, the current treatment regimen involves surgical resection followed by concurrent irradiation and chemotherapy, but the median survival time of GBM patients remains approximately 16 months [4]. This poor prognosis stems from tumor relapse due to residual tumor cells following treatment [9-12]. The chemotherapeutic of choice for newly diagnosed GBM, Temodar ® (Temozolomide, TMZ), is orally administered but despite its lipophilic makeup and ability to cross the blood brain barrier (BBB), patient survival time was only slightly improved [4, 13]. TMZ is still limited in its efficacy due to its inability to sufficiently accumulate in the CNS and fully eliminate residual infiltrative tumor cells. Furthermore, TMZ is highly restricted by its dose limiting systemic toxicities of myelosuppression and lymphopenia [14-16]. Nanotechnology based therapeutics are a promising strategy to more effectively target and treat these residual tumor cells but they must be engineered to effectively overcome multiple hurdles including the brain tissue barrier to achieve enhanced therapeutic distribution within the tumor.

2.2. Barriers to effective therapeutic NP delivery to the brain

Two main barriers exist to prevent effective delivery of therapeutics to the brain; the blood brain barrier (BBB) is the first hurdle that systemically administered nanocarriers must overcome [17].

Passive passage through the BBB requires the molecules to be lipophilic and less than 500 Daltons in size [18]. Therefore, most NPs are effectively barred from entering the brain through the systemic route. Several strategies have been developed to transiently disrupt or bypass the BBB [19-21]; however, the dose of therapeutic that is achieved in the brain following this delivery method remains low. Thus, direct intratumoral administration of the therapeutic remains the most promising in being able to achieve high concentrations of the therapeutic within the local tumor bulk. If the nanocarrier is able to overcome or bypass the BBB, the brain tissue barrier (BTB) serves as a second obstacle to effective therapeutic delivery. The BTB is composed of the nanoporous and highly adhesive brain extracellular matrix (ECM) that sterically or adhesively traps therapeutic NPs upon their entry into the brain parenchyma [2, 22, 23]. In addition, tumor microenvironments often possess increased cellular density and upregulated proteoglycan concentrations, both of which further prevent therapeutic NPs from reaching the target cells [24].

To address the limitations of nanotechnology delivery to overcome the BTB, two strategies have recently been developed: 1) effectively engineer a NP to minimize the interactions that entrap the NP and 2) utilize improved delivery methods such as CED to drive the therapeutic to overcome those hindering interactions.

2.3. Strategy 1: Optimized nanocarriers for brain delivery

In both preclinical and clinical studies, intracranial infusion of nanocarriers leads to suboptimal distributions if the nanocarrier characteristics are poorly considered [25, 26]. In order to improve the delivery of therapeutic NPs, recent studies have detailed the optimal NP characteristics for brain penetration to comprise a small size (<100 nm in diameter) and a near neutral surface chemistry to minimize adhesive interactions with the brain ECM [2, 20]. When our lab synthesized these “brain penetrating” NPs in this fashion, we demonstrated that these NPs can rapidly diffuse within the brain parenchyma to achieve higher distribution [2] and prolong survival of orthotopically implanted, glioma-bearing rodents [27]. These parameters have been further corroborated by high impact publications that have intracranially delivered therapeutic “brain penetrating” drug and gene nanocarriers and have achieved significant improvement in survival of tumor-bearing rodents [28, 29]. Thus, although the need to overcome the BTB has long been overlooked in comparison to the BBB, addressing the BTB through the tailoring of NP physicochemical characteristics has slowly gained attention as an essential step towards effective therapeutic delivery to the brain.

2.4. Strategy 2: Local delivery – Convection enhanced delivery

Local administration of chemotherapeutics, such as implantation of the carmustine-loaded Gliadel® wafer, has demonstrated promising results as an adjuvant therapy [30] by circumventing the BBB, reducing potential systemic toxicities, and increasing concentration of drug in the tumor [31]. However, topically administered therapeutics suffer from decreased penetration into the tumor parenchyma and rapid clearance from the extracellular space, thereby limiting the overall benefits [31, 32]. Simultaneously, other researchers have employed convection enhanced delivery (CED) as an alternative strategy to increase therapeutic distribution [33]; however, studies have demonstrated that even with CED, poorly designed NPs are unable to distribute in the brain which leads to poor efficacy of the treatment [26, 33].

CED of therapeutics has shown promise in preclinical studies for improving therapeutic distribution in the brain parenchyma but its clinical success has been largely limited. A number of recently completed or ongoing clinical trials focused on combatting the diffuse pathology of malignant gliomas or Parkinson's disease currently deliver therapeutics into the brain using CED [5, 34]. Unfortunately, most of these trials have not met their primary endpoint which is hypothesized to be due to poor distribution of the therapeutic from the injection site, sequestration of therapeutic within perivascular spaces, lack of training and poor implementation of CED by surgeons, and failure to normalize the CED hardware across multiple institutions [8, 34]. As our understandings of CED grow as a result of improved real-time monitoring and imaging techniques [35], very promising preclinical results employing CED against malignant glioma have recently come to light [28, 29], yet their therapeutic of choice (viruses, PLGA paclitaxel) still face numerous obstacles prior to translation to clinical trials and into the clinic.

Here, we hypothesize that the combination delivery of a brain penetrating NP platform using optimized CED parameters is a promising therapeutic modality for treating neurological diseases such as GBM.

3. INTRACRANIAL ADMINISTRATION OF NON-ADHESIVE NANOCARRIERS USING CONVECTION ENHANCED DELIVERY (CED)

3.1. Introduction

Convection enhanced delivery (CED) was first described in 1994 [36] as a strategy to drive therapeutics to farther distances within the brain interstitium using the bulk flow of a fluid. Even today, the fact that numerous clinical trials have or currently implement CED for treatment of Parkinson's disease and recurrent malignant glioma continues to underscore the enthusiasm for this delivery method [5, 31]. This excitement stems from the fact that many brain diseases are characterized by the presence of pathological cells or abnormal extracellular structures that are highly disseminated throughout the brain tissue. Thus, NPs must be able to follow and target these widely distributed entities, which may theoretically be achieved through CED [20]. However, in practice, non-homogeneous distribution of the administered therapeutic occurs with high concentrations remaining near the catheter implantation site, confined within perivascular spaces, or localized within white matter tracts [7, 8, 25, 37]. Conventionally designed therapeutics, even when delivered via the bulk flow of CED, are often found associated with components of the brain extracellular matrix (ECM), which sterically and adhesively prevents infused therapeutics from effectively distributing throughout the brain. These challenges have led to a significant number of terminated CED-based clinical trials that have failed to meet their primary and secondary outcome measures likely due to suboptimal distribution of the therapeutic [8, 25, 38]. Indeed, very promising preclinical results have recently come to light which detail significant survival benefits in malignant glioma bearing rodents when viral or NP therapeutics are specifically engineered for brain penetration and are intracranially administered using CED [28, 29]. Therefore, optimizing and delivering a NP therapeutic that is able to achieve maximal distribution within the brain parenchyma may result in even further improvements in both preclinical and clinical investigations for CNS diseases.

We have previously developed and demonstrated that a NP up to 114 nm in diameter, if shielded with a dense layer of polyethylene glycol (PEG), can minimize interactions with the brain ECM and rapidly diffuse through the intercellular spaces (ICS) in the brain parenchyma [2]. However, relying solely on diffusion to distribute therapeutic NP throughout the ICS achieves only sub-optimal therapeutic concentrations at farther distances [20]. Therefore, we hypothesize that the combined delivery of a non-adhesive NP using CED may be a promising strategy to overcome the brain ECM and achieve therapeutically relevant distribution in the brain.

3.2. Methods

3.2.1. NP preparation and characterization

Forty nm dark red fluorescent carboxylated polystyrene microspheres (PS-COOH) (Life Technologies, Grand Island, NY) were modified by conjugating a dense layer of 5 kDa methoxy-PEG-amine (Creative PEGworks, Winston Salem, NC), onto the surface, according to a previously published protocol [2], to obtain densely PEGylated polystyrene NPs (PS-PEG). NP size and surface chemistry were characterized in a standard 10 mM NaCl solution through dynamic light scattering and laser doppler anemometry techniques using a Zetasizer NanoZS (Malvern Instruments, Southborough, MA).

3.2.2. In vivo CED of various nanocarriers

When preparing NPs for intracranial CED, stock PS-PEG and PS-COOH were each diluted 25-fold in 0.9% saline and mixed at a 1:1 ratio for a final concentration of 1 mg/mL. Additional NP concentrations were also investigated including final concentrations of 25 mg/mL and 0.1 mg/mL in normal saline.

Female CF-1 mice weighing 20-30 g in mass or male Sprague Dawley rats weighing 300-400 g in mass were anesthetized with a mixture of ketamine (75 mg/kg) and xylazine (7.5 mg/kg). For mice, a 2 cm sagittal incision was made on the head and a burr hole was made 2 mm lateral to the bregma. All NP solutions or infusate solutions were loaded into a 50 μL Hamilton Neurosyringe with a 33 gauge syringe and set with a 1 mm step (Hamilton, Reno, NV). The syringe was vertically mounted on a Chemyx Nanojet Injector Module (Chemyx, Stafford, TX) which was held on a small animal stereotactic frame (Stoelting, Wood Dale, Il). The loaded syringe was lowered to a depth of 2.5 mm below the mouse dura and a total of 2 μL of the solution was administered over 10 minutes at a rate of 0.2 μL/min. For rats, a burr hole was made 3 mm lateral to the bregma and a total solution of 20 μL of solution was administered at a depth of 3.5 mm at a rate of 0.33 μL/min. In both rodents, the cannula was allowed to sit for 5 minutes following the completion of infusion and was then withdrawn at a rate of 1 mm/min. The animal was then sutured (Covidien, Mundelein, Il) and placed on a heating pad.

We conducted a single CED administration into the *ex vivo* harvested brain of a female New Zealand rabbit. The animal was euthanized using an overdose of pentobarbital and the brain was excised and placed on ice to maintain structural integrity *ex vivo*. PS-PEG nanoparticles were administered at a concentration of 1 mg/mL at a rate of 0.33 uL/min for 90 minutes at the following coordinates: 23 mm posterior to the bregma, 3 mm lateral to midline, and 9 mm ventral. The thalamus was targeted given its high grey matter content, similar to the striatum in rodents. The brain was flash frozen and sliced/imaged for nanoparticle distribution.

3.2.3. Tissue processing for NP imaging

Animals were sacrificed 1 hour post-CED and the brains were fixed in formalin for 24 hours and subsequently exposed to a 10%, 20%, and 30% sucrose gradient. The same procedure was followed for animals that were sacrificed 24 hours, 72 hours, and 7 days post-administration. Brains were mounted and cryosectioned at a thickness of 50 μm (Leica Biosystems, Buffalo Grove, Il). Distances ± 1.5 mm from the injection site were carefully obtained. Slices were fixed with Dako fluorescence mounting medium (Dako, Carpinteria, CA) and imaged using a Zeiss confocal 710 laser scanning microscope (Zeiss, Jena, Germany) in the GFP and Cy5 channels at 5x magnification. The presence of background fluorescence was determined by comparing to the striatum of the contralateral hemisphere with no injection. Brain slice images were quantified for fluorescent distribution of PS-PEG or PS-COOH NPs by running the confocal laser scanning microscope images through a custom MATLAB script which thresholded the images at 10% of the maximum intensity (Fig S.4). Fluorescent distribution of NP in the ventricles or white matter tracts were avoided and not included in the quantification. The area of distribution calculated from each slice was multiplied by the slice thickness of 50 μm and summated across all images to obtain a total volume of distribution. If a slice was lost during cryosection procedure, the area of distribution was taken as the average of the previous and following slices. Rarely was more than 1 slice lost from a brain specimen. Furthermore, to ensure that the observed volume of distribution (Vd) differences between the PS-COOH and PS-PEG NPs was not due to the use of GFP and Cy5 channels, we switched the fluorescent markers and confirmed that fluorescent PS-PEG NPs (Yellow-green, GFP) exhibited significantly enhanced distribution as compared to PS-COOH NPs (Dark-red, Cy5).

3.2.4. Staining of brain slices for specific cellular markers

Tissues were harvested, post-fixed, and cryosliced at 10 μm thickness. Tissues were mounted on glass slides, washed 3 times with PBS, and blocked with blocking buffer composed of 5% normal goat serum (Sigma Aldrich, St. Louis, MO) and 1% bovine serum albumin (Sigma Aldrich, St. Louis, MO) in PBS for 1 hour at room temperature. Tissue slices were incubated with primary rabbit anti-mouse Iba1 antibody (Abcam ab107159, Cambridge, MA), rabbit polyclonal anti-mouse NeuN (Millipore ABN78A4, Billerica, MA), or anti-glial fibrillary acidic protein (GFAP) (eBioscience, San Diego, CA) each diluted at 1:250 in blocking buffer for 16 hours at 4^{o} C. Tissues were washed 3 times with PBS. For Iba-1 stain, tissues were further incubated with AF488 labeled goat anti-rabbit secondary antibody (Life Technologies, Grand Island, NY) diluted 1:500 in blocking buffer for 1 hour at room temperature. Tissues were washed 3 times with PBS, and then incubated with DAPI (Life Technologies, Grand Island, NY) at a 1:1000 dilution in PBS for 15 minutes at room temperature. Slides were washed 3 times with

PBS and allowed to dry before mounting with Dako fluorescence mounting medium (Dako, Carpinteria, CA).

3.2.5. Confocal imaging and MATLAB image-based processing

Slices were fixed with Dako fluorescence mounting medium (Dako, Carpinteria, CA) and imaged using a Zeiss confocal 710 laser scanning microscope (Zeiss, Jena, Germany) in the GFP and Cy5 channels at 5x magnification. The presence of background fluorescence was determined by comparing to the striatum of the contralateral hemisphere with no injection. Brain slice images were quantified for fluorescent distribution of PS-PEG or PS-COOH NPs by running the confocal laser scanning microscope images through a custom MATLAB script which thresholded the images at 10% of the maximum intensity (Fig S.4). Fluorescent distribution of NP in the ventricles or white matter tracts were avoided and not included in the quantification. The area of distribution calculated from each slice was multiplied by the slice thickness of 50 μm and summated across all images to obtain a total volume of distribution. If a slice was lost during cryosection procedure, the area of distribution was taken as the average of the previous and following slices. Rarely was more than 1 slice lost from a brain specimen. Furthermore, to ensure that the observed Vd differences between the PS-COOH and PS-PEG NPs was not due to the use of GFP and Cy5 channels, we switched the fluorescent markers and confirmed that fluorescent PS-PEG NPs (Yellow-green, GFP) exhibited significantly enhanced distribution as compared to PS-COOH NPs (Dark-red, Cy5).

To image for cell-specific markers, confocal images of stained slides were taken at high magnification (40x) for Iba-1 (microglia), NeuN (neurons), and GFAP (astrocytes).

3.2.6. Statistical analysis

Statistical testing between two groups were conducted using a two sample student t-test. If statistical comparisons involved more than two groups, testing was conducted with SPSS 18.0 software (IBM Inc.) using one-way ANOVA followed by Tukey honestly significant difference. Differences for t-test, ANOVA, and Tukey tests were considered statistically significant at $p < 0.05$.

3.3. Results and Discussion

3.3.1. NP characterization

Fluorescently labeled 40 nm PS-COOH NP probes were modified with exceptionally dense surface PEG coatings according to our previously published protocol [2]. These densely PEGylated NP were approximately 60 nm with a near neutral surface charge (as indicated by ζ-potential), whereas unmodified, PS-COOH possessed a significantly anionic surface charge (Figure 3.1A).

3.3.2. Surface chemistry of NPs affects volume of distribution

Previous studies that have used CED to administer sub-100 nm, non-shielded NP fail to achieve significant NP distribution, likely due to adhesive interactions between the NP and the brain ECM [39]. We have shown that NP as large as 114 nm with exceptionally dense PEG coatings can rapidly diffuse in healthy and tumor rodent brain tissues, thereby leading to improved therapeutic outcome [2, 40]. Here, we discovered that the pressure-driven flow provided by CED further improves the distribution of non-adhesive NP throughout the brain interstitium in both CF-1 mice and Sprague Dawley rats (Figure 3.1B). Following infusion at a NP concentration of 1 mg/mL, the volume of distribution (Vd) of non-adhesive NP was consistently higher (~6-7 fold) than that of unmodified PS-COOH in both species (Figure 3.1B, C). We conclude that even the continuous pressure-driven flow provided by CED cannot adequately overcome the adhesive interactions that occur between conventional NP (i.e. PS-COOH) and the brain ECM. Thus, a well-coated, non-adhesive NP surface is essential towards achieving significant distribution of NP away from the point of administration following CED.

Given that we observed a scalable increase in the Vd of our PS-PEG NPs when increasing the volume of infusion from 2 μL (in mice) to 20 μL (in rats), we believe that further improvements in the Vd may be realized in larger animals that can tolerate larger volume of infusions. Indeed, in our single administration in a New Zealand rabbit, we found that a 30 μL administration yielded a significantly higher than expected Vd of 110 mm^3. But given that this study currently consists of 1 specimen which was conducted in an *ex vivo* setting, further investigations with this animal model must be undertaken. Furthermore, this author acknowledges that the anatomical differences present in the brain of larger mammalian species (i.e. non-human primates and/or humans) would require careful placement of catheters and further adjustment of infusion parameters, as demonstrated in previous preclinical studies [41, 42] to truly achieve this improved Vd.

3.3.3. Concentration-dependent NP distribution

In an attempt to address the limited NP distribution, several groups have administered high concentrations of small, conventional NP that saturate the available binding domains throughout the ECM, thereby enabling residual NP to distribute away from the point of infusion [26, 33, 43]. We therefore sought to determine the correlation between Vd of NP and infused NP concentration. When PS-PEG and PS-COOH were coinfused at 0.1 mg/mL, 1 mg/mL, and 25 mg/mL, Vd of PS-PEG was 10.7-fold, 3.6-fold, and 1.3-fold higher than that of PS-COOH, respectively (Figure 3.3A). Importantly, the Vd of PS-COOH increased with increasing concentrations of infused NP whereas PS-PEG achieved high Vd independent of concentration (Figure 3.3A, B).

3.3.4. Cell specific uptake of NPs following intracranial infusion

To mechanistically understand the fate of NPs following their infusion into the brain striatum, we imaged for the presence of PS-PEG and PS-COOH at 24 hours, 72 hours, and 7 days post-administration. At each timepoint, we found that the Vd of both PS-PEG and PS-COOH were qualitatively similar to their respective Vd at 1 hour post-CED (Figure 3.3A). Additionally, the PS-PEG fluorescence appeared significantly punctated, indicating accumulation of the NPs at specific locations within the striatum whereas PS-COOH remained confined near the point of administration (Figure 3.4A).

Given that the appearance PS-PEG NPs at longer timepoints demonstrated cell-specific accumulation, we further investigated the cell-specific uptake of PS-PEG and PS-COOH NPs at high magnification at a timepoint of 24 hours after CED administration. Qualitative images of individual cellular stains (Figure 3.4B) depict significant colocalization of PS-PEG NPs with microglia, whereas little to no colocalization was observed with neurons and astrocytes. Of note, the microglia exhibit a ramified phenotype, indicating that they remain unactivated, as opposed to the pro-inflammatory activated status indicated by an amoeboid morphology that may induce further injury [44]. Furthermore, PS-COOH NPs did not associate with any specific cell marker and instead, remain entrapped near the point of administration. Therefore, we hypothesize that a biodegradable NP that is engineered to be brain penetrating similar to our PS-PEG NPs may be safely administered, uptaken, and degraded/cleared by microglia, whereas a conventional NP may remain within the brain interstitium for longer periods of time. Detailed clearance and retention analysis needs to be further tested and analyzed.

3.4. Conclusion

We establish that non-adhesive NP, when administered using CED, can overcome the brain ECM and achieve significant distributions within the rodent brain interstitium, even when administered at low concentrations. Furthermore, the non-adhesive nature of these NPs enable them to be safely uptaken and cleared from the brain intercellular spaces into microglia. On the other hand, conventional NP remain entrapped near the point of administration and can only overcome the brain ECM following CED if they are administered at extremely high NP concentrations (Figure 3.2A, B), which may not be translationally applicable for highly immunogenic and/or toxic drug payloads.

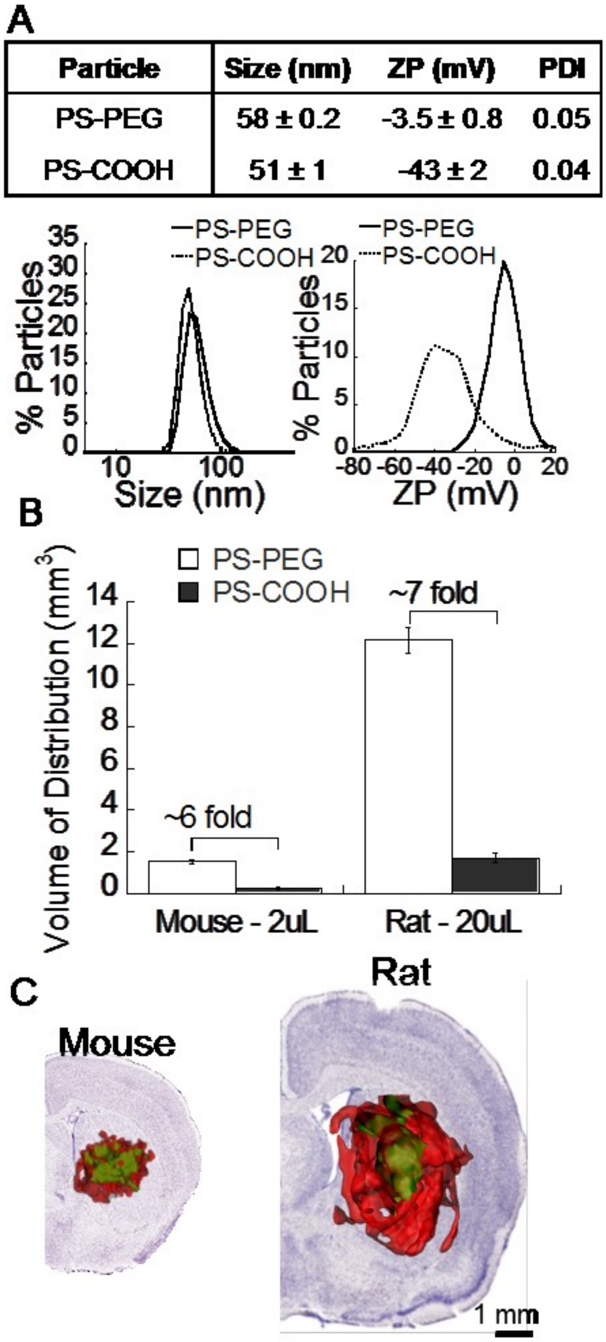

Particle	Size (nm)	ZP (mV)	PDI
PS-PEG	58 ± 0.2	-3.5 ± 0.8	0.05
PS-COOH	51 ± 1	-43 ± 2	0.04

Figure 3.1: In vivo administration of PS-PEG and PS-COOH. (A) Physicochemical characterization of model polystyrene based nanoparticles. (B) Nanoparticle volume of distributions in CF-1 mouse and Sprague Dawley rats. (C) Representative 3D nanoparticle distribution volumes injected into rodent striatum. Images are overlayed on coronal brain slices derived from mouse and rat brain atlases.

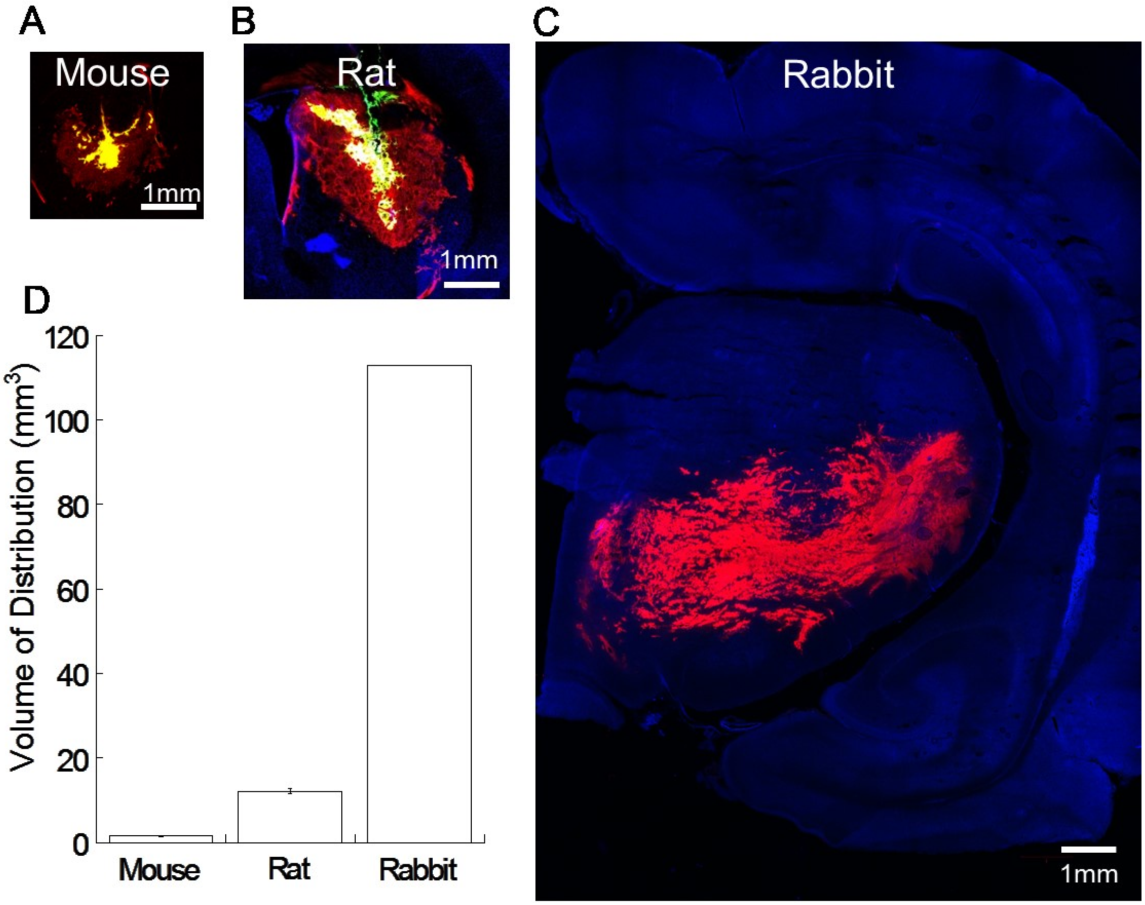

Figure 3.2: In vivo nanoparticle distribution in mouse, rat, and rabbit. (A, B, C) Qualitative coronal slice images depicting the area of distributions of PS-PEG nanoparticles (red) in (A) mouse, (B) rat, and (C) rabbit. (D) Quantitative volume of distribution (Vd) following 2 uL (mouse), 20 uL (rat), and 30 uL (rabbit) injections of PS-PEG nanoparticles. N ≥ 3 for mouse and rat quantitative calculations. N = 1 for rabbit. Note: Mouse and rat Vd reproduced from Figure 3.1B

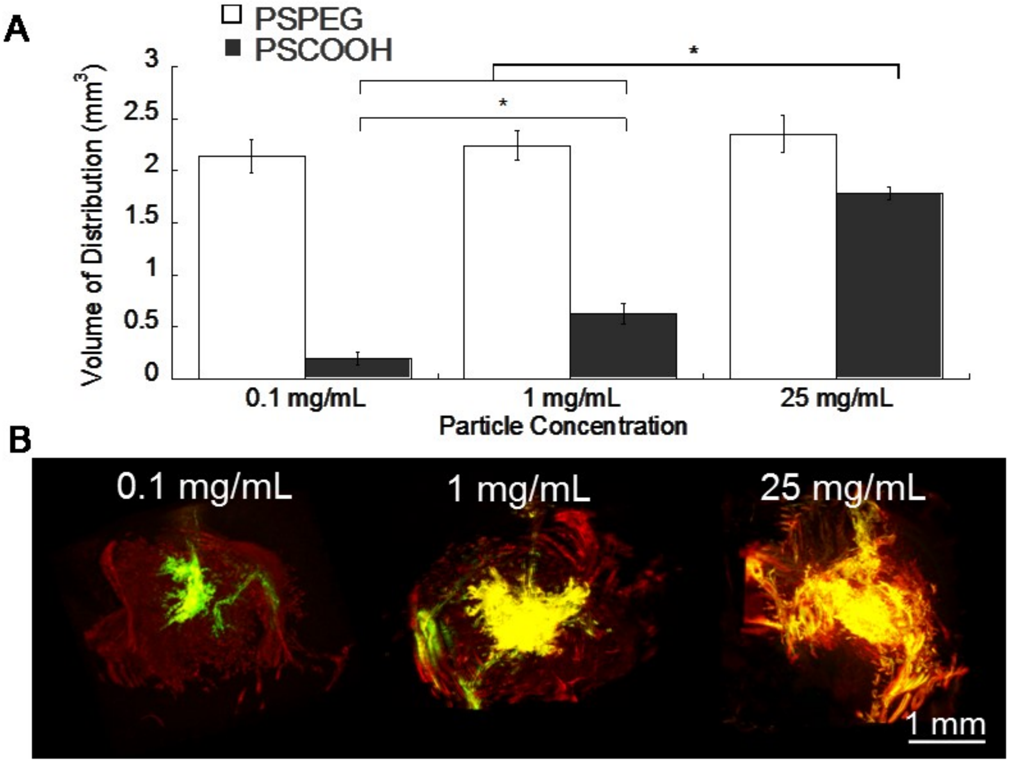

Figure 3.3: Volume of distribution dependence on particle concentration. (A) Quantitative volume of distributions of PS-PEG and PS-COOH nanoparticles in relation to the concentration of particles administered. Statistical significance denoted by * $P < 0.05$. (B) 3D reconstruction of PS-PEG (red) and PS-COOH (green) nanoparticles in the mouse striatum following CED administration.

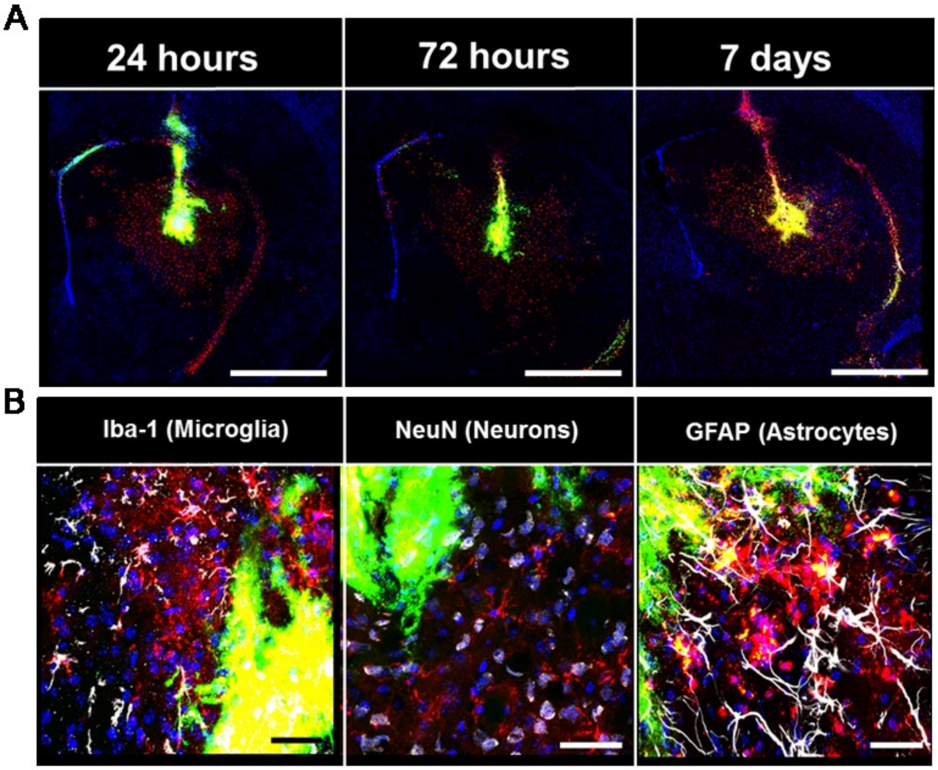

Figure 3.4: Time dependent uptake/clearance of nanoparticles in the brain. (A) Presence of PS-PEG (red) and PS-COOH (green) nanoparticles in the striatum at specific timepoints following CED infusion. Scale bar = 1mm. (B) Cell specific staining for microglia, neurons, and astrocytes depict uptake of PS-PEG nanoparticles in microglia at 24 hours following CED administration. Scale bar = 50 μm.

4. DEVELOPMENT OF BIODEGRADABLE BRAIN-PENETRATING NANOPARTICLES FOR DELIVERY TO THE CENTRAL NERVOUS SYSTEM

4.1. Introduction

The development of therapeutic-loaded NPs represents a promising strategy to deliver drugs into the brain for the treatment of primary brain tumors such as GBM. Furthermore, many of these NP platforms are now engineered from biocompatible polymers that can readily degrade in the physiological microenvironment, effectively delivering the target payload without negatively impacting the normal functioning of surrounding healthy tissue [45]. Given that efforts on therapeutic delivery to the brain has primarily focused on overcoming the BBB, the majority of these biodegradable NPs have been engineered to solely address the specific criteria to enable NP entrance into the brain from systemic circulation. However, the presence of the BTB has only been recently elucidated, which has led to the subsequent emphasis that in order to achieve effective therapeutic delivery to the brain, therapeutic, biodegradable NPs must also be similarly engineered to overcome this hurdle [2, 22].

NP delivery to tumors has focused on both passive (enhanced permeability and retention effect [46]) and active delivery methods. Leading NP formulations that have been developed for active transport across the BBB have mainly focused on modifying the surface chemistry of a NP [47]. For example, numerous groups have conjugated transferrin antibodies on the NP surface and experienced increased uptake across the BBB due to the high abundance of transferrin receptors that are overexpressed in GBM [48-50]. Alternatively, a leading NP candidate developed by Dr. Jorg Kreuter (Goethe University of Frankfurt) focuses on coating a PLGA-based NP with a P80 surfactant [51, 52]. The presence of this surfactant leads to the adsorption of a serum protein (apolipoprotein-E; ApoE), which binds to the receptors expressed on the endothelial cells of the BBB [53]. This leads to the transcytosis of the NP construct across the BBB and into the brain [54]. Although this NP is able to pass through the BBB, its ability to navigate through the heterogeneous brain tissue barrier has not been investigated.

To address the hindrance imposed by the BTB, studies have shielded the NP surface chemistry [27] or have driven NP distribution through the brain using convection enhanced delivery (CED) [33]. However, a combination of the two strategies has not been previously investigated. Our previous work employed the former strategy by developing sub-100nm, biodegradable NPs derived from PLGA-PEG and coated with cholic acid (CHA), a small molecule surfactant. When injected into brain tissue slices, these NPs rapidly diffused due to their densely PEG-shielded surfaces [27]. Furthermore, when loaded with the chemotherapeutic paclitaxel, these NPs were able to significantly delay the tumor growth progression of malignant glioma-bearing rodents [55].

Here, we first compare the “brain penetrating” abilities of our biodegradable PLGA-PEG NPs to the gold-standard ApoE-coated NP that is able to cross the BBB. Furthermore, we circumvent the BBB altogether and administer our lead PLGA-PEG NPs into the brain using CED. We find that this combined delivery approach effectively avoids the BBB and also addresses the limitations imposed by the BTB, thereby achieving widespread therapeutic distribution in the brain that may lead to further improved treatment of patients with GBM.

4.2. Materials and Methods

4.2.1. NP preparation, labeling, and characterization

PLGA (75:25) (MW: 15kDa; Jinan Daigang Biomaterials Co. Ltd., Jinan, China) and PLGA-PEG (75:25) (25 wt% PEG; Jinan Daigang Biomaterials Co. Ltd., Jinan, China) NPs were formulated using the single emulsion process according to a previously published protocol [40]. Briefly, PLGA-PEG and PLGA polymer were fluorescently labeled with AlexFluor 647 and AlexaFluor 555 cadaverine dye (Molecular Probes, Eugene, OR) respectively as previously described [40]. Polymers were dissolved in dichloromethane and emulsified using a probe sonicator in 1% P80, 1% F68, 1% F127, 1% polyvinyl alcohol (PVA), or 0.5 wt% cholic acid (Sigma Aldrich, St. Louis, MO). Samples were allowed to spin at 700 rpm for 3 hours to evaporate all solvent. NPs were filtered through a 1 μm filter (Whatman, GE Healthcare, Pittsburgh, PA). PLGA-PEG were collected and washed using centrifugal filter units (MWCO: 100 kDa, Millipore, Billerica, MA) at a speed of 3600g for 12 min. PLGA NPs were collected using a two-step procedure. NPs were centrifuged at 8000g and the supernatant was recovered and further ultra-centrifuged at 100,000g. The pellet was then washed once and collected again at 100,000g before being resuspended for further use.

Human serum albumin NPs either uncoated (rHSA-NP), with PEG (PEG-rHSA-NP) or Apoliprotein-E targeting ligand (ApoE-rHSA-NP) were kindly provided by Dr. Jorg Kreuter. Physichochemical characteristics were previously determined prior to shipping to and testing in Hanes Lab.

NP size and surface chemistry were characterized in a standard 10 mM NaCl solution through dynamic light scattering and Laser Doppler Anemometry techniques using a Zetasizer NanoZS (Malvern Instruments, Southborough, MA).

4.2.2. Rodent brain slice preparation

Healthy rat brain tissue slices were prepared according to a slightly modified protocol of a previously publication [2]. The rodent brain was removed and the tissue was sliced into 1.5 mm thick slices using a Zivic Mouse Brain slicer (Zivic instruments, Pittsburgh, PA) and placed in custom-made microscopy chambers. Half a microliter of fluorescently labeled particles was injected at a depth of 1 mm into the cerebral cortex using a 10 μL Hamilton Neuros Syringe (Hamilton, Reno, NV). The chambers were sealed using a coverslip to minimize convective bulk flow so that particle movement could be fully attributed to Brownian diffusion. The transport rate of particles was calculated by analyzing the particle trajectories in brain tissue slices as described previously [2].

4.2.3. Multiple particle tracking in rodent brain slices

The particle trajectories were recorded as 20 s movies at an exposure of 66 ms using an EMCCD camera (Evolve 512; Photometrics, Tuscon, AZ) mounted on an inverted epifluorescence microscope (Axio Observer D1, Carl Zeiss, Hertfordshire, UK) equipped with a 100x oil-immersion objective. N = 3 rat brain tissue specimens were used for each particle type. Mean squared displacement (MSD) of particles were calculated and compared at a time scale of $\tau = 1$ s. Theoretical MSD of NP in ACSF was calculated using theoretical Stokes-Einstein equation and the mean particle diameter calculated through dynamic light scattering.

4.2.4. CED of non-adhesive PLGA-based NPs

NPs were lyophilized overnight and resuspended at a concentration of 1 mg/mL in 0.9% saline. Female CF-1 mice weighing 20-30 g were anesthetized with a mixture of ketamine (75 mg/kg) and xylazine (7.5 mg/kg). A 2 cm sagittal incision was made on the head and a burr hole was made 2 mm lateral to the bregma. The loaded syringe was lowered to a depth of 2.5 mm below the mouse dura and a total of 2 μL of the solution was administered over 10 minutes at a rate of 0.2 μL/min. The cannula was allowed to sit for 5 minutes following the completion of infusion and was then withdrawn at a rate of 1 mm/min. The animal was then sutured (Covidien, Mundelein, Il) and placed on a heating pad.

4.2.5. Tissue processing and image-based analysis of NP distribution

Slices were fixed with Dako fluorescence mounting medium (Dako, Carpinteria, CA) and imaged using a Zeiss confocal 710 laser scanning microscope (Zeiss, Jena, Germany) in the GFP and Cy5 channels at 5x magnification. The presence of background fluorescence was determined by comparing to the striatum of the contralateral hemisphere with no injection. Brain slice images were quantified for fluorescent distribution of PS-PEG or PS-COOH NPs by running the confocal laser scanning microscope images through a custom MATLAB script which thresholded the images at 10% of the maximum intensity. Fluorescent distribution of NP in the ventricles or white matter tracts were avoided and not included in the quantification. The area of distribution calculated from each slice was multiplied by the slice thickness of 50 μm and summated across all images to obtain a total volume of distribution.

4.2.6. Statistical analysis

Statistical testing between two groups were conducted using a two sample student t-test. If statistical comparisons involved more than two groups, testing was conducted with SPSS 18.0 software (IBM Inc.) using one-way ANOVA followed by Tukey honestly significant difference. Differences for t-test, ANOVA, and Tukey tests were considered statistically significant at $p < 0.05$.

4.3. Results

4.3.1 Characterization and transport of Apolipoprotein-E NPs in brain tissue

We first tested the brain penetrating abilities of HSA-based NPs given that they are considered one of the leading NP for delivery across the BBB. Using multiple particle tracking (MPT), we tracked the individual trajectories of naked HSA-NP, PEG-coated HSA-NP (PEG-HSA-NP) and the gold standard Apolipoprotein-E coated NP (ApoE-HSA–NP) in healthy rodent brain tissue and compared their mean squared displacements to our PS-PEG NPs. NP physicochemical characteristics are detailed in Figure 4.1A. All three HSA-based NPs were around 200 nm in diameter and exhibited significantly anionic surface charges.

HSA-NP, PEG-HSA-NP, and ApoE-HSA-NP all displayed completely immobilized motion within the brain tissue, with approximate MSD values of 10^{-3} μm^2. In comparison, at a representative timescale of $\tau = 1$ second, our PS-PEG NPs from

Chapter 3 were able to diffuse approximately 2500 times faster than HSA-based NPs (Figure 4.1A, B).

4.3.2 Characterization and transport of PLGA-based NPs in brain tissue

PLGA and PEG-PLGA NPs were engineered with the varying surfactant coatings and collected using their respective centrifugation methods to ensure that their sizes would be below the previously detailed brain pore sizes [2]. All particles are sub-100 nm in diameter and all PEG-PLGA NPs exhibited near neutral surface charge regardless of surfactant choice. PLGA NPs were highly anionic except for those coated with 1% PVA which were also near neutral in surface charge (Table 4.1).

The ability of PLGA and PEG-PLGA NPs to penetrate brain tissue was conducted using multiple particle tracking in *ex vivo* healthy rodent brain tissue slices. Interestingly, both PLGA and PEG-PLGA NPs that were coated with surfactants that have previously been implicated to help in NP crossing of the BBB (P80 and F68) demonstrated completely immobilized motion (Figure 4.2). In fact, their MSD were similar, if not slower, than the MSD of ApoE-HSA-NP at a timescale of $\tau = 1$ second (Table 4.1). PEG-PLGA NPs coated with 1% F127 or 1% PVA exhibited 6-fold and 5.4-fold increased MSD respectively as compared to the MSD of ApoE-HSA-NP. Again, non-PEGylated PLGA NPs coated with these same surfactants were immobilized. On the other hand, PEG-PLGA NPs formulated in ultrapure water or 0.5% CHA diffused 19-fold and 80-fold faster than ApoE-HSA-NP (Figure 4.2, Table 4.1).

4.3.3 Volume of distribution of PLGA-based NPs following CED

Following our *ex vivo* characterization, we wanted to investigate whether the improved diffusion of PLGA-PEG NPs formulated with 0.5% CHA could translate to improved distribution *in vivo* following administration using CED. Indeed, compared to similarly sized and formulated PLGA (0.5% CHA) NPs, PEG-PLGA (0.5% CHA) NPs were able to achieve widespread distribution throughout the striatum (Figure 4.3A). In fact, the final Vd of PEG-PLGA NPs was 0.48 mm^3, which was a 12-fold improvement over the Vd of PLGA NPs of only 0.04 mm^3.

4.4. Discussion

Effective delivery of NP therapeutics to the brain for treatment of primary brain tumors such as GBM requires addressing two main barriers: 1) the blood brain barrier and 2) the brain tissue barrier. Biodegradable NPs remain the main delivery vehicle of choice given its tailorable size and surface chemistry; however, the main focus has been on developing NPs specifically for overcoming the BBB instead of also addressing the nascent understanding of the necessary design criteria for effective NP delivery through the BTB. The inability to tackle both barriers has resulted in limited advancements in utilizing nanotechnology strategies for improving therapeutic outcome of GBM patients. In this chapter, we begin by demonstrating that the optimized biodegradable NPs that have been designed for passage through the BBB fail to address the hindrances of the BTB. In comparison, we find that our PLGA-PEG based NPs are able to rapidly diffuse in brain tissue, but only if coated with the CHA surfactant. When intracranially delivered using

CED, these NPs achieve widespread distribution in the rodent striatum and represent a promising strategy for the treatment of GBM.

The use of surfactant coatings on biodegradable NP has been widely investigated given the ease of adsorbing these different molecular chains to the NP surface. This modification has been shown to stabilize the NP and maximize drug encapsulation efficiency, both essential considerations for effective drug delivery [56]. In addition, the use of specific surfactants has been shown to have further implications for overcoming both the BBB and BTB [54]. Our previous work has shown that a CHA surfactant coated on the surface of PLGA-PEG NPs can lead to improved NP distribution [40]. Here, PLGA-PEG NP coated with our surfactant of choice, CHA, diffuse faster than ApoE coated HSA NP in the brain tissue. In fact, P80 coated NP, which has been shown to associated with ApoE and facilitate BBB transcytosis, are immobilized once in the brain parenchyma. Thus, although systemically administered P80 coated NPs and HSA-NP are able to transcytose across the BBB, they would not be able to distribute through the brain parenchyma. However, we do note that Kreuter and coworkers have shown that these P80 coated NPs traffic to the cytoplasm of neurons in the brain [54]. In light of our findings, the transport of Kreuter et al.'s P80 coated NPs through the brain parenchyma is likely an active transport process, which traffics them away from the endothelial cells of the BBB and localizes them within specific neurons.

Surface modification to render a NP surface non-interactive is an essential factor towards maximizing therapeutic distribution in the brain parenchyma. In addition to steric limitations, distribution of PLGA-based NP systems is most likely hindered by hydrophobic interactions with components of the brain ECM. Sufficient PEG shielding of

PLGA NPs allows them to more effectively distribute as compared to its non-shielded counterpart. The importance of appropriate NP design and delivery is further reflected by a promising study recently conducted by Zhou et al. who observed significant survival benefits when glioma-bearing rodents were treated with paclitaxel-loaded PLGA NPs that were coated with PVA surfactant and intracranially administered with CED [33]. Interestingly, we found that PLGA-PEG NPs coated with PVA surfactant did not exhibit brain penetrating abilities; rather, these NPs were hindered and immobilized by the brain ECM. The discrepancy between our findings and Zhou et al. can be attributed to their method of administration (CED) and higher NP concentration (100 mg/mL) that was infused into the brain, which has previously been shown to significantly improve NP distribution (also observed in Figure 3.2). In our study, we demonstrate that brain penetrating PLGA-PEG NPs coated with CHA surfactant can distribute to a large volume of the rodent striatum when administered via CED, even if delivered at very low concentrations (1 mg/mL). Thus, this CHA-coated PLGA-PEG NP will enable the delivery of highly cytotoxic drugs whose toxicities would be prohibitive if administered at high concentrations.

4.5. Conclusion

In this chapter, we compared the “brain penetrating” abilities of our lead, PLGA-PEG NPs to the HSA-NPs that have been engineered to overcome the BBB. We believe that when delivering a therapeutic to the brain, the presence of the brain tissue barrier must be heavily weighted, perhaps even moreso in comparison to the BBB. Although our brain penetrating PEG-PLGA NPs are not specifically designed to pass through the BBB, their delivery using CED can avoid the BBB altogether and achieve widespread therapeutic distribution in the brain. Thus, we believe that the delivery of a non-adhesive PLGA NP into the brain using CED represents a promising treatment platform for the delivery of other chemotherapeutics such as docetaxel and digoxin.

A

Nanoparticle	Mean Diameter ± SEM (nm)	ζ-potential ± SEM (mV)	$MSD_{particle}/MSD_{ApoE\text{-}HSA\text{-}NP}$
PS-PEG	69 ± 2	-2.8 ± 0.4	2500
PS-COOH	57 ± 2	-39 ± 2.5	0.5
HSA NP	199.9*	-44.3*	1.05
PEG – HSA – NP	211.3*	-33.6*	0.92
ApoE – HSA – NP	218.9*	-40.5*	1

B

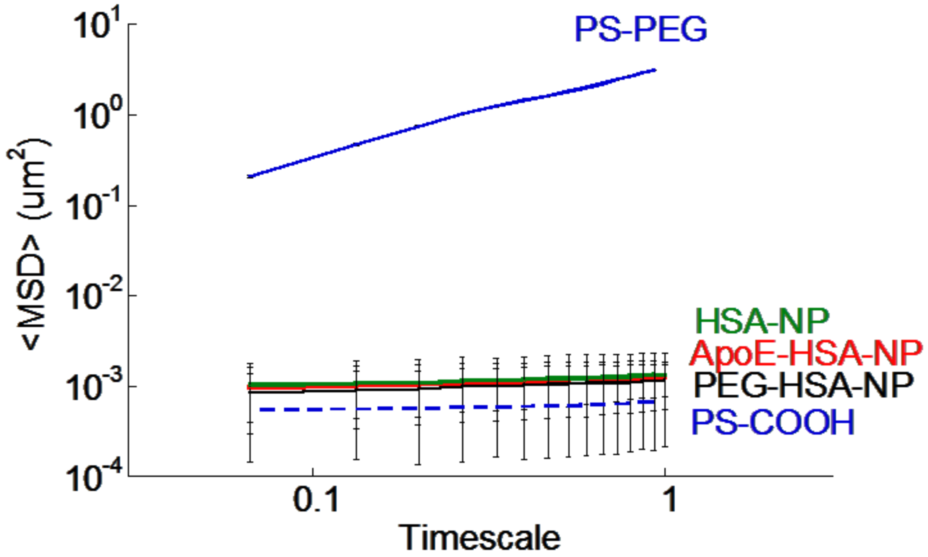

Figure 4.1: Characterization of human serum albumin nanoparticles (HSA-NP) (A) Physicochemical characteristics of PS-NP and HSA-NP. * Values provided by Kreuter and coworkers. (B) Mean squared displacement (MSD) of tracked nanoparticles in healthy rodent brain tissue slices.

Table 4.1: Physicochemical properties of biodegradable PLGA and PLGA-PEG nanoparticles coated with varying surfactants. Size and ζ-potential were measured in ACSF at pH 7.0. Data are presented as average of at least 3 measurements.

Particle	Emulsifier	Mean Diameter ± SEM (nm)	ζ-potential ± SEM (mV)	$MSD_{PLGA\text{-}NP}$/ $MSD_{ApoE\text{-}HSA\text{-}NP}$
PLGA	NA	86 ± 4	-33 ± 1	0.5
PEG-PLGA	NA	66 ± 2	-2.8 ± 0.1	**19**
PLGA	1% P80	85 ± 4	-16 ± 1	1
PEG-PLGA	1% P80	95 ± 3	-4.4 ± 0.3	0.5
PLGA	1% F68	82 ± 1	-16 ± 1	1.1
PEG-PLGA	1% F68	66 ± 0.3	-2.7 ± 0.2	0.5
PLGA	1% F127	88 ± 5	-23 ± 1	0.8
PEG-PLGA	1% F127	79 ± 2	-4.9 ± 1	6
PLGA	1% PVA	94 ± 2	-2.0 ± 1	1.2
PEG-PLGA	1% PVA	86 ± 4	-3.2 ± 0.3	5.4
PLGA	0.5% CHA	88 ± 2	-48 ± 1	0.7
PLGA-PEG	0.5% CHA	69 ± 2	-2.2 ± 0.1	**80**

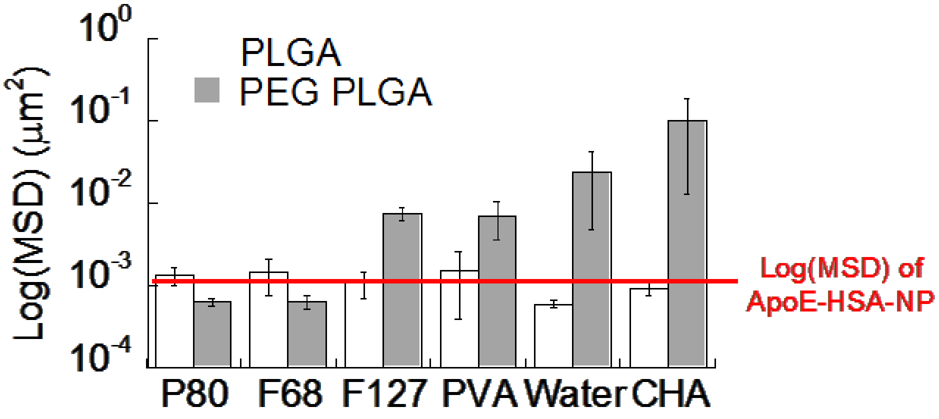

Figure 4.2: ***Ex vivo*** **characterization of PLGA and PEG-PLGA NP.** Mean squared displacement (MSD) at a timescale of 1 sec for individual PLGA-based NP formulated with varying surfactants as compared to the MSD of ApoE-HSA-NP.

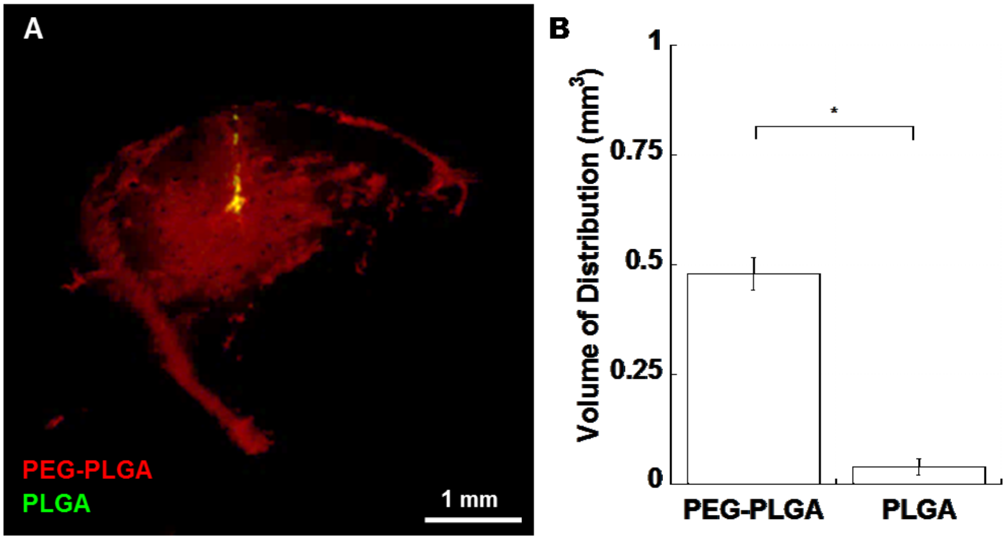

Figure 4.3: ***In vivo*** **distribution of therapeutic PLGA nanoparticles in mouse striatum administered via CED** (A, B) Representative coronally-sliced images of PLGA-PEG (red) and PLGA (green) nanoparticles infused in 0.9% saline Data represent the average of $N \geq 3$ mouse brain specimen for each solution. (B) Quantified PLGA-PEG and PLGA volume of distributions in rodent striatum. Inset depicts the Vd of PLGA based nanoparticles. $*P < 0.05$ denotes statistical significance.

5. DEVELOPMENT AND IN VIVO CHARACTERIZATION OF A BRAIN PENETRATING NON-VIRAL DNA NANOPARTICLE (DNA-NP)

5.1. Introduction

Patients with neurological diseases, including Parkinson’s disease, Alzheimer’s disease, brain tumors and most neurogenetic disorders, suffer from severe debilitating symptoms and lack of effective treatments. The accumulated knowledge of specific genetic targets that can alter or reverse the progression of central nervous system (CNS) diseases makes gene therapy an attractive therapeutic strategy [57, 58]. Multiple preclinical and clinical studies have aimed to improve the delivery of nucleic acids to the CNS using leading viral or non-viral gene vectors, with specific focus on enhancing the level and distribution of transgene expression throughout the brain tissue [57, 59].

Viral gene vectors, though relatively efficient, have been limited by low packaging capacity, technical difficulties in scale-up, high cost of production [60] and/or risk of mutagenesis [61]. Furthermore, despite the immune-privileged nature of the CNS, neutralizing immune responses may occur with repeated administrations or after prior exposures [25, 58, 62-65]. Non-viral gene vectors are an alternative strategy for gene delivery without many of the limitations of viral vectors [57]. Cationic polymer-based gene vectors provide a tailorable platform for DNA condensation and gene transfer *in vitro* and *in vivo*. The positive charge density allows for stable compaction of negatively charged nucleic acids [66, 67], protecting the nucleic acids from enzymatic degradation [68]. Also, the protonatable amines provide increased buffering capacity that may facilitate endosome escape via the “proton sponge effect”, leading to transfection [69]. A wide variety of cationic polymers have been developed for nucleic acid delivery, enabling the design of gene vector platforms with diverse physicochemical profiles and *in vivo* behaviors [70, 71].

However, non-viral gene vectors must overcome numerous biological barriers to reach target cells in the brain [57]. Various strategies have been developed to manipulate or bypass the BBB [72, 73], which is the primary barrier to the systemic delivery of gene vectors to the brain. These approaches include, but are not limited to, direct administration to the CNS [74] and reversible disruption of the BBB via focused ultrasound [75] or chemical agents [76]. However, once beyond the BBB, the anisotropic and electrostatically charged brain ECM found between brain cells has been widely recognized as another critical barrier [2, 77, 78]. This BTB hampers widespread distribution of macromolecules and NP in the brain, thereby limiting their access to target cells in disseminated neurological diseases [2, 25, 26, 77]. Given that polymeric gene vectors are typically derived from cationic backbone polymers, the negatively charged components of the ECM, comprising hyaluronan, chondroitin sulfate, proteoglycans, link proteins and tenascins, represent a significant electrostatic barrier to the penetration of DNA-NP [77, 79].

Convection enhanced delivery (CED) can further enhance the distribution of therapeutics by providing a pressure gradient during intracranial administration [20]. However, CED is unlikely to provide a significant benefit if DNA-NP are trapped in the brain parenchyma due to adhesive interactions and/or steric obstruction. Previous reports have demonstrated that, even following CED, the interactions between positively charged gene vectors and the negatively charged ECM confine NP to the point of injection and perivascular spaces, and limit their penetration into, and distribution throughout, the brain parenchyma [26, 80, 81]. Thus, designing particles with surfaces that minimize interactions with the brain ECM is critical for achieving CED-mediated enhanced particle distribution in the brain [20, 80].

In this study, we aimed to develop a DNA-NP platform with the physicochemical properties required for efficient brain penetration by polymeric NP, namely, a non-adhesive surface coating and small particle diameter in comparison to the average ECM mesh spacing [2]. To formulate a compact, colloidally-stable gene vector platform for CNS delivery, we were guided by our previous work toward optimizing PEG density to formulate gene vectors capable of efficiently penetrating human mucus secretions [82, 83]. Here, we formulated densely PEGylated brain-penetrating DNA-NP (DNA-BPN), conventionally PEGylated (lower density) DNA NP (DNA-CPN), and un-PEGylated DNA NP (DNA-UPN) and characterized their toxicity, cell uptake, and transfection efficiency *in vitro*. We then used high resolution MPT to compare their transport rates in freshly excised *ex vivo* rodent brain tissues. Finally, we investigated NP distribution and transfection throughout the brain tissue following administration *in vivo* by CED.

5.2. Materials and Methods

5.2.1. Gene vector synthesis and DNA labeling

Methoxy PEG N-hydroxysuccinimide (mPEG-NHS, 5 kDa, Sigma-Aldrich, St. Louis, MO) was conjugated to 25 kDa branched polyethyleneimine (PEI) (Sigma-Aldrich, St. Louis, MO) to yield a PEG_{5k}-PEI copolymer as previously described [82]. Briefly, PEI was dissolved in ultrapure distilled water, the pH was adjusted to 7.5 – 8.0 and mPEG-NHS was added to the PEI solution at various molar ratios and allowed to react overnight in 4^{o}C. The polymer solution was extensively dialyzed (20,000 MWCO, Spectrum Laboratories, Inc., Rancho Dominguez, CA) against ultrapure distilled water and lyophilized. Nuclear magnetic resonance (NMR) was used to confirm PEG: PEI ratios of 8, 26, 37 and 50. 1H NMR (500 MHz, D2O): δ 2.48 – 3.20 (br, CH2CH2NH), 3.62 – 3.72 (br, CH2CH2O). The poly-L-lysine 30-mer (PLL) and PEG_{5K}-PLL block copolymers were synthesized and characterized as previously published.[82, 84] The lyophilized polymers were dissolved in ultrapure distilled water and pH was adjusted to ~6.5 – 7.

The pd1GL3-RL plasmid DNA was a kind gift from Professor Alexander M. Klibanov (M.I.T) and pEGFP plasmid was purchased by Clontech Laboratories Inc. (Mountainview, CA). The plasmid DNA was propagated and purified as previously described [82]. Mirus Label IT® Tracker™ Intracellular Nucleic Acid Localization Kit (Mirus Bio, Madison, WI) was used to fluorescently tag plasmid DNA with a Cy3 or Cy5 fluorophore. Gene vectors were formed by the drop-wise addition of 10 volumes of labeled or non-labeled plasmid DNA (0.2 mg/ml) to 1 volume of a swirling polymer solution. PEI solutions were prepared at previously optimized nitrogen to phosphate (N/P) ratio of 6 and at PEG_{5k}-PEI to PEI molar ratio of 3. For the formulation of free PEI (DNA-UPN) and $(PEG_{5k})_8$-PEI (DNA-CPN) based gene vector controls, the PEI solutions were prepared at N/P ratio of 6 using 100% of free PEI or $(PEG_{5k})_8$-PEI, respectively. For fluorescence imaging, Cy3- or Cy5-labeled DNA was used to assemble fluorescently labeled gene vectors. The plasmid/polymer solutions were incubated for 30 min at room temperature to form gene vectors. Gene vectors were washed twice with 3 volumes of ultrapure distilled water, and re-concentrated to 1 mg/ml using Amicon®

Ultra Centrifugal Filters (100,000 MWCO, Millipore Corp., Billerica, MA) to remove free polymers. DNA concentration was determined via absorbance at 260 nm using a NanoDrop ND-1000 spectrophotometer (NanoDrop Technologies, Wilmington, DE). PEG-PLL gene vectors were similarly prepared at an N/P ratio of 2 as previously described [82, 84, 85].

5.2.2. NP physicochemical characterization and in vitro stability

Hydrodynamic diameter, ζ-potential and polydispersity index (PDI) were measured in 10 mM NaCl at pH 7.0 by dynamic light scattering and laser Doppler anemometry, respectively, using a Nanosizer ZS90 (Malvern Instruments, Southborough, MA). Gene vectors were imaged using transmission electron microscopy (TEM, Hitachi H7600, Japan) to determine their morphology and dimensions. PEI gene vector stability was assessed by incubating gene vectors in artificial cerebrospinal fluid (aCSF; Harvard Apparatus, Holliston, MA) at 37 ^{o}C and conducting dynamic light scattering every 30 min for 24 h. At 1 h of incubation, a fraction of the NP solution was used for TEM.

5.2.3. Ex vivo brain penetration of non-adhesive DNA-NP

Multiple particle tracking (MPT) was used to estimate the MSD of fluorescent gene vectors in *ex vivo* rodent brain slices as previously described [2]. Briefly, brains were harvested from adult Fischer rats and incubated in aCSF for 10 min on ice. The brains were sliced into 1.5 mm coronal slices using a Zivic brain matrix slicer (Zivic Instruments, Pittsburgh, PA) and placed on custom made slides. Half a microliter of fluorescently labeled gene vectors was injected on the cerebral cortex at a depth of 1 mm using a 50 μl Hamilton Neuro Syringe (Hamilton, Reno, NV) mounted on a stereotaxic frame. Tissues were covered by a 22 mm x 22 mm coverslip to minimize tissue movement and bulk flow. Particle trajectories were recorded over 20 s at an exposure time of 66.7 ms by an Evolve 512 EMCCD camera (Photometrics, Tucson, AZ) mounted on an inverted epifluorescence microscope (Axio Observer D1, Zeiss; Thornwood, NY) equipped with a 100x/1.46 NA oil-immersion objective. Movies were analyzed with a custom made MATLAB code to extract x, y-coordinates of gene vector centroids over time and calculate the MSD of each particle as a function of time [2, 86]. The spatial resolution to the noise/signal ratio correlation was estimated using immobilized gene vectors on a glass slide [87, 88]. We estimated the average resolution of our MPT experiments to be ~0.009 μm^2 at 1 s. At least three rat brains were used per gene vector type, and at least 500 gene vectors were tracked per brain sample. The ensemble-averaged MSD (<MSD>) for all gene vectors in a sample was calculated and then averaged over different samples as a function of time. Histograms were generated from the MSD data for each individual vector at a time scale of 1 s. The theoretical MSD of gene vectors in aCSF was calculated using the Stokes-Einstein equation and the mean particle diameter calculated through dynamic light scattering.

5.2.4. CED administration of brain penetrating DNA-NP

To study the distribution of PEI-based gene vectors following CED in the rodent striatum, six rats for each vector type were used. A 33 gauge 50 μl Hamilton Neuro Syringe mounted to a stereotaxic headframe was lowered to a depth of 3.5 mm. A 20 μl solution of Cy3-labeled DNA-CPN and Cy5-labeled DNA-BPN at a plasmid concentration of 500 µg/ml for each particle type in normal saline was administered. The rate of infusion was set at 0.33 µl/min, using a Chemyx Inc. Nanojet Stereotaxic syringe pump (Chemyx, Stafford, TX). Animals were sacrificed 5 h following the injection. To examine the concentration-dependence of particle distribution, we also performed co-injections at half the plasmid concentration, 250 µg/ml for each particle type, in normal saline.

5.2.5. Expression of reporter transgene following CED of brain penetrating DNA-NP

To assess the distribution of transgene expression following CED administration of gene vectors, at least four rats for each particle type were used; plasmid encoding fluorescent eGFP reporter protein with a cytomegalovirus (CMV) promoter was complexed into the various PEI-based gene vector formulations and infused in a 20 µl solution of 1 mg/ml plasmid solution using the same parameters described above. Animals were sacrificed 48 h following CED administration, and harvested brains were fixed in 4% formaldehyde.

5.2.6. Image based quantification of DNA-NP distribution and transgene expression

Freshly harvested brains were fixed in 4% formaldehyde overnight followed by a gradient sucrose solutions before cryosection. Tissues were sectioned coronally into 100 µm thick slices using Leica CM 1905 cryostat. Slices were stained with DAPI (Molecular Probes, Eugene, OR) to visualize cell nuclei, and imaged for the fluorescence originated from DAPI, Cy3 and Cy5 or Alexa Fluor 488 (eGFP) using confocal LSM 710 microscope (Carl Zeiss; Hertfordshire, UK) under 5x and 10x magnification. Settings were carefully optimized to avoid background fluorescence based on non-injected control rat brains. Laser power, pinhole, gain, offset and digital gain were selected separately for each magnification and kept constant throughout the study.

The volume of gene vector distribution following CED administration was quantified using a custom MATLAB script that subtracted the background fluorescence and thresholded the fluorescent intensities at 10% of the maximum intensity. NP fluorescence in the white matter tracts due to backflow was excluded from quantification. Every 100 µm slice within 2 mm of the injection plane was imaged. The area of distribution on each slice was summated to calculate the total volume of gene vector distribution. The identical process was utilized for the analysis of the distribution of transgene expression mediated by various PEI-based gene vectors carrying eGFP plasmid. To reconstruct three dimensional images of NP distribution and distribution of transfection within the rodent striatum, we stacked and aligned the previously acquired images using Metamorph ® Microscopy Automation & Image Analysis Software (Molecular Devices, CA). We used Imaris ® Software (Bitplane, CT) to create 3D isosurfaces of the reconstructed images.

5.2.7. Quantification of transgene expression using Western Blot

For western blot analysis of *in vivo* transfection following CED of gene vectors, three rats for each particle type were used and the same experimental procedures followed for imaging-based analysis of distribution of transfection were used. Animals were sacrificed 48 h following CED administration and immediately placed on ice and a 4 mm thick coronal slice of the striatum from -2 mm to 2 mm from the injection site was dissected and stored in -80°C for western blot analysis. The antibodies, anti-GFP (B-2): sc-9996 and anti-β-actin:sc-47778 (Santa Cruz Biotechnology, Santa Cruz, CA), were used for the detection of transgene expression (eGFP) and housekeeping protein (actin), respectively. Brain tissues were lysed using brief sonication in ice PBS buffer (1 mM PMSF, and 1 μg/ml each of aprotinin, leupeptin, and pepstatin A). Sampling buffer (10% glycerol, 2% SDS, 62.5 mM Tris–HCl, 2% β-mercaptoethanol, pH 6.8) was added and samples were boiled at 100^{o}C for 10 min. Samples were resolved by SDS–polyacrylamide gel electrophoresis (PAGE) and proteins on the gels were transferred to nitrocellulose (Bio-Rad, Hercules, CA) using a semidry blotter (Bio-Rad, Hercules, CA). The membrane was blocked with 3% BSA in TBST (10 mM Tris-Cl, pH 8.0, 150 mM NaCl, 0.5% Tween-20) and incubated overnight at 4 °C with primary antibodies. Immunoblots were visualized by enhanced chemiluminescence method. Quantification of western blot results was performed using the Multi Gauge program (Fujifilm, Tokyo, Japan) [89].

5.2.8. In vivo safety of DNA-NP

To evaluate the safety profile of the gene vectors *in vivo* following CED administration, three rats for each group were used. Various PEI-based gene vector formulations were infused in a 20 μl solution at a 1 mg/ml plasmid concentration as described above. A normal saline solution was infused as a negative control. Animals were sacrificed 4 d following administration and the harvested brains were fixed in 4% formaldehyde, processed, sectioned and stained with hematoxylin and eosin. Blind histopathological analysis was performed by a board certified neuropathologist and tissues were scored from 0-3 for indications of inflammation and hemorrhage (0: no inflammation/hemorrhage, 1: mild, 2: moderate, 3: severe).

5.2.9. Statistical analysis

Statistically significant differences between two groups were analyzed with a two-tailed Student's t test assuming unequal variances or paired student's t test when allowed. Multiple comparisons were performed using one-way analysis of variance (ANOVA), followed by post hoc test using SPSS 18.0 software (SPS S Inc., Chicago, IL).

5.3. Results

5.3.1. In vitro characterization and stability of DNA-NP

To effectively shield the positive surface charge intrinsic to cationic gene vectors, we formulated gene vectors using copolymers of polyethyleneimine (PEI) conjugated to multiple 5 kDa PEG molecules (PEG_{5k}-PEI) with a range of PEG to PEI molar ratios. As previously reported, PEGylation of cationic polymers may have a negative influence on DNA complexation due to reduction of available positive charges and additional steric hindrance by the PEG chains after conjugation [90]. Thus, using only highly PEGylated PEI to condense DNA copolymers yields loose, unstable gene vectors that are not likely to retain their stability in biological environments [82]. In order to achieve compact and colloidally stable gene vectors, we formulated vectors with a blend of PEG_{5k}-PEI and free PEI, with 25% of the total amines deriving from free PEI [82]. Using a fixed amount of free PEI, we achieved DNA compaction into ~50 nm DNA NP using PEG_{5k}-PEI copolymers with a wide range of PEG to PEI molar ratios. Importantly, we found that the use of a copolymer with a PEG to PEI ratio of 26, which is substantially higher than PEGylation ratios used typically [90-92], is sufficient to form gene vectors with a near neutral ζ-potential (Table 1) (DNA-BPN); near-neutral ζ-potential has been shown to be key to enabling NP diffusion in brain tissue [2]. We also prepared DNA-CPN consisting of PEGylated PEI with a more conventional PEG to PEI ratio of 8 [55, 90, 93], and un-PEGylated PEI DNA NP (DNA-UPN). The physicochemical properties of DNA-BPN, DNA-CPN and DNA-UPN are summarized in Table 5.1. Of note, DNA-CPN possessed a larger particle diameter and more positive surface charge compared to DNA-BPN, (59 nm and 9.3 mV for DNA-CPN; 43 nm and 2.9 mV for DNA-BPN) suggesting looser compaction and/or inferior surface coating of DNA-CPN.

To predict the particle stability of gene vectors following *in vivo* administration, we characterized *in vitro* stability in artificial cerebrospinal fluid (aCSF) at 37^{o}C over time (Figure 5.1A). DNA-UPN aggregated immediately after addition to aCSF; the hydrodynamic diameter increased 8.3-fold, from 47 nm ± 2 nm to 392 nm ± 32 nm. After 7 h, the polydispersity index (PDI) was greater than 0.5, indicating loss of colloidal stability. DNA-CPN diameter increased ~3-fold 30 min after addition to aCSF, from 59 nm ± 1 nm to 172 nm ± 5 nm, and then remained stable at the larger size for the remaining 24 h. We found that DNA-BPN exhibited improved stability in aCSF compared to both DNA-UPN and DNA-CPN. DNA-BPN size remained unchanged over the first 30 min in aCSF at 50 nm ± 17 nm, followed by a 1.6-fold increase in diameter that remained stable over the remaining 24 h (Table 5.1, Figure 5.1A). These observations were further confirmed by transmission electron micrographs (TEM) of gene vectors in ultrapure water (Figure 5.1B, upper row) and after 1 h incubation in aCSF at 37^{o}C (Figure 5.1B, lower row). Incubation of DNA-UPN in aCSF resulted in the formation of large aggregates. DNA-CPN increased in size and demonstrated some signs of aggregation, while DNA-BPN modestly increased in size, but did not appear to aggregate.

5.3.2. Ex vivo brain penetration of DNA-NP with varying PEG densities

We next used MPT to assess the diffusion of DNA-BPN, DNA-CPN and DNA-UPN in the brain parenchyma. We have previously demonstrated, using model NP, that MPT results in *ex vivo* brain tissue predicts well NP penetration into the brain parenchyma *in vivo* [2]. As expected, due to their positive surface charge, the DNA-UPN were largely immobilized by the brain ECM, as shown by their constrained, non-Brownian trajectories (e.g. Figure 5.2A). Similarly, the average DNA-CPN exhibited hindered motion, though not completely immobilized (Figure 5.2A). In contrast, the trajectory of a typical DNA-BPN spanned much greater distances, indicating relatively unhindered diffusion in brain tissue (Figure 5.2A). At a timescale of 1 s, the ensemble-averaged mean squared displacement (<MSD>) of DNA-BPN was 5- and 29-fold higher than that of DNA-CPN and DNA-UPN, respectively (Figure 5.2B). The diffusion rates of DNA-UPN and DNA-CPN in brain tissue were 6,900- and 930-fold lower than their theoretical diffusion rates in aCSF, respectively, while DNA-BPN moved only 260-fold slower in brain than in aCSF (Table 5.1). When examining histograms displaying the range of logarithmic MSD values ($\log_{10}$MSD) for individual gene vectors, we found that the transport behavior was largely unimodal for DNA-UPN and DNA-BPN; the majority of DNA-UPN displayed low MSD values, whereas most DNA-BPN exhibited increased MSD values indicative of diffusion in brain tissue. DNA-CPN were largely immobilized in brain tissue, but a minor population was able to penetrate the brain parenchyma (Figure 5.2C). Defining diffusing

DNA NP as having $\log_{10}\mathrm{MSD} \geq -1$ [86], we found that 10.3%, 32.9% and 63% of DNA-UPN, DNA-CPN and DNA-BPN, respectively, were able to diffuse in the brain parenchyma. To test whether the enhanced *ex vivo* diffusion in brain tissue would improve the distribution of the vectors in the brain parenchyma *in vivo*, we performed a bolus co-injection of fluorescently labeled DNA-CPN and DNA-BPN in the rodent striatum. As shown in Figure 5.2D, DNA-CPN largely remained localized to the injection site, whereas DNA-BPN spread approximately 300 µm from the injection site only 2 h after administration.

5.3.3. DNA-NP volume of distribution following CED administration

We next aimed to determine the effect of vector surface characteristics on distribution in brain following CED. To directly compare the spatial distribution of the gene vectors, we co-infused Cy5-labeled DNA-BPN and Cy3-labeled DNA-CPN. DNA-BPN distributed homogeneously throughout the rodent striatum, whereas DNA-CPN were confined in the injection site (Figure 5.3A, B). Within the coronal plane of injection, DNA-BPN covered a 3-fold larger tissue area than DNA-CPN (Figure 5.3C, $p < 0.05$). Moreover, the overall volume of distribution in the brain achieved with DNA-BPN was found to be 3.1-fold higher than the volume of distribution achieved with DNA-CPN (Fig. 5.3D).

5.3.4. Widespread delivery and high levels of a reporter transgene

We then sought to determine whether increased tissue distribution would also lead to an increase in the volume of tissue transfected following CED administration of gene vectors carrying plasmid DNA encoding eGFP. DNA-UPN and DNA-CPN treated animals demonstrated significant eGFP expression surrounding the injection site (Figure 5.4A-B, D-E). In contrast, DNA-BPN provided widespread transfection throughout the rat striatum (Figure 5.4C, F), which correlated well with the gene vector distribution analysis (Fig. 5.3A, B). In particular, DNA-BPN resulted in a statistically significant ($p < 0.05$) increase in the eGFP transgene expression with a 2.4- and 3.2-fold higher volume of tissue transfection compared to DNA-CPN and DNA-UPN, respectively (Figure 5.4G). We also quantitatively determined total transgene eGFP expression mediated by CED of DNA-UPN, DNA-CPN and DNA-BPN, using western blot analysis. DNA-BPN demonstrated a statistically significant, 2-fold higher overall transgene expression in the striatum in comparison to DNA-CPN and DNA-UPN (Figure 5.4H).

5.4. Discussion

As previously discussed with drug delivery, efficacious gene therapy for diffuse and debilitating CNS disorders requires that transgene expression occur throughout the broadly disseminated, diseased area at therapeutically relevant levels [25, 94, 95]. Regardless of delivery method, the limited spatial distribution of non-viral gene vectors in the brain remains a key challenge to achieving clinically-relevant therapeutic results [94, 96]. In this chapter, we demonstrated that exceptionally dense PEG coatings, only achieved by blends of PEG-PEI and PEI, are critical to NP stability, safety, and distribution and transfection within the brain. We further establish that the BPN gene vector platform is non-adhesive to the brain parenchyma, leading to improved distribution in the brain. Further, the synergistic effect of combining polymeric gene vectors engineered to penetrate the brain parenchyma and the convective bulk flow provided by CED resulted in highly efficient and widespread transgene expression in the brain parenchyma. Importantly, this was achieved with no signs of vector-induced toxicity. This strategy provides a tailorable polymer-based platform that may significantly improve the efficacy of non-viral gene therapy in CNS diseases.

NP diffusion in the brain predominantly takes place through the narrow, tortuous space between cells [77]. The ECM, the main component of the extracellular space, imposes an adhesive and steric barrier to the movement of NP through the brain parenchyma. Non-specific electrostatic interactions with the abundant negative charges of the ECM hinder the diffusion of poorly-shielded cationic polymer-based gene vectors [79, 97], as shown with DNA-UPN (uncoated) and DNA-CPN (less densely coated) in this study. Hence, rapid brain penetration of DNA-BPN is most likely attributed to the efficient shielding of the positive surface charge intrinsic to the cationic polymer-based gene vectors. Moreover, the dense surface PEG coating achieved by blending highly PEG-conjugated polymer with unmodified polymer allows DNA-BPN to retain their compact sub-100 nm size in physiological conditions (i.e. CSF) required to move through the pores in the ECM without being hindered by steric obstruction. In comparison, the loose compaction, lack of stability and the tendency towards aggregation of conventionally PEGylated cationic particles, including DNA-CPN, does not allow for efficient penetration through the large proportion of ECM pores that are smaller than 200 nm in diameter [2, 26]. These results demonstrate the importance of designing gene vectors capable of overcoming both the adhesive interactions and steric hindrance imposed by the brain ECM.

CED has been applied to further enhance the distribution of locally administered therapeutics. However, CED of non-PEGylated liposomal non-viral gene vectors for the treatment of unresectable or recurrent glioblastoma has demonstrated limited success in a phase I/II clinical trial. Voges et al. underlined the fact that, even following CED, the heterogeneous ECM can act as a barrier, hence limiting the spatial distribution of gene vectors [25, 98]. Namely, the physicochemical characteristics of gene vectors leading to adhesive and/or steric interactions with the brain parenchyma significantly impact their flow through brain tissue [20, 26]. Previous studies have reported that cationic charge, even if shielded, greatly restricts the convection of NP away from the point of administration [26, 94]. Here, we demonstrate that the diffusion of DNA-BPN in the brain parenchyma translates to enhanced distribution of gene vectors *in vivo* and, therefore, widespread transgene expression throughout the brain when administered using CED. It should be noted that a high density surface coating is required to achieve improved CED-facilitated distribution of gene vectors; the insufficiently shielded DNA-CPN were unable to escape the injection site and failed to mediate enhanced distribution of transgene expression compared to unshielded DNA-UPN following CED.

PEGylation as a stealth coating strategy has previously been shown to decrease cell uptake, endosome escape and subsequent transgene expression [99, 100]. However, we found that PEGylation of cationic polymer-based gene vectors did not decrease entry in primary astrocytes (rat, rabbit) or 9L glioma, as demonstrated in previous reports [101, 102], but led to significantly lower transfection efficacy *in vitro* [103, 104]. The increased stability of DNA-BPN may decrease *in vitro* transfection efficiency by hindering DNA unpackaging, and the conjugation of PEG to primary amines may reduce the buffering capacity and subsequent endosome escape by the PEI-based vectors [103, 105]. Regardless, CED administration of DNA-BPN resulted in double the total amount of *in vivo* transgene expression in comparison to DNA-UPN and DNA-CPN, suggesting that the ability of DNA-BPN to maintain small size and reach and transfect cells over a larger area of the striatum more than offsets the inferior intracellular delivery capacity often observed with PEG-coated gene vectors.

Although cationic polymer-based gene vector have been safely tested in clinical trials [106], their possible cytotoxicity remains a concern [90, 92]. In good agreement with previous observations [90, 107, 108], conventional PEGylation (i.e. DNA-CPN) was not sufficient to significantly improve the *in vitro* safety profile of cationic polymer-based gene vectors. However, we demonstrated that the dense PEG coatings achieved using our polymer blending approach significantly decreased the toxicity of PEI-based gene vectors. DNA-BPN was associated with a favorable safety profile, similar to the widely used PEG-PLL NP system shown to be safe in animal brain [109, 110] and lung [111, 112], as well as the human airways [113]. The reduced toxicity of DNA-BPN *in vivo* in combination with the widespread distribution in the brain when administered by CED overcomes important limitations of conventional cationic polymer-based gene vectors.

5.5. Conclusion

Non-viral gene vectors have emerged as a promising platform for the treatment of CNS diseases. However, achieving high spatial distribution of therapeutically relevant transgene expression remains a challenge. In this study, we describe a strategy for designing cationic polymer-based gene vectors that can penetrate through the brain parenchyma, leading to enhanced vector distribution throughout the entire striatum following CED. This strategy can be adapted to a variety of cationic polymers with different attributes that may further enhance gene transfer to the brain [82]. The combination of the DNA-BPN gene vector technology with plasmids encoding for sustained or selective expression can further enhance the transfection profile of DNA-BPN [110, 114]. The combined result of high-level and widespread transgene expression achieved with DNA-BPN has promise for improving the therapeutic efficacy of gene-based treatments for CNS diseases.

Table 5.1: Physicochemical properties and diffusivity of gene vectors in rodent cortical tissue.

	PEG/PEI w/w[a]	Hydrodynamic Diameter ± SEM (nm)[b]	ζ-potential ± SEM (mV)[b]	PDI[b]	Hydrodynamic Diameter in ACSF[c]	$\mathrm{MSD_{AQ}/MSD_{Brain}}$[d]
DNA-UPN	0	47 ± 2	26 ± 1.2	0.15	1071 ± 53	6900
DNA-CPN	1.6	59 ± 1	9.3 ± 0.5	0.17	193 ± 4	930
DNA-BPN	3.9	43 ± 5	2.9 ± 0.3	0.19	80 ± 9	260

[a] PEG/PEI weight to weight ratio used to formulate respective NP.

[b] Size, ζ-potential and polydispersity (PDI) were measured by dynamic light scattering (DLS) in 10 mM NaCl at pH 7.0 and are presented as an average of at least 3 measurements ± standard error of the mean (SEM).

[c] Hydrodynamic diameter in aCSF was measured by DLS following incubation in aCSF at 37 °C for 1 h.

[d] MSD at 1 s was measured using MPT of fluorescently labeled gene vectors in rodent brain slice. NP diffusivity in aCSF was calculated using the Stokes-Einstein equation and the mean particle diameter.

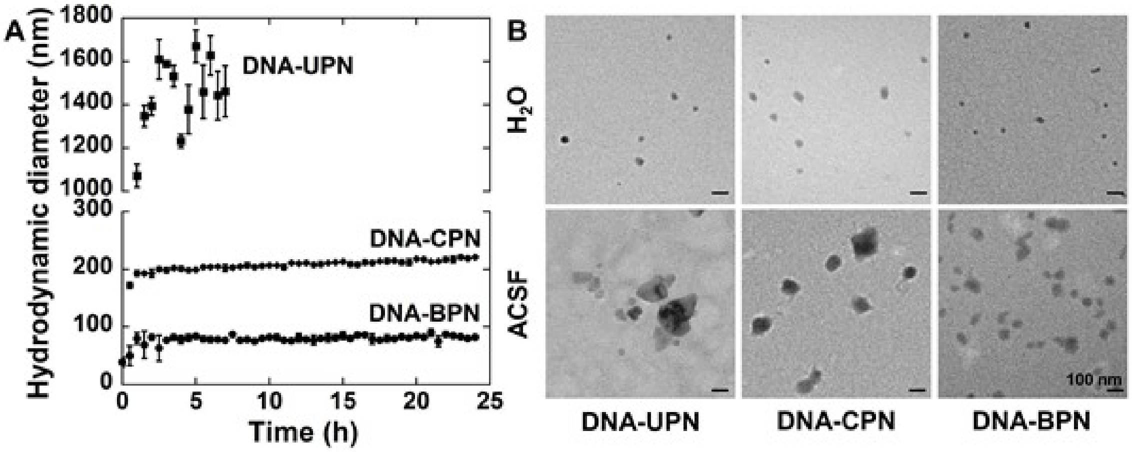

Figure 5.1: Gene vector stability (A) Gene vector hydrodynamic diameter in aCSF at 37 °C was measured by dynamic light scattering (DLS). Measurements were taken every half an hour up to 24 hours or until polydispersity (PDI) > 0.5. Data represents the mean ± SEM. (B) Transmission electron microscopy images of gene vectors in ultrapure water (top panel) and following 1 h incubation in aCSF at 37 °C (bottom panel).

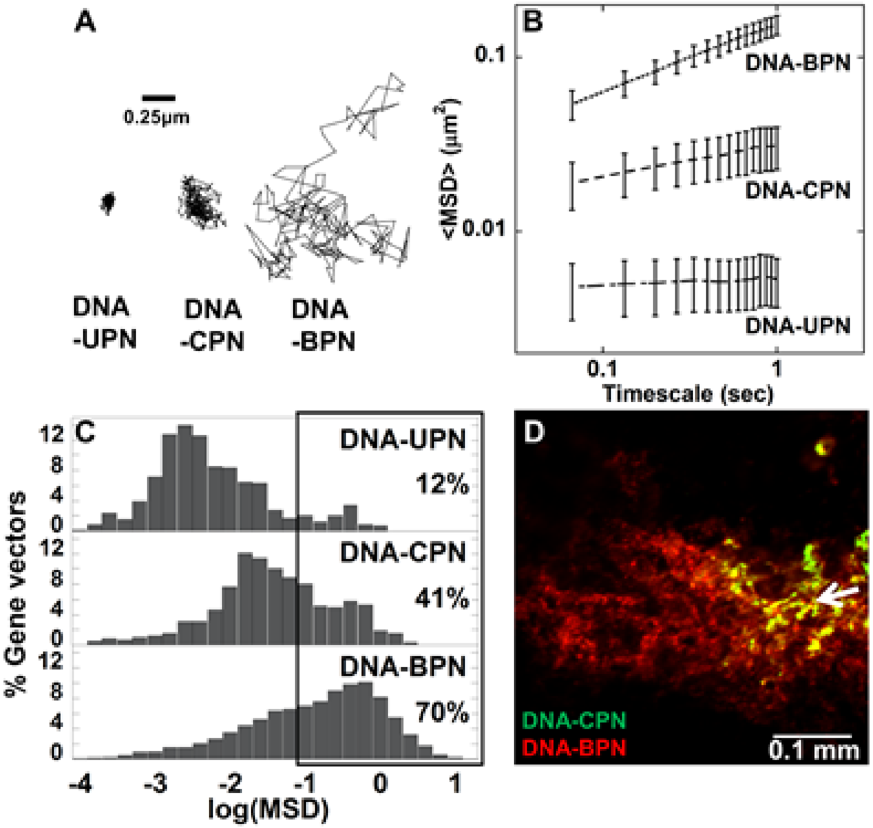

Figure 5.2: Gene vector penetration of rodent brain tissue (A) Representative particle trajectories over 20 s in *ex vivo* rodent brain tissue. Trajectories shown are of particles that had an MSD equal to the ensemble average at a time scale of 1 s. Scale bar = 0.25 µm (B) Ensemble-averaged geometric mean of MSD of PEI-based gene vectors as a function of time. Data represent the ensemble average of at least three independent experiments, with n ≥ 500 particles tracked for each experiment. (C) Histograms of individual MSD of respective gene vectors from at least three independent experiments at a timescale of $\tau = 1$ s. (D) *In vivo* spread of Cy5- labeled DNA-CPN (Green) and Cy3-labeled DNA-BPN (Red) following bolus co-injection in the striatum. Scale bar = 100 µm. Co-localization of DNA-BPN and DNA-CPN in each image is represented as yellow. White arrow demonstrates point of injection.

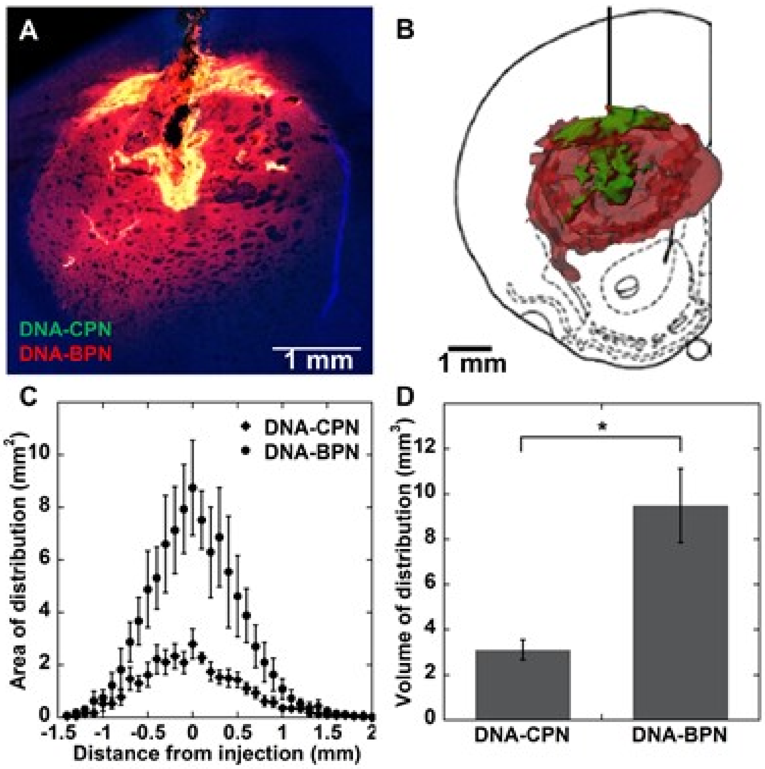

Figure 5.3: ***In vivo* distribution of PEI-based gene vectors following CED** (A) Representative distribution of labeled Cy3 DNA-CPN (green) and Cy5 DNA-BPN (red) in rat striatum using confocal microscopy; DAPI staining for cell nuclei (blue). Colocalization of DNA-BPN and DNA-CPN in each image represented as yellow. Scale bar 1 mm. (B) Representative 3D reconstruction of labeled Cy3 DNA-CPN (green) and Cy5 DNA-BPN (red) distribution in the rat striatum following CED. (C) Image-based MATLAB quantification of area of distribution of PEI-based NP as a function of distance from the injection site (n = 6). (D) Summated image-based MATLAB quantification of volume of distribution for DNA-BPN and DNA-CPN (n = 6). * Denotes statistical significance $p < 0.05$.

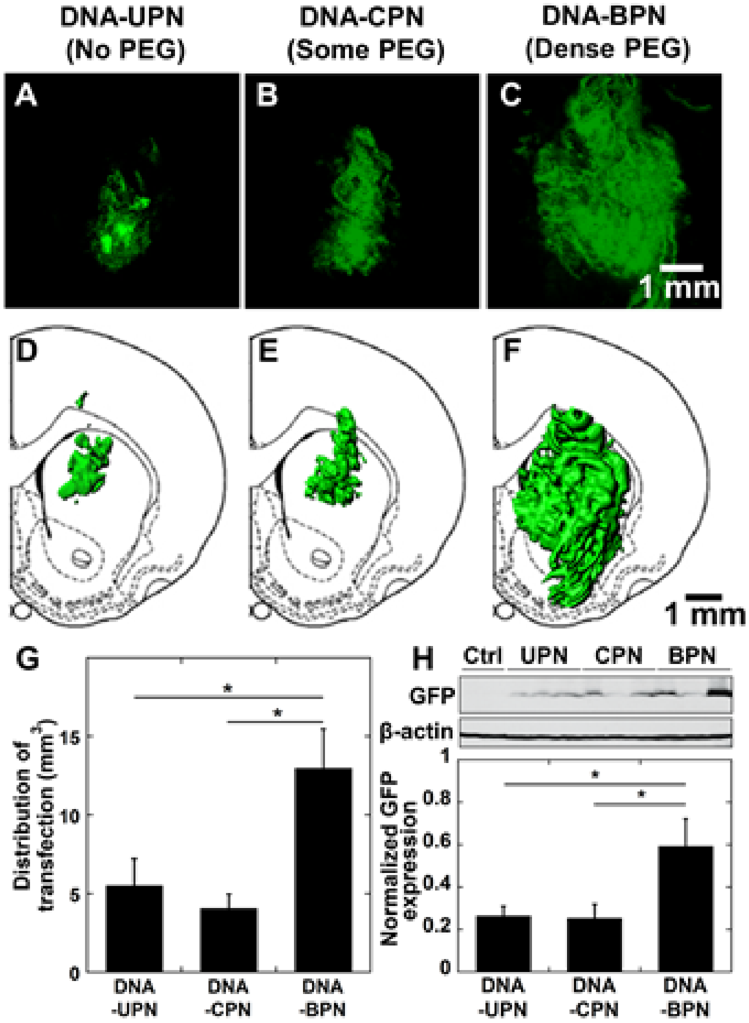

Figure 5.4: ***In vivo*** **distribution and overall level of eGFP transgene expression following CED of various PEI-based gene vectors carrying eGFP plasmid DNA** (A-C) Representative stacked and aligned confocal images of eGFP expression (Green) following administration of the respective PEI-based gene vectors in the rodent caudate putamen. Scale bar = 1mm. (D-F) Isosurface 3D re-construction of distribution of *in vivo* eGFP expression using multiple sequential confocal fluorescence images of respective PEI-based gene vectors. (G) Image-based MATLAB quantification of volume of distribution of eGFP expression $*p < 0.05$ (n = 4-6). (H) Transgene expression following NP CED administration in rodent striatum. eGFP expression was analyzed using Western blot. The band quantification was performed using Multi Gauge software (Fujifilm). The expression level of eGFP was normalized with β-actin. Data represents the mean ± SEM. * Denotes statistical significance $p < 0.05$.

6. THERAPEUTIC BRAIN-PENETRATING CISPLATIN NANOPARTICLES REDUCE TOXICITY AND IMPROVE EFFICACY AGAINST MALIGNANT GLIOMA

6.1. Introduction

The introduction of orally administered temozolomide (TMZ), the current chemotherapeutic of choice for treatment of GBM, has resulted in only minor improvements in patient survival, despite its relative ability to cross the blood brain barrier (BBB) [4, 13]. The effectiveness of TMZ is diminished due to its rapid degradation in physiological conditions, low potency as an alkylating agent and development of tumor resistance [13, 15, 115]. Furthermore, TMZ has dose limiting systemic toxicities in the forms of myelosuppression and lymphopenia [14-16]. For these reasons, current efforts are focused on identifying additional chemotherapeutics that may supplant or be used in combination with TMZ as a treatment for GBM [116].

Cis-diamminedichloroplatinum (Cisplatin, CDDP) is a highly potent anti-cancer drug and has demonstrated success in treating neoplasms such as testicular, ovarian, bladder and lung cancers [117]. Additionally, systemic CDDP has been widely adopted as an adjuvant therapy for several brain tumors in pediatric patients, such as neuroblastoma and medulloblastoma [118]. However, adult GBM clinical trials that employ systemic administration of CDDP have demonstrated limited success due to the high occurrence of nephrotoxicity and neurotoxicity manifesting even at sub-therapeutic levels [119-122]. Thus, clinical trials for GBM have administered alternative platinum agents (i.e. carboplatin) that exhibit reduced toxicities but are also less efficacious [123]. If the toxicity manifestations that are associated with CDDP can be effectively managed, then it may be a highly relevant chemotherapeutic for achieving improved therapeutic outcome in patients with GBM.

Local administration of chemotherapeutics is clinically applied as an adjuvant therapy for the treatment of GBM [124], and is an excellent strategy for avoiding off-site toxicities [31]. Intracerebral infusion of CDDP at low doses has been safely conducted in humans to treat malignant glioma [125, 126], but therapeutic benefit has not observed, indicating that higher chemotherapeutic concentrations was required. Recent preclinical studies have achieved promising results following intratumoral administration of CDDP [127, 128] but the local, neurotoxic effects of CDDP remain a significant limitation to direct intracranial administration [128, 129]. Nanotechnology enables the design of drug-delivery platforms that provide controlled release of chemotherapeutics and can lead to simultaneous enhancement of therapeutic efficacy while ensuring safety of the treatment [117, 124]. Combined with local administration, this approach offers the opportunity to achieve sustained therapeutic levels of CDDP in the tumor with reduced off-target effects.

Despite the aforementioned advantages, locally administered drug delivery platforms attain limited efficacy due to their inability to escape from the point of administration and distribute throughout the tumor tissue [32]. As previously stated in this thesis, only NP with diameters smaller than the average mesh-spacing of the brain ECM and shielded with a bio-inert coating are able to diffuse within the brain parenchyma [2]. Rational NP design [2, 130] and convection enhanced delivery (CED) [29, 33], are being investigated to overcome this barrier but only recently have efforts been made to combine both strategies [131]. We have previously shown that when manually administered into the tumor, brain-penetrating nanoparticles (BPN) loaded with paclitaxel were highly effective at delaying the growth rate of an orthotopically implanted rodent gliosarcoma but failed to achieve a substantial improvement in survival [2, 40]. Here, we hypothesize that the intracranial delivery of a CDDP-loaded BPN (CDDP-BPN) combined with CED may provide widespread homogeneous delivery of CDDP throughout the tumor and lead to improved therapeutic efficacy.

We have designed a sub-100 nm poly-aspartic acid (PAA)-based NP that possesses a dense surface layer of polyethylene glycol (PEG) and a high CDDP content that can be released in a sustained manner. This NP is able to diffuse in healthy and tumor rat brain tissue *ex vivo* and demonstrate improved distribution within the brain parenchyma *in vivo*. When manually administered, these BPN delayed the growth rate of a highly aggressive rat glioma as compared to conventionally designed NP. Furthermore, when delivered using CED, these CDDP-BPN significantly extended the survival of orthotopic GBM-bearing rodents. Therefore, administering CDDP-BPN using CED addresses the toxicity limitations of CDDP and represents a promising therapeutic strategy for the treatment of malignant gliomas.

6.2. Materials and Methods

6.2.1. Peptide conjugation, labeling, and NP synthesis

PAA (MW: 27kDa, Alamanda Polymers, Huntsville, AL) was reacted with PEG (MW: 5kDa, Creative PEGworks, Winston Salem, NC) at a 1:10 molar ratio with the addition of 1-Ethyl-3-(3-dimethylaminopropyl) carbodiimide (EDC, Invitrogen, Carlsbad, CA) at stoichiometric concentrations mixed in 50 mM 2-(N-morpholino)ethanesulfonic acid

(MES Buffer, pH 5.0, Sigma Aldrich, St. Louis, MO). The reaction was carried out for 72 h at room temperature followed by dialysis against deionized water using a 20kDa MWCO cassette (Spectrum Lab, Rancho Dominguez, CA) for 120 h. The solution was then lyophilized to obtain the PEG-PAA polypeptide which was then stored at -20°C until use. The PAA:PEG ratio was confirmed through nuclear magnetic resonance (NMR) to be ~1:10. ^{1}H NMR (500 MHz, D_2O): δ 2.70-2.80 (br, $CH\underline{CH_2}COOH$) 3.55-3.75 (br, $\underline{CH_2CH_2}O$), 4.40-4.55 (br, $NH\underline{CH}CH_2$). Immediately prior to NP formulation, the lyophilized polymers were dissolved in ultrapure distilled water.

Fluorescent labeling dye AlexaFluor 555 and AlexaFluor 647 carboxylic acid, succinimidyl ester (AF555 and AF647, Molecular Probes, Eugene, OR) was conjugated to PAA-PEG and PAA polypeptide respectively by dissolving in 200 mM borate buffer (pH 8.2) and reacting for 72 h at room temperature. The solution was dialyzed against deionized water using a 20kDa MWCO cassette (Spectrum Lab) for 120 h followed by lyophilization after which the labeled polypeptide was recovered and stored at -20°C until use.

CDDP-UPN and CDDP-BPN were formulated using the following protocol. For the CDDP-UPN, 7.5 mM of CDDP (Sigma Aldrich) was mixed with 5 mM of aspartic acid in RNAse free water for 72 h at room temperature. For CDDP-BPN, 5 mM of CDDP was mixed with a 5 mM of aspartic acid (9:1 ratio of PEG-PAA:PAA) in RNAse free water for 72 h at room temperature. Particles were then collected using filters (Amicon Ultra, 100kDa MWCO; Millipore, Billerica, MA) by centrifuging at 1000 g for 10 min and stored at room temperature until further use.

6.2.2. Physicochemical characteristics and in vitro release characterization

Physicochemical characteristics of NP were determined using a Zetasizer NanoZS (Malvern Instruments, Southborough, MA). All particles were diluted in 10 mM NaCl (diluted from phosphate buffered saline) and dynamic light scattering was employed to determine the hydrodynamic diameter and PDI at a backscattering angle of 173°. The surface charge (ζ-potential) of the particles was determined through Laser Doppler Anemometry. Quantification of CDDP within the NP was conducted through flameless atomic absorbance spectroscopy (AAS) (Perkin Elmer, Waltham, MA) and loading was calculated as the % mass of CDDP in the total sample. NP imaging was conducted using a Hitachi H7600 transmission electron microscope (TEM, Hitachi, Japan).

To determine CDDP release, CDDP-UPN or CDDP-BPN were dispersed in 1 mL of ACSF (Harvard Apparatus, Holliston, MA) within a 100kDa MWCO dialysis membrane (Spectrum Lab). The chamber was then placed in a 13 mL ACSF sink and shaken at 37°C. At specific timepoints, 1 mL of the sink was removed and replaced with 1 mL of fresh ACSF. Samples were then diluted accordingly in ACSF and quantified using AAS.

6.2.3. Ex vivo NP tracking in healthy and tumor rodent brain tissue

Healthy or tumor rat brain tissue slices were prepared according to a slightly modified protocol of a previously publication [2]. F98 tumor bearing rats were sacrificed 12 days after tumor inoculation ($1x10^5$ cells) to ensure a significantly large tumor bulk for investigation. Healthy or tumor brain tissue was sliced into 1.5 mm thick slices using a Zivic Mouse Brain slicer (Zivic instruments, Pittsburgh, PA) and placed in custom-made microscopy chambers. Half a microliter of fluorescently labeled particles was injected at a depth of 1 mm into the cerebral cortex using a 10 µL Hamilton Neuros Syringe (Hamilton, Reno, NV). The chambers were sealed using a coverslip to minimize convective bulk flow so that particle movement could be fully attributed to Brownian diffusion. The transport rate of particles was calculated by analyzing the particle trajectories in brain tissue slices as described previously [2]. The particle trajectories were recorded as 20 s movies at an exposure of 66 ms using an EMCCD camera (Evolve 512; Photometrics, Tuscon, AZ) mounted on an inverted epifluorescence microscope (Axio Observer D1, Carl Zeiss, Hertfordshire, UK) equipped with a 100x oil-immersion objective. N = 3 rat brain tissue specimens were used for each particle type. MSD of particles were calculated and compared at a time scale of $\tau = 1$ s. Theoretical MSD of NP in ACSF was calculated using theoretical Stokes-Einstein equation and the mean particle diameter calculated through dynamic light scattering.

6.2.4. In vivo NP distribution following manual or CED administration

Fluorescently labeled CDDP-UPN or CDDP-BPN (12 µg of CDDP) were loaded in a 50 µL Hamilton Neuros Syringe (Hamilton) and co-injected at a ratio of 1:1 into the striatum of Male Sprague Dawley Rats weighing 200-220g. A burr hole was drilled 3 mm lateral and 1 mm posterior to the bregma. For a manual injection, the catheter was lowered to a depth of 4.0 mm and raised up 0.5 mm. The NP mixture was manually administered at a rate of 2 µL/min for a total of 10 µL. Catheter was then withdrawn at a rate of 1 mm/min. For CED, the catheter was vertically mounted on a Chemyx Nanojet Injector Module (Chemyx, Stafford, TX), which was held on a small animal stereotactic frame (Stoelting, Wood Dale, Il). The catheter tip was lowered to a depth of 3.5 mm and NP were infused at a rate of 0.33 μL/min followed by catheter withdrawal at a rate of 1 mm/min. Animals were sacrificed 1 h post-administration and the brains were removed and immediately frozen on dry ice. Tissues were cryosectioned (Leica CM 3050S, Leica Biosystems, Buffalo Grove, Il) into 100 μm coronal slices and imaged using a Zeiss confocal 710 laser scanning microscope in the DS Red (AF555, CDDP-UPN), and Cy5 (AF647, CDDP-BPN) channels. As previously conducted [132], brain slice images were quantified for fluorescent distribution of NP within the striatum using a custom MATLAB script which thresholded the images at 10% of the maximum intensity. Fluorescent distribution of NP in the ventricles or white matter tracts (WMT) were avoided and not included in the quantification. The area of distribution calculated from each slice was multiplied by the slice thickness of 100 μm and summated across all images to obtain a total volume of distribution.

6.2.5. CDDP dose escalation for in vivo toxicity

A 10 μL solution of CDDP-FD (12 μg and 24 μg) or CDDP-BPN (12 μg, 24 μg, and 48 μg) was administered intracranially using a manual injection. For 5 days following CDDP administration, the rats were evaluated 3 times a day for physical deficiencies and subsequently once every day. Weights were recorded every other day and rats were sacrificed when necessary due to clinical presentation of symptoms. The study was terminated 30 days after CDDP administration.

6.2.6. In vivo F98 tumor inoculation

Female Fischer F344 rats weighing 100-140 g were anesthetized with a mixture of ketamine-xylazine as previously described [133] and inoculated with luminscence expressing F98 glioma cells (1×10^5 cells). Briefly, a sagittal incision was made to expose the skull followed by the drilling of a burr hole 1 mm posterior and 3 mm lateral to the bregma. A 10 μL solution of F98 glioma cells was administered into the striatum at a depth of 3.5 mm. The head was then closed using biodegradable sutures (Polysorb™ Braided Absorbable Sutures 5-0, Covidien, Mundelein, Il) and Bacitracin was applied generously.

6.2.7. In vivo bioluminescence monitoring of tumor progression

Rat weights were measured every other day and optical imaging of the tumor was conducted every 3 days following treatment. Briefly, rats were injected intraperitoneally with 8 mg/mL luciferin (Sigma Aldrich) and were imaged 10 min later. The rats were subjected to a continuous flow of isoflurane and imaged using IVIS optical imaging for the presence of luciferase expressing tumor cells. Monitoring of tumor growth was terminated when the first normal saline treated rat was sacrificed due to clinical symptoms attributed to tumor progression.

6.2.8. Treatment of F98 glioma-bearing rodents

At the predetermined days post-inoculation, rats were randomized into treatment groups. The burr hole was re-accessed and 10 μL of the therapeutic solution (12 μg of CDDP) was administered intracranially at the same coordinates. Animals were returned to their cages and continuously monitored for deficiencies. For animals undergoing radiotherapy, rodents were anesthetized and a focused radiation beam (2 Gy/min for a total of 15 Gy) was administered on the ipsilateral hemisphere where the tumor was implanted.

6.2.8. Efficacy involving human xenograft GBM

On Day 0, nude mice were inoculated with 10^5 luciferase expressing GBM-1 human xenograft cells in collaboration with Dr. Eberhart's lab. The striatum was similarly targeted in mice (as was conducted in rats) at the following coordinates: 0 mm anterior/posterior and 2 mm lateral to bregma. Syringe was lowered to 2.5 mm prior to administration of the tumor cell solution (2 µL).Tumors were allowed to grow for 30 days and tumors were luminescently imaged to confirm establishment of GBM-1 xenografts. Briefly, animals were injected intraperitoneally with 15 mg/mL luciferin and 8 minutes later, imaged using IVIS optical imaging. Animals were randomized into two treatment groups. On Day 31, the burr hole was accessed in the animals that were to be treated with CDDP-BPN. 2 µL of a 0.9 mg/mL CDDP-BPN solution was administered at a rate of 0.2 uL/min at the same coordinates as before. The animal's heads were sutured, bacitracin was generously applied on the wound, and mice were returned to their cages.

6.2.10. Monitoring of animal survival

Animals were monitored for deficiencies daily and weighed every other day. Animals were sacrificed when deemed humanely necessary in a blinded manner according to John's Hopkins Animal Care and Use policy.

6.2.11. Statistical analysis

Statistical significance testing between two groups was conducted using a two-sample t-test. Significance was considered at $p < 0.05$. Comparisons between more than two groups included a one-way ANOVA test followed by a Games Howell test. Kaplan Meier analysis was conducted using a Log-Rank test. Statistical significance was considered at $p < 0.05$.

6.3. Results

6.3.1. NP characterization

We engineered conventional un-PEGylated CDDP NPs (CDDP-UPN) and highly PEGylated CDDP-BPN with diameters smaller than the brain pore size [2] (Table 6.1). CDDP-BPN was uniformly formed with low polydispersity index (PDI) (0.11 ± 0.02) and near neutral surface charge as indicated by ζ-potential (-8.6 ± 1.1 mV), whereas the similarly sized CDDP-UPN exhibited higher PDI (0.2 ± 0.01) and highly anionic surface charge (-35 ± 2.0 mV) as expected from the carboxyl side groups of PAA. Both NP formulations were spherical in shape (Figure 6.1A, B) and were able to encapsulate a high concentration of CDDP (w/w) with a higher drug quantity loaded in a CDDP-BPN (19.5 ± 1.4%) as compared to the CDDP-UPN (9.5 ± 1.6%) (Table 6.1). Controlled, linear CDDP release kinetics were observed with both formulations over the course of 24 h in artificial cerebrospinal fluid (ACSF) (Figure 6.1C).

6.3.2. Ex vivo diffusion of CDDP-NP in brain tissue

To determine whether the densely PEGylated NP can diffuse within the tissue parenchyma, we administered fluorescently labeled CDDP-UPN and CDDP-BPN formulations in freshly excised healthy rat brain or rat tumor tissues, tracked the individual particle trajectories, and quantified their mean square displacements (MSD). In healthy rat brain tissue, the dense surface PEG coating significantly improved the ability of CDDP-BPN to rapidly diffuse within the rat brain parenchyma. Representative NP trajectories over 20 s demonstrated unhindered diffusion of CDDP-BPN that traversed over greater distances compared to CDDP-UPN (Figure 6.2A, C). We quantified the MSD using multiple particle tracking (MPT). At a timescale of $\tau = 1$ s, the ensemble-averaged MSD (<MSD>) of the CDDP-UPN was 17,100-fold lower in healthy rat brain tissue than in ACSF, as opposed to the <MSD> of CDDP-BPN, which was only 285-fold lower (Table 6.1). Therefore, CDDP-BPN were able to diffuse 60-fold faster than CDDP-UPN in healthy rat brain tissue. We similarly characterized *ex vivo* NP diffusion in F98 tumor tissue through MPT (Figure 6.2B, D) and found that at $\tau = 1$ s, the <MSD> of CDDP-BPN was only 115-fold slower than in ACSF whereas CDDP-UPN was 1,000-fold slower than in ACSF (Table 6.1), corresponding to a 9-fold difference between NP types ($p < 0.05$) (Figure 6.2D).

6.3.3. Improved in vivo distribution of CDDP-BPN when administered with CED

To verify our *ex vivo* findings, we manually co-administered fluorescently labeled CDDP-BPN and CDDP-UPN *in vivo* into the rat striatum and investigated the respective NP volume of distribution (Vd). When manually administered, the Vd of CDDP-BPN in the striatum is improved 14-fold as compared to Vd of CDDP-UPN (Figure 6.3A, C). We further co-administered CDDP-BPN and CDDP-UPN using CED to determine whether the pressure-driven flow could improve NP Vd. CDDP-BPN achieved homogeneous distribution throughout the striatum (Figure 6.3B, C) with a 6.5-fold enhancement in Vd as compared to its administration using a manual injection (Figure 6.3C). Similarly, the Vd of CDDP-UPN was also enhanced, albeit only by a factor of 3. Thus, this corresponds to a 29-fold higher Vd of CDDP-BPN than CDDP-UPN when both are administered using CED (Figure 6.3C).

6.3.4. CDDP-BPN significantly improves CDDP therapeutic index

Given that CDDP-FD is highly toxic when administered into the brain [129], we next evaluated whether the controlled release of CDDP from BPN provided an improved safety profile following intracranial administration. Healthy rats were treated with a manual administration of either CDDP-FD or CDDP-BPN at different CDDP doses administered in 10 μL. Rats treated with CDDP-BPN at doses of 12 μg (100% survival) and 24 μg (80% survival) fared better than those treated with CDDP-FD at those same doses (47% survival and 23% survival, respectively) (Figure 6.4A). Furthermore, 40% of rats treated with 48 μg CDDP-BPN were long-term survivors, representing an improvement in CDDP tolerability over those treated with CDDP-FD at half that dose. Of note, a dose of 48 μg of CDDP-FD could not be tested due to the limited solubility of CDDP in water. We similarly utilized CED to administer CDDP-FD at 12 μg (60% survival) and CDDP-BPN at 12 μg (100% survival) and 24 μg (80% survival), demonstrating that the difference in manual and CED administration did not yield differences in animal tolerability to CDDP. Thus, the CDDP-BPN formulation enables the administration of higher CDDP doses provided that the dose is well tolerated. Prior studies have safely administered 6 μg of CDDP-FD intracranially [129]. We found that the maximum tolerable dose (MTD) of intracranially administered CDDP when delivered in CDDP-BPN is 2-fold higher at 12 μg (Figure 6.4A, B).

6.3.5. CDDP-BPN delays tumor progression following manual administration

We next evaluated the ability of CDDP-BPN (12 μg of CDDP) to delay tumor growth rate compared to CDDP-FD, CDDP-UPN, and normal saline (NS) following intracranial administration into rats bearing a high inoculum of orthotopically implanted F98 rat glioma cells. In accordance with our findings in the neurotoxicity study (Figure 6.4 A, B), the CDDP-FD treatment was prohibitive as the majority (>50%) of rats demonstrated seizure-like symptoms within 5 days following the treatment. Continuous monitoring of tumor size through optical imaging of tumor bioluminescence revealed a statistically significant reduction in the rate of tumor growth in the CDDP-BPN treated group on Days 7 and 10 compared to groups treated with saline or CDDP-UPN ($p < 0.05$) (Figure 6.5B, C). The tumor growth rates were similar between the CDDP-UPN and saline-treated groups, suggesting that CDDP-UPN failed to provide a therapeutic benefit. In good agreement with previously documented F98 tumor inoculations [133], saline-treated rats presented with symptoms of significant lethargy and weakness on Day 12 and animals were sacrificed when deemed humanely necessary.

6.3.6. Improved survival of animals treated with CED administered CDDP-BPN

Given that a manual injection of CDDP-BPN achieved significant tumor growth delay, we further evaluated efficacy of CDDP-BPN and CDDP-UPN against F98 glioma when administered using CED. Animals that were treated with saline had a median survival of 28 days whereas manually administered CDDP-UPN and CDDP-BPN achieved a median survival of 37 and 42 days respectively (Figure 6.6B, C). In combination with CED, the therapeutic efficacy of CDDP-UPN did not significantly improve (median = 40 days), although a minor population (30%) exhibited extended survival (greater than 100 days). CDDP-BPN delivered using CED achieved significantly improved survival ($p < 0.05$) as compared to all other treatment groups (Figure 6.6B, C). The majority of animals (80%) remained alive at day 100 and were deemed long-term survivors. No signs of F98 tumor was evident in CED administered CDDP-BPN treated rodents (Figure 6.7).

A second efficacy study was initiated to interrogate the efficacy of CDDP-BPN upon treatment of larger sized tumors. Therefore, we inoculated 10^5 F98 glioma cells and withheld CDDP-BPN treatment until 3 days, 6 days, or 9 days post-inoculation (Figure 6.8A). Regardless of treatment day, animals that received CDDP-BPN exhibited improved survival ($p < 0.05$) as compared to the non-treated group. However, no significant survival differences were observed between animals treated on Day 3, Day 6, and Day 9.

A third efficacy study was conducted to investigate whether the addition of radiotherapy, an essential component in the current treatment regimen for human GBM, could further improve the efficacy of CDDP-BPN. Thus, we inoculated animals with 10^5

F98 glioma cells and treated with CDDP-FD (6 μg) and CDDP-BPN (24 μg) on Day 3, followed by radiotherapy 1 day later. Radiotherapy alone improved the median survival time (MST) to 28 days, a significant improvement as compared to non-treated animals (MST = 20 days). Intriguingly, all 4 treatment groups that received CDDP (either FD or BPN) demonstrated some percentage of cures and there was no statistical significance between these 4 groups. CDDP-FD and CDDP-BPN treated animals exhibited the best survival with 70% and 60% of those animals exhibiting long term survival, respectively. However, the combination of radiotherapy with CDDP-FD and CDDP-BPN appeared to have worsened their outcome.

6.3.7. Efficacy of CDDP-BPN against human xenograft GBM-1 cells

Having observed promising efficacy results using CDDP-BPN against aggressive rodent models of GBM, we next wanted to determine the therapeutic efficacy of this nanoparticle against alternative GBM models (i.e. human xenografts). The GBM-1 *in vivo* model, conducted in collaboration with Dr. Eberhart's group, establishes at a slower rate in comparison to the rodent models of GBM (i.e. F98 and 9L). Thus, we treated 31 days post-inoculation and observed for long term survival. However, both *in vivo* luminescent imaging of tumor size (Figure 6.10b) and overall survival (Figure 6.10c) did not yield improved therapeutic effects of CDDP-BPN treatment as compared to non-treated controls.

6.4. Discussion

Improving the distribution of a chemotherapeutic within the tumor parenchyma following intracranial administration is essential for achieving improved therapeutic outcome [20, 33], but current drug delivery strategies have been unable to effectively address this requirement. For example, small molecule drugs administered directly into the brain fail to distribute as they are rapidly metabolized or eliminated [20] . Conventionally designed NP avoid rapid clearance but they remain largely immobilized within the tumor extracellular space in the immediate vicinity of the point of administration [25, 26]. We methodically engineered CDDP-BPN and tailored its physicochemical characteristics (sub-100 nm, near neutral surface charge) to allow for homogeneous, widespread distribution throughout the tumor parenchyma [2, 20, 27]. These densely PEGylated CDDP-BPN can deliver higher concentrations of the chemotherapeutic in a sustained manner to a larger population of infiltrating tumor cells, thereby leading to decreased rates of glioma recurrence and improved therapeutic outcome.

The effects of PEG coating on the NP surface have been well-documented and shown to provide several benefits including a monodisperse NP population as well as improved particle condensation and stability [99]. In good agreement with prior findings, the inclusion of a high density PEG yielded uniformly small CDDP NP with a near neutral surface charge that can rapidly diffuse through healthy [2] and tumor brain parenchyma [27]. However, effective CDDP complexation into a PAA-based NP is dependent on the number of available carboxyl groups for the formation of coordination bonds [134]. Hence, we anticipated that the conjugation of a large number of PEG chains to the carboxyl groups of PAA would compromise CDDP loading. Following a strategy previously described by our lab to improve NP condensation [135], a minor wt% (10%) of non-PEGylated PAA was incorporated into the CDDP-BPN formulation. This provides additional carboxyl groups that bind with CDDP, thereby improving the CDDP loading without compromising the dense PEG layer on the surface of the NP. A suitable dense PEG layer on the NP surface was further confirmed by the near neutral surface ζ-potential and the ability of the NP to rapidly diffuse *ex vivo* and *in vivo* within rat brain tissues.

CDDP is known for its high anti-tumor potency, but its applicability for treating human GBM has been limited by significant toxicities when locally or systemically administered [117]. Controlling the release kinetics of CDDP has been shown to alleviate its toxicities in a variety of tumor models by preventing the exposure of cytotoxic concentrations to the surrounding healthy tissues [136-139]. Here, both CDDP-UPN and CDDP-BPN formulations exhibited linear release of CDDP over 24 h in ACSF, triggered by the presence of chloride, calcium, and magnesium ions that compete with CDDP for carboxylate coordinate bonds [140]. We found that controlled release of CDDP significantly reduces local neurotoxicity compared to CDDP-FD administration in both healthy and tumor-bearing rats. Thus, CDDP-BPN enables the administration of significantly higher doses of the chemotherapeutic that can further lead to improved therapeutic efficacy. Given that the high incidence of CDDP-associated toxicities has led to the early termination of many clinical trials, the improved safety profile of CDDP when delivered in a BPN represents a significant improvement in the relevance of CDDP as a chemotherapeutic for treating GBM [121, 141].

Local administration of chemotherapeutics has the potential to achieve high concentrations of therapeutics in the tumor and has achieved significant clinical success as demonstrated by the Gliadel® wafer [30, 142], but limited diffusion of the drug from the implantation site has minimized its therapeutic efficacy [143]. Here, we characterized the distribution of CDDP NP using two, well-detailed strategies: 1) manual injection [29] and 2) CED [29, 33]. When administered using a manual injection, CDDP-BPN achieved higher Vd within the rodent striatum as compared to the Vd of conventionally designed CDDP-UPN but a high percentage of CDDP-BPN was found in the WMT, likely due to fluid backflow that resulted from the rapid injection. When administered using CED, CDDP-BPN was able to harness the advantages of the pressure-driven fluid flow provided by CED and achieved more homogeneous and significantly higher Vd within the striatum while minimizing its presence in white matter tracts (WMT). This establishes that both appropriate NP design and method of delivery are important considerations as only the combination of CDDP-BPN delivered using CED significantly enhanced survival of tumor-bearing rodents.

Radiotherapy has been shown to be synergistic in preclinical studies when combined with the platinum chemotherapeutics against orthotopic rodent GBM [127, 144]. Thus, we investigated the combination therapy of CDDP-BPN and CDDP-FD with radiotherapy (XRT) in hopes of further enhancing the survival efficacy of the treatment. In good agreement with previous studies, XRT alone significantly enhanced survival but we found that rodents treated with the combination of CDDP and XRT exhibited far decreased survival efficacy. We believe that toxicities may have come into play as all CDDP treated groups (regardless if radiotherapy was included or not) exhibited early rodent deaths, indicating that the CDDP doses that were administered may have been too high. Thus, the addition of XRT may have further enhanced the toxicities. Future tailoring of the CDDP-FD and CDDP-BPN doses in combination with XRT must be conducted in order to fully understand whether the combination of CDDP-BPN and XRT are synergistic. However, we note that CDDP remains a highly promising treatment as a significant number of animals that survived CDDP-associated toxicities remained alive up to 120 days post-inoculation.

In the clinical setting, CED has been widely employed in clinical trials for intracranial administration of therapeutics following tumor resection of patients diagnosed with high grade gliomas [145-147]. These studies were conducted under the notion that CED can achieve therapeutic distribution up to centimeters away from the administration site [148], but investigational studies following the failure of these clinical trials have revealed that the distribution remains poor and nonhomogeneous [6]. We demonstrate that CED of a CDDP-BPN can achieve widespread distribution within the rodent striatum, which leads to a significantly improved therapeutic outcome, as demonstrated by all 3 of our efficacy studies (Figures 6.6, 6.8, 6.9). Of note, CED of CDDP-UPN or manual administration of CDDP-BPN was not as efficacious as the CED administration of CDDP-BPN, emphasizing the importance of the combination of CED with a BPN. In light of these positive results, we admit that there remain further hurdles to overcome in evaluating this CDDP-BPN technology before clinical applications in humans can be started. Namely, further investigations involving human xenograft tumors as well as larger animal models will be required. Nevertheless, the translational applicability of this CDDP NP platform for treatment of tumors has been established by a similar, peptide-based CDDP NP which has demonstrated promising Phase I/II results and is currently under investigation in a Phase III clinical trial for pancreatic cancer [149]. With our findings to date, we anticipate that local, intratumoral administration of CDDP-BPN using CED may be a promising adjuvant therapy for patients diagnosed with high grade gliomas.

6.5. Conclusion

The development of a CDDP-BPN addresses two major concerns pertaining to the use of CDDP as a chemotherapeutic agent and enables us to harness the potency of CDDP for the treatment of GBM. Namely, administering CDDP-BPN using CED (1) reduces the inherent toxicities associated with CDDP and (2) delivers high concentrations of CDDP throughout the tumor bulk, yielding improved therapeutic efficacy. As a therapeutic platform, we anticipate that CDDP-BPN delivered using CED can be rapidly combined with additional adjuvant therapies such as radiotherapy that may further improve the treatment and outcome of patients with GBM.

Table 6.1: Characterization of the size, ζ-potential, and MSDs of CDDP NP in normal and tumor rat brain tissue compared to their theoretical MSDs in ACSF. Size and ζ-potential were measured in ACSF at pH 7.0. Data are presented as average of at least 3 measurements.

Peptide Carrier	Mean Diameter ± SD (nm)	ζ-potential ± SD (mV)	Polydispersity Index (PDI)	CDDP Loading% (w/w)	MSD_{ACSF}/ MSD_{brain}	MSD_{ACSF}/ MSD_{tumor}
CDDP-UPN	65 ± 3	-35 ± 2	0.20 ± 0.01	9.5 ± 1.6%	17,000	1,000
CDDP-BPN	74 ± 2	-8.6 ± 1.1	0.11 ± 0.02	19.4 ± 1.4%	285	115

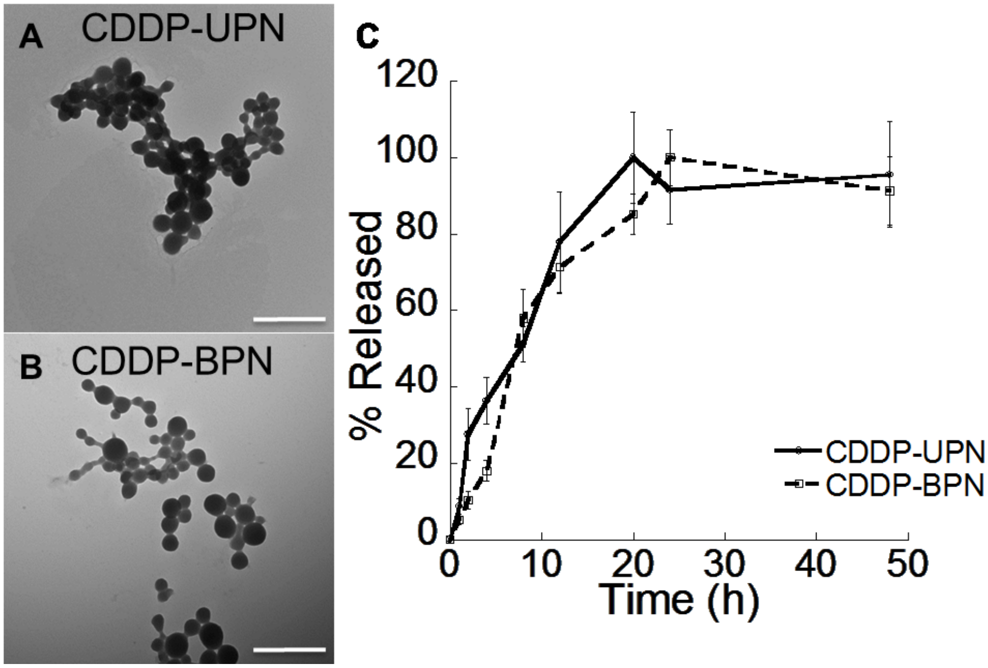

Figure 6.1: *In vitro* characterization of CDDP NP. (A, B) TEM imaging of CDDP-UPN and CDDP-BPN formulations. Scale bar = 500nm. (C) Quantified *in vitro* release kinetics in ACSF (pH 7.0) demonstrating similar, linear release of CDDP from both CDDP-UPN and CDDP-BPN formulations.

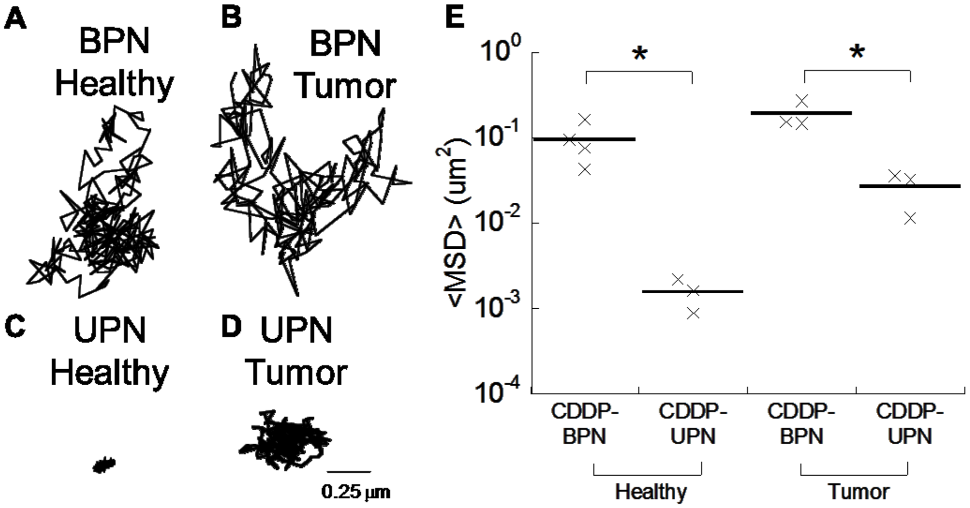

Figure 6.2: Particle diffusion in healthy rodent brain tissue. (A-D) Representative trajectories of (A, B) CDDP-BPN and (C, D) CDDP-UPN in healthy and rodent brain tumor tissue over 20 s of tracking. (E) <MSD> of CDDP-BPN and CDDP-UPN at a timescale of $\tau = 1$ s in at least N=3 *ex vivo* healthy or tumor rodent brain tissue samples. Greater than 100 NP were tracked per sample. * $p < 0.05$ denotes statistically significant differences between groups.

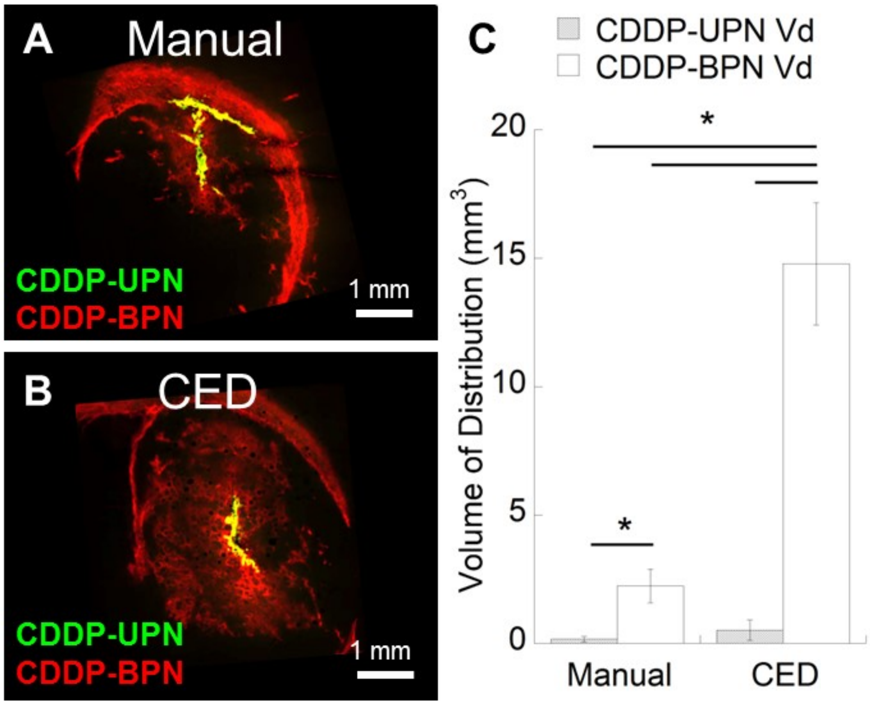

Figure 6.3: Distribution of CDDP-UPN and BPN *in vivo*. (A-B) Representative images of a 10 μL co-administration of CDDP-UPN (green) and CDDP-BPN (red) into the rodent striatum using (A) a manual injection or (B) CED. NP overlay depicted as yellow. N ≥ 3 for each administration. Scale bar = 1 mm. (C) Vd of CDDP-BPN and CDDP-UPN following manual or CED administration. Calculations were conducted using image-based MATLAB quantification. * $p < 0.05$ denotes statistical significance between NP administration groups.

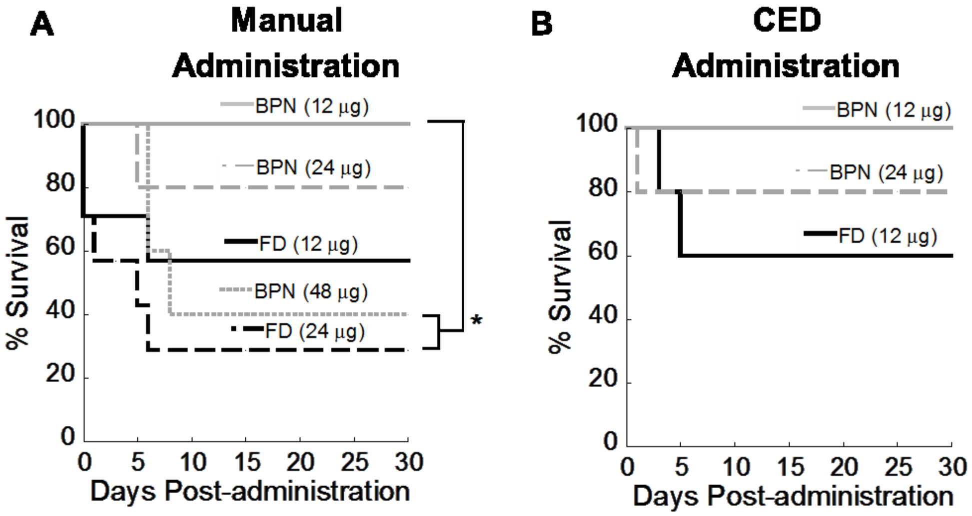

Figure 6.4: *In vivo* CDDP toxicity: (A) Kaplan Meier survival curve of CDDP-FD and CDDP-BPN (N ≥ 5 in each group) administered in healthy rodents using a manual injection. * $p < 0.05$ for both 24 ug FD and 48 ug CDDP-BPN groups as compared to 12 ug CDDP-BPN group that experienced no deaths from the treatment. (B) Kaplan Meier survival curve of CDDP-FD and CDDP-BPN (N = 5 in each group) administered in healthy rodents using CED.

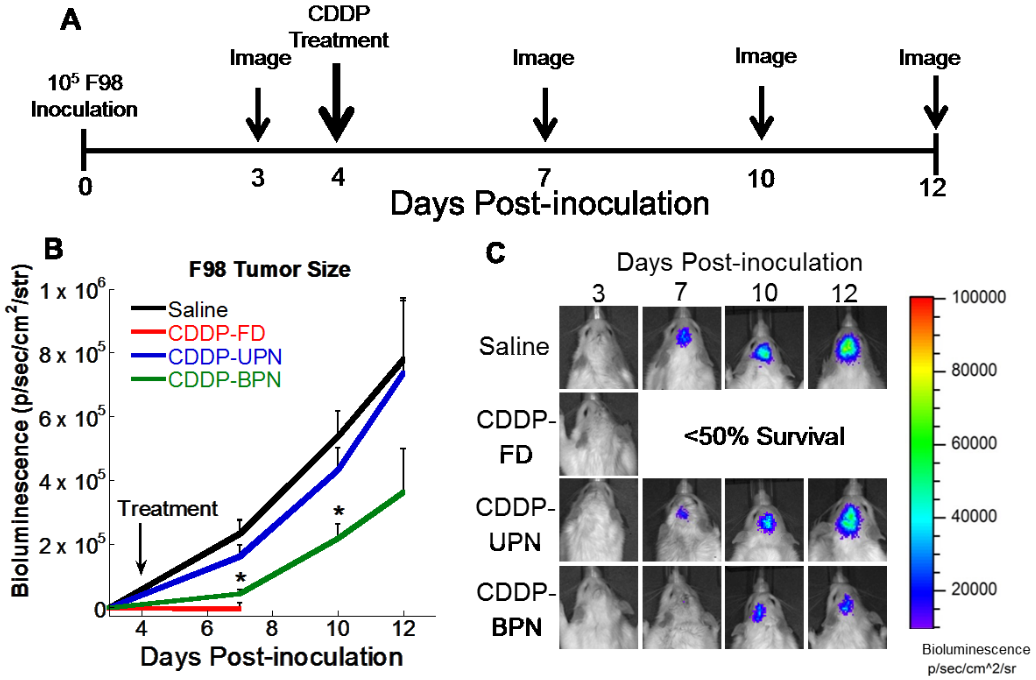

Figure 6.5: *In vivo* tumor growth delay: (A) Tumor inoculation and CDDP treatment scheme for monitoring tumor growth delay. (B) Bioluminescent monitoring of F98 tumor size following a 1x10^5 inoculation. Rodents were treated with 10 µL of Saline, CDDP-FD, CDDP-UPN, or CDDP-BPN. Delayed tumor growth occurred at Day 7 and 10 post-inoculation when rodents were treated with CDDP-BPN. * $p < 0.05$ significance between CDDP-BPN and both Saline/CDDP-UPN groups. (C) Representative bioluminescent expression of F98 glioma in respective treated rodent groups.

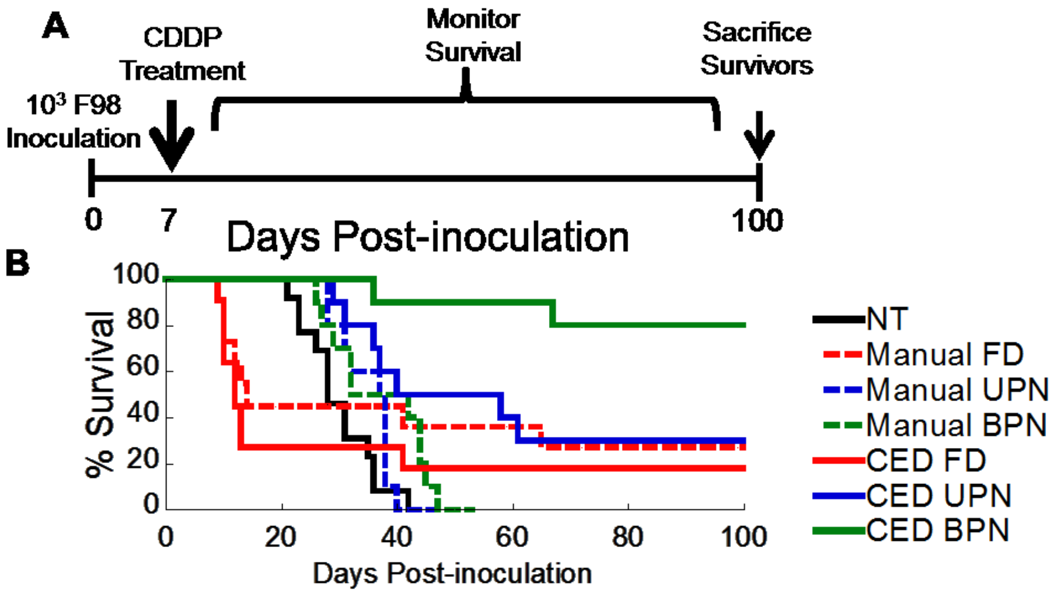

C

Treatment	Rats per group (N)	Survival Time		p-value compared to CED BPN
		Range (days)	Median (days)	
Saline	13	21-42	28	$p < 0.001$
Manual FD	11	9-100$^{\#}$	14	$p = 0.008$
Manual UPN	10	28-40	37	$p < 0.001$
Manual BPN	9	26-47	42	$p < 0.001$
CED FD	11	9-100$^{\#}$	12	$p = 0.001$
CED UPN	10	29-100$^{\#}$	40	$p = 0.019$
CED BPN	10	36-100$^{\#}$	N/A	N/A

Figure 6.6: ***In vivo* survival efficacy**. **(A)** Tumor inoculation and CDDP treatment scheme for investigating long term survival. **(B, C)** Rats inoculated with 10^3 F98 glioma cells were treated on Day 7 following inoculation with 1) Saline, 2) Manual injection of CDDP-FD, 3) Manual injection of CDDP-UPN, 4) Manual injection of CDDP-BPN, 5) CED of CED-FD, 6) CED of CDDP-UPN, and 7) CED of CDDP-BPN. Kaplan Meier survival curve depicts significantly improved ($p < 0.05$) long term survival of the combination of CED administered CDDP-BPN as compared to all other treatment groups. # indicates the presence of long term survivors (greater than 100 days) in the respective treatment groups.

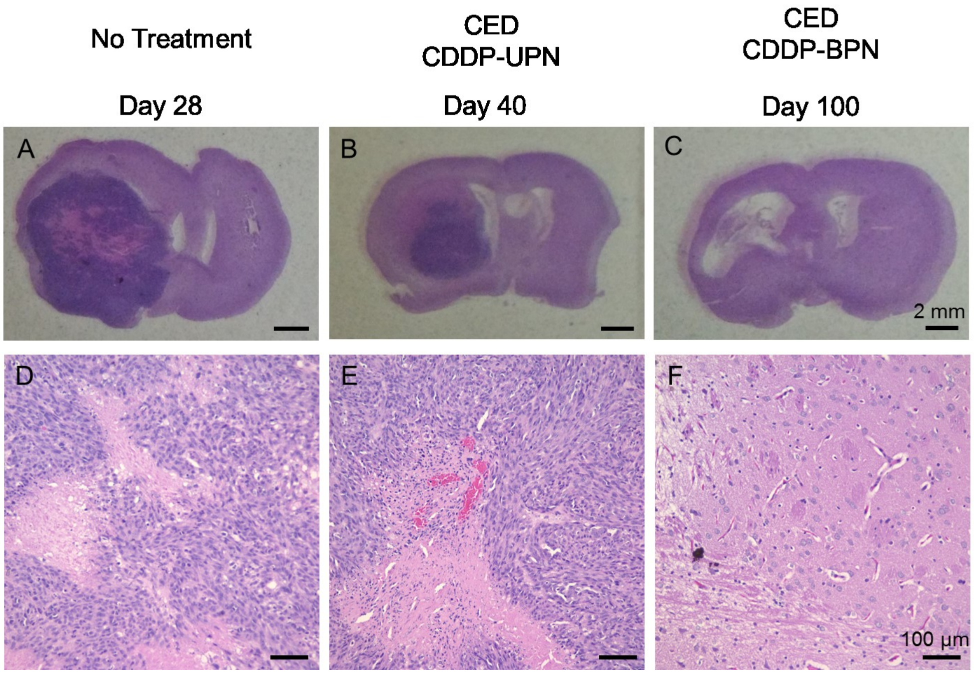

Fig 6.7: Coronal slice of H&E stained rodent brains following tumor inoculation and treatment. At their median survival dates, large F98 tumors are seen in the striatum of (A) non-treated and (B) CED administered CDDP-UPN treated rodents. (D, E) High magnification images illustrate the presence of pseudopalisading fronts and necrotic cores that are characteristic of F98 tumors. (C) On the contrary, CED administered CDDP-BPN treated rodents show no remnants of F98 tumors upon their sacrifice at 100 days following tumor inoculation.

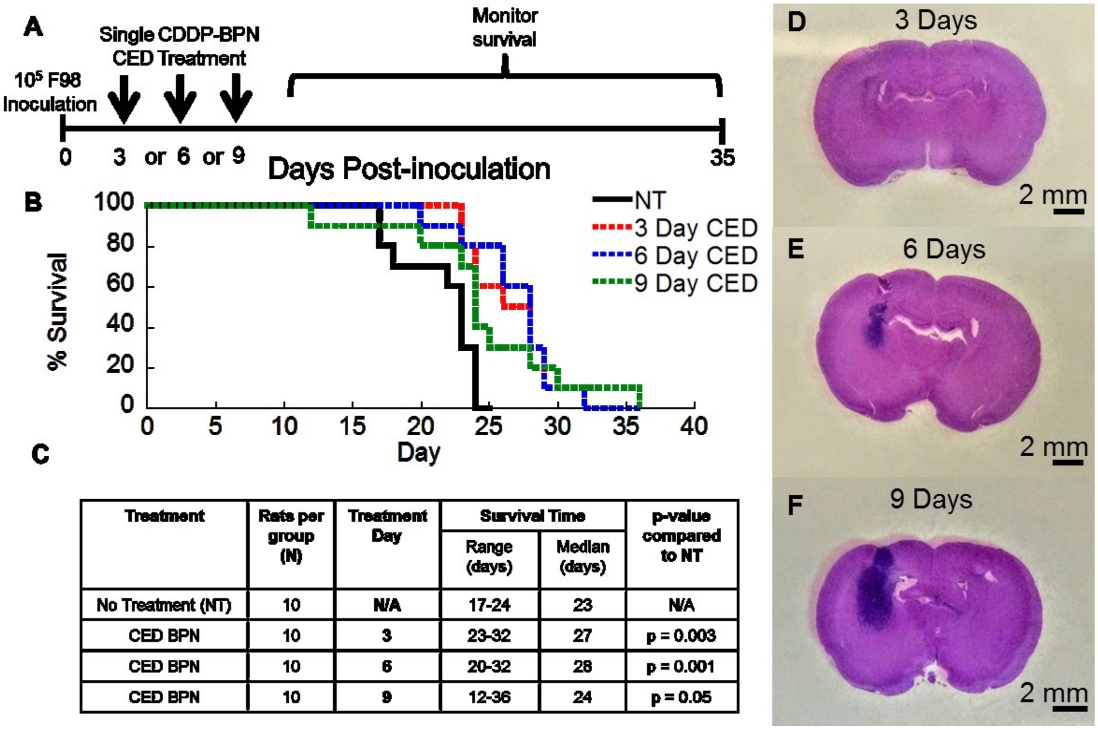

Treatment	Rats per group (N)	Treatment Day	Survival Time		p-value compared to NT
			Range (days)	Median (days)	
No Treatment (NT)	10	N/A	17-24	23	N/A
CED BPN	10	3	23-32	27	p = 0.003
CED BPN	10	6	20-32	28	p = 0.001
CED BPN	10	9	12-36	24	p = 0.05

Fig 6.8: Time dependent efficacy of CDDP-BPN against orthotopic 10^5 inoculation of F98 glioma cells in rats. **(A)** Tumor inoculation and CDDP treatment scheme for investigating long term survival. **(B, C)** F98 glioma bearing rats were treated with CDDP-BPN on Day 3, Day 6, or Day 9 using CED. Kaplan Meier survival curve depicts improved ($p < 0.05$) long term survival of CED administered CDDP-BPN as compared to no treatment. **(C)** Statistics and breakdown of individual treatment conditions. **(D, E, F)** Histological images of F98 glioma tumors on the three different days of treatment.

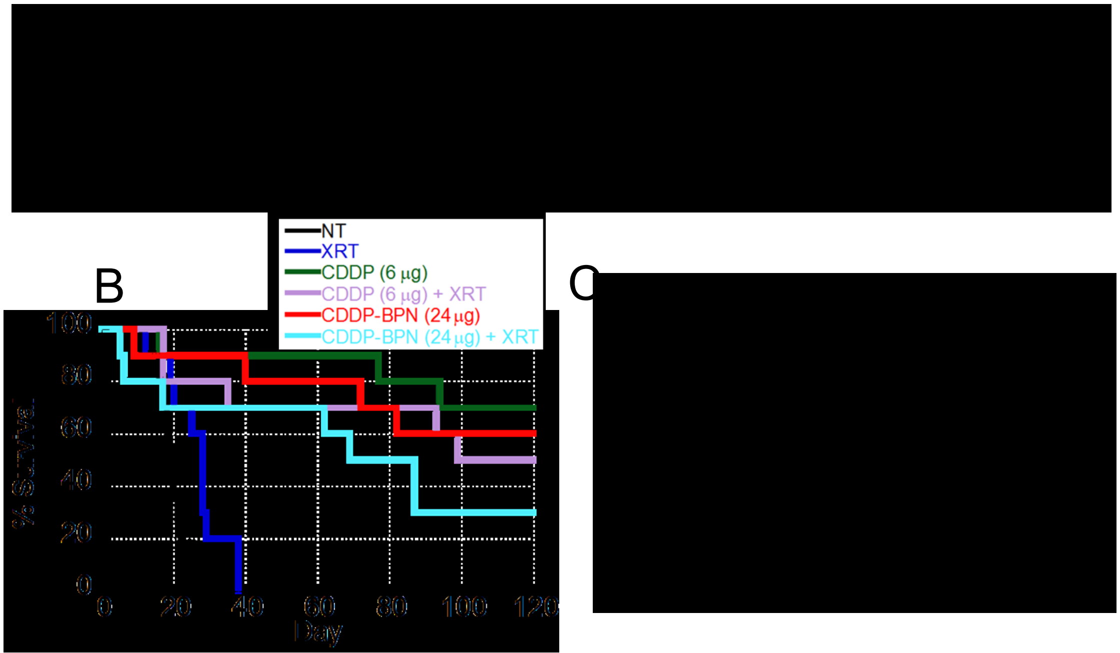

Fig 6.9: Efficacy of CDDP-BPN in combination with radiotherapy against orthotopic 10^5 inoculation of F98 glioma cells in rats. (A) Tumor inoculation and treatment scheme **(B, C)** Kaplan Meier survival curve depicts improved ($p < 0.05$) long term survival of CDDP treated animals (both FD and BPN) as compared to radiotherapy only and no treatment animals. **(C)** Statistics and breakdown of individual treatment conditions.

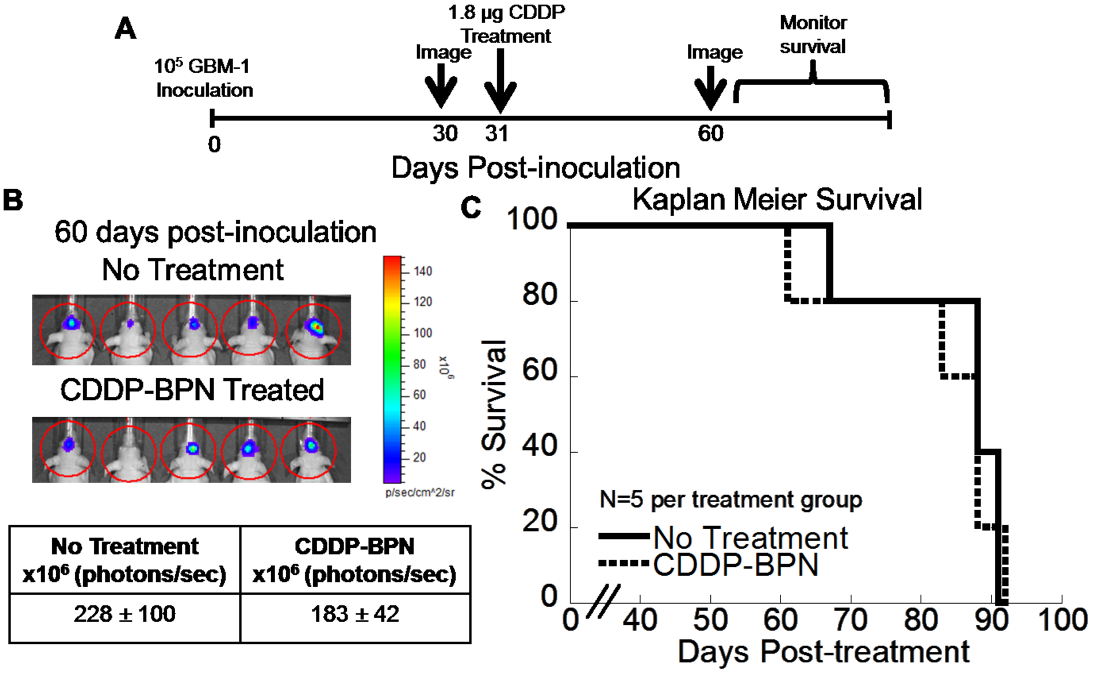

No Treatment x10⁶ (photons/sec)	CDDP-BPN x10⁶ (photons/sec)
228 ± 100	183 ± 42

Fig 6.10: Efficacy of CDDP-BPN against human xenograft GBM. (A) Tumor inoculation and CDDP treatment scheme for investigating long term survival of GBM-1 bearing nude mice. **(B)** Luminescent imaging of GBM-1 cells at day 60 following tumor inoculation. Average luminescence was quantified and no statistically significant difference was observed. **(C)** Kaplan Meier survival curve depicting similar survival of non-treated and CDDP-BPN treated groups

7. IMPROVING CED THROUGH THE ADMINISTRATION OF NON-ADHESIVE NANOPARTICLES IN A HYPEROSMOLAR INFUSATE SOLUTION

7.1. Introduction

CED is an effective delivery strategy to circumvent the blood brain barrier (BBB) and can theoretically achieve widespread NP distribution by harnessing a pressure driven bulk flow [20, 36, 150]. However, recent advances in technological imaging have determined that administering a NP using CED still fails to achieve therapeutically favorable distribution [7]. Intracranially administered NP travel through the brain interstitium, which comprises two distinct spaces: the intercellular space (ICS) and perivascular space (PVS). NP distribution in the ICS is limited by hindrances imposed by the extracellular matrix (ECM) components [2]. Moreover, the preferable flow of NP through, and subsequent confinement within, the low resistance, fluid-filled PVS reduces their ability to reach the target cells [7, 151]. These revelations have shed light on prior terminated CED-based clinical trials that failed to meet their primary and secondary outcomes [5, 152] and have spurred the development of the next generation of NP systems optimized for CED [28, 29].

PVS are cerebrospinal fluid (CSF) filled canals surrounding large brain vessels and are responsible for the clearance of metabolites to maintain homeostasis in the brain [153]. When administered into the brain, NP encounter a higher resistance when traveling through the ICS than through the PVS [154]; therefore, significant quantities of infused NP have been visually confirmed to traffic through PVS [7, 8]. Once localized in the PVS, NP remain sequestered due to the glia limitans, the anatomical barrier that separates the PVS and ICS [155]. More importantly, NP accumulation and entrapment in PVS occurs following all available delivery strategies to the brain, including administrations using intranasal, intracisternal, or intrathecal routes [151, 156, 157]. Given that NP confinement in PVS has been suggested to lead to a reduction in therapeutic efficacy in clinical trials [8, 35], an effective strategy to reduce PVS sequestration is essential.

We propose a delivery strategy that combines the delivery of a well-shielded NP with the osmotic modulation of the brain tissue in order to minimize the hindrances of the brain ECM and preferable NP accumulation in PVS. More specifically, we utilize a previously developed, non-adhesive probe NP [2], and locally administer it in a hyperosmolar, 3% saline infusate solution into the rodent striatum using CED. We demonstrate that these improvements can be extended to a similarly engineered, therapeutically relevant drug nanocarrier. The results gleaned from this mechanistic study may be adapted to improve the clinical relevance of CED and must be further considered in future attempts at therapeutic delivery to the brain.

7.2. Materials and Methods

7.2.1. NP characterization in solutions of varying osmolarities

To test NP stability, the particles were diluted 200-fold in the following infusate solutions: water, saline (0.9%, 3%) and mannitol (10%, 25%) and allowed to incubate for 15 minutes at room temperature. NPs were then sized again using dynamic light scattering to determine hydrodynamic diameters using a Zetasizer NanoZS.

7.2.2. Preparation of ex vivo tissues in solutions of varying osmolarities

The brains from female CF-1 mice were harvested and MPT was conducted on NPs injected into 1.5 mm thick brain slices according to a slightly modified protocol of a previous publication [2]. Briefly, the harvested rodent brain was rinsed in chilled artificial spinal fluid and sliced at 1.5 mm intervals using a Zivic mouse brain mold (Zivic Instruments, Pittsburgh, PA). Individual brain slices were immersed in infusate solutions (water, 0.9% saline, 3% saline, 10% mannitol, or 25% mannitol) for 5 minutes. Brain slices were removed and mounted on a custom made well and 0.5 μL of fluorescently labeled PS-PEG NPs were injected into the cortex. A coverslip was glued on top of the specimen to prevent bulk flow in the tissue.

7.2.3. Multiple particle tracking of PS-PEG NPs in treated ex vivo tissue slices

The particle trajectories were recorded as 20 second movies at an exposure of 66 ms using an EMCCD camera (Evolve 512; Photometrics, Tuscon, AZ) mounted on an inverted epifluorescence microscope (Axio Observer D1, Zeiss; Thornwood, NY) equipped with a 100x oil-immersion objective (N.A., 1.3). NP mean squared displacements (MSD) were calculated based on a custom MATLAB NP tracking code and histograms of particle MSD were determined at a timescale of $\tau = 1$ second.

7.2.4. In vivo CED administration of non-adhesive NPs

When preparing NPs for intracranial CED, stock PS-PEG and PS-COOH were each diluted 25-fold in water, 0.9% saline, 3% saline, 10% mannitol, or 25% mannitol and mixed at a 1:1 ratio for a final concentration of 1 mg/mL. For PLGA and PLGA-PEG, NPs were lyophilized overnight and resuspended at a concentration of 1 mg/mL in 0.9% saline or 3% saline for administration.

Female CF-1 mice weighing 20-30 g in mass were anesthetized with a mixture of ketamine (75 mg/kg) and xylazine (7.5 mg/kg). For mice, a 2 cm sagittal incision was made on the head and a burr hole was made 2 mm lateral to the bregma. All NP solutions or infusate solutions were loaded into a 50 μL Hamilton Neurosyringe with a 33 gauge syringe and set with a 1 mm step (Hamilton, Reno, NV). The syringe was vertically mounted on a Chemyx Nanojet Injector Module (Chemyx, Stafford, TX) which was held on a small animal stereotactic frame (Stoelting, Wood Dale, Il). The loaded syringe was lowered to a depth of 2.5 mm below the mouse dura and a total of 2 μL of the solution was administered over 10 minutes at a rate of 0.2 μL/min. The cannula was allowed to sit for 5 minutes following the completion of infusion and was then withdrawn at a rate of 1 mm/min. The animal was then sutured (Covidien, Mundelein, Il) and placed on a heating pad.

7.2.5. Toxicity of infusate solutions

Following intracranial administration of the various infusate solutions (no NP), CF-1 mice were monitored for adverse signs of toxicity. Mice were sacrificed either 1 hour or 72 hours post-administration. Brains were harvested and fixed in formalin for 24 hours followed by H&E staining analysis conducted by the Johns Hopkins Reference Histology. The injection point was identified by the tissue cavity imparted by the needle and the region immediately adjacent was imaged and evaluated for evidence of toxicity or hemorrhage by a board certified neuropathologist (C.G.E.).

7.2.6. Tissue processing and staining for cellular nuclei or blood vessels

Mice were co-injected with fluorescent dark red PS-PEG and red PS-COOH NPs. Tissues were harvested, post-fixed, and cryosliced at 10 μm thickness at designated intervals from the coronal plane of injection (0 mm, 0.5 mm, 1.0 mm, and 1.5 mm). Tissues were mounted on glass slides and immersed in pepsin solution (Dako, Carpinteria, CA) at 37^{o} C for 10 minutes. Slides were washed 3 times with PBS and blocked with blocking buffer composed of 5% normal goat serum (Sigma Aldrich, St. Louis, MO) and 1% bovine serum albumin (Sigma Aldrich, St. Louis, MO) in PBS for 1 hour at room temperature. Tissue slices were incubated with primary rabbit anti-mouse collagen IV antibody (Abcam ab6586, Cambridge, MA) diluted 1:250 in blocking buffer for 16 hours at 4^{o} C. Tissues were washed 3 times with PBS and incubated with a AF488 labeled goat anti-rabbit secondary antibody (Life Technologies, Grand Island, NY) diluted 1:500 in blocking buffer for 1 hour at room temperature. Tissues were washed 3 times with PBS, and then incubated with DAPI (Life Technologies, Grand Island, NY) at a 1:1000 dilution in PBS for 15 minutes at room temperature. Slides were washed 3 times with PBS and allowed to dry before mounting with Dako fluorescence mounting medium (Dako, Carpinteria, CA).

7.2.7. Image-based quantification of NP distribution

Animals were sacrificed 1 hour post-CED and the brains were fixed in formalin for 24 hours and subsequently exposed to a 10%, 20%, and 30% sucrose gradient. Brains were mounted and cryosectioned at a thickness of 50 μm (Leica Biosystems, Buffalo Grove, II). Distances ± 1.5 mm from the injection site were carefully obtained. Slices were fixed with Dako fluorescence mounting medium (Dako, Carpinteria, CA) and imaged using a Zeiss confocal 710 laser scanning microscope (Zeiss, Jena, Germany) in the GFP and Cy5 channels at 5x magnification. The presence of background fluorescence was determined by comparing to the striatum of the contralateral hemisphere with no injection. Brain slice images were quantified for fluorescent distribution of PS-PEG or PS-COOH NPs by running the confocal laser scanning microscope images through a custom MATLAB script which thresholded the images at 10% of the maximum intensity. Fluorescent distribution of NP in the ventricles or white matter tracts were avoided and not included in the quantification. The area of distribution calculated from each slice was multiplied by the slice thickness of 50 μm and summated across all images to obtain a total volume of distribution. If a slice was lost during cryosection procedure, the area of distribution was taken as the average of the previous and following slices. Rarely was more than 1 slice lost from a brain specimen.

7.2.8. Investigating NP presence in perivascular spaces

Using a Zeiss confocal 710 laser scanning microscope, high resolution images (40x magnification) were taken at the designated intervals away from the main NP bulk and imaged for DAPI, collagen IV, PS-PEG, and PS-COOH. Images were derived from N=3 mice specimen with at least N=3 images per animal. Presence of fluorescent PS-PEG and PS-COOH in PVS and ICS were qualitatively determined in all images. Presence of NP in ECS and ICS were categorized into the following groups: 1) consistent in 100% of images, 2) consistent in 90% of all images, 3) consistent in 80% of all images, and 4) consistent in less than 20% of all images.

7.2.9. Quantifying NP escape from perivascular spaces

The lateral striate arteries in the rodent striatum were visually identified in the imaged slices by identifying elongated and flattened endothelial cells following a DAPI stain (Life Technologies, Grand Island, NY). Co-staining these endothelial cells with blood vessel basement membrane (Collagen IV) confirmed their lining of the striate artery. High resolution images using a Zeiss confocal 710 laser scanning microscope (40x magnification) were taken of PS-PEG and PS-COOH in the striate artery. To determine the extent of NP escape from PVS, images were processed through a custom MATLAB script. A line was drawn parallel along DAPI-stained endothelial cells that defined the striate artery. Fluorescent NPs intensities were averaged at 10 μm intervals up to 100 μm away from the striate artery. At least N=3 striate artery vessels were quantified in each condition. The percent NP coverage within the parenchymal ICS on each high resolution image (40x magnification) was calculated by using the custom MATLAB quantification script which thresholded the images at 10% of the maximum intensity. Flattened, DAPI-stained endothelial cells that line the striate artery were used to delineate the PVS and the ICS and only detectable fluorescence throughout the ICS was quantified. At least N=3 striate artery images were quantified for each condition.

7.2.10. Statistical analysis

Statistical testing between two groups were conducted using a two sample student t-test. If statistical comparisons involved more than two groups, testing was conducted with SPSS 18.0 software (IBM Inc.) using one-way ANOVA followed by Tukey honestly significant difference. Differences for t-test, ANOVA, and Tukey tests were considered statistically significant at $p < 0.05$.

7.3. Results and Discussion

7.3.1. Physicochemical characterization of NPs in varying solutions

To determine the optimal infusate solution, the stability of PS-PEG and PS-COOH NPs were first characterized to ensure that the solution does not significantly impact their physicochemical characteristics or lead to aggregation. The sizes of both NPs remained unchanged in water and normal saline solutions. PS-COOH NPs aggregated in 3% saline concentrations and form substantially larger complexes, whereas PS-PEG NPs remained stable (Table 7.1). Both PS-PEG and PS-COOH NPs increased in size when immersed in higher mannitol concentration solutions (Table 7.1).

7.3.2. Ex vivo NP diffusion in treated brain tissues

For non-adhesive NP that are shielded from adhesive interactions with the brain ECM, the steric obstruction imposed by the ECM components constitutes the main limitation to efficient NP distribution [2, 77]. To overcome this barrier, prior studies have modulated the brain tissue to enlarge the pore sizes of the brain ECM and enhance therapeutic distribution [158-161]. Nicholson and coworkers have previously demonstrated that exposure of brain tissues to modestly hyperosmolar solutions (500 mOsmol/kg) increases the volume of ICS and minimizes the tissue's cumulative resistance to NP diffusion [162]. Here, we sought to alter the pore sizes of the brain ECM by administering well-shielded NP in infusate solutions of varying osmolarities. We selected hyperosmolar saline and mannitol solutions given that they have both been administered in clinical settings for reducing elevated intracranial pressure [163]. Furthermore, mannitol has been extensively investigated as a hyperosmolar infusate solution for CED of therapeutics in preclinical studies [158, 161, 164]. All infusate solutions were deemed safe following histological analysis of H&E stained mouse brains by a board-certified neuropathologist (Figure 7.1).

To determine the changes in ECM pore sizes following exposure of the brain microenvironment to solutions of different osmolarities, we probed the pore sizes of the brain by using a previously established *ex vivo* technique [2, 19]. Of note, we ensured that the PS-PEG physicochemical characteristics were unaffected in the infusate solutions (Table 1) in order to accurately assess the effect of osmolarity on ECM pore size. Specifically, we incubated brain slices in hypo-osmolar water, iso-osmolar 0.9% saline, or hyperosmolar 3% saline and used MPT to quantify the diffusion of non-adhesive PS-PEG probes [2]. At a timescale of 1 second, brain slices treated with hyperosmolar 3% saline yielded 1.5-fold higher NP MSD compared to brain slices incubated in normal saline (Figure 7.2A). This indicates that water drawn into ICS via the osmotic gradient generated by hyperosmolar saline has enlarged the ECM mesh spacing [159, 162], thereby reducing the steric hindrances imposed on PS-PEG traveling within the brain ICS. On the contrary, brain slice treatment with hypo-osmolar water solution yielded 2-

fold lower MSD values (Figure 7.2A). This reduced PS-PEG diffusivity is due to an increase in steric hindrances resulting from the engorging of cellular structures driven by water intake and subsequent reduction of ICS [159].

7.3.3. Improved NP distribution when administered in hyperosmolar saline solutions

To verify that the osmotic modulation of ICS observed *ex vivo* translates *in vivo, w*e administered NP using CED in saline infusate solutions with varying osmolarities and determined their effect on the Vd of NP. We discovered that the Vd of non-adhesive PS-PEG was positively correlated with the osmolarity of the infusate solution. However, higher osmolarity solutions did not significantly affect the Vd of PS-COOH (Figure 7.2B, C). This indicates that even when steric hindrances were minimized, adhesive interactions remained a dominating limitation for conventional NP. In fact, when infused in iso-osmolar and hyperosmolar solutions, Vd of PS-PEG was 5.8-fold and 6.8-fold higher than that of PS-COOH, respectively. In contrast, the Vd of PS-PEG and PS-COOH were not significantly different when hypo-osmolar water was used as an infusate solution, suggesting that the elevated steric hindrances stemming from a reduction in ECM pore sizes serve as the dominant limitation to NP distribution. These observations emphasize the importance of simultaneously minimizing adhesive interactions and steric hindrances in order to maximize NP distribution in the brain interstitium following CED.

7.3.4. Instability of NPs in mannitol yields no improvement in distribution

It should be noted that CED of a non-adhesive NP in a hyperosmolar infusate solution is valid only if the NP physicochemical characteristics are retained. We found that increasing the osmolarity of mannitol infusate solutions (from 10% to 25%) reduced PS-PEG diffusivity in brain tissues *ex vivo* (Figure 7.3A) and distribution *in vivo* (Figure 7.3B, C). Since the osmolarity is a colligative property independent of solute type, the contradictory findings are not likely due to any unique effect mannitol-based osmotic driven water flow. Rather, the results can be attributed to the marked increase in the size of PS-PEG in 25% mannitol infusate solution (Table 7.1), which offset the effect of enlarged ECM pores.

7.3.5. Trafficking of NPs through perivascular spaces

PVS, also known as Virchow Robin spaces in the brain, serve as a conduit for rapid flow of CSF into the brain from the subarachnoid space [165] and are responsible for the clearance of small metabolic molecules and waste products [153]. Numerous studies have demonstrated that the distribution of therapeutics at large distances away from the injection site takes place predominantly through the PVS [7, 8]. However, preferential trafficking and subsequent sequestration of intracranially administered NP in PVS [166] significantly reduce the available NP dose for treating target cells. Excessive therapeutic buildup within PVS has also resulted in toxic side effects to neighboring macrophages [26], undesired immune responses [8], and an overall reduction in therapeutic efficacy [7, 8].

We hypothesize that the fraction of NP that distribute through the ICS as opposed to the PVS will be increased by modulating the brain tissue to reduce the resistance of the brain ECM to NP diffusion. We thus investigated the extent of NP trafficking within PVS when infused in water, 0.9%, and 3% saline. PS-PEG administered in water were largely confined in the PVS (Figure 7.4A-D, Table 7.2). However, when administered in normal saline, PS-PEG were found in the ICS up to 1.0 mm away from the plane of injection (Figure 7.4E-G, Table 7.2), and were localized only within PVS at 1.5 mm (Figure 7.4H, Table 7.2). Furthermore, PS-PEG infused in hyperosmolar 3% saline were found in both the ICS and PVS up to 1.5 mm away (Figure 7.4M, Table 7.2), suggesting that NP distribution in ICS may be enhanced by reducing ECM resistance. Reduced NP accumulation in the PVS and improved NP distribution throughout the ICS achieved by a hyperosmolar infusate solution offers a promising strategy to overcome a critical limitation of CED.

Regardless of the infusate solution, PS-COOH were found solely associated with blood vessels (Figure 7.4A-M, Table 7.2). In fact, increasing saline concentration reduced the overall distance that PS-COOH trafficked through PVS. When infused in water and 0.9% saline, PS-COOH were found in PVS up to 1.5 mm away from the plane of administration, whereas PS-COOH infused in 3% saline were located in PVS only up to 0.5 mm away. The reduced distance can be attributed to the instability of PS-COOH in hyperosmolar saline (Table 7.1) as their rapid aggregation to sizes larger than 1 μm would significantly increase the steric hindrances encountered when trafficking through the PVS of arterioles that are sub-1 μm in width [167].

7.3.6. NP escape from perivascular spaces in lateral striate arteries

Due to the intrinsically lower physical resistance of the PVS compared to that of ICS [156], NP trafficking in the PVS is inevitable regardless of administration parameters or NP characteristics. Furthermore, NP remain sequestered in the PVS, unable to pass through the glia limitans [168], a barrier formed by astrocytic endfeet that strictly delineates the PVS from the ICS with only ~20 nm intercellular openings [153, 155, 169]. We hypothesize that by modulating the glia limitans using a hyperosmotic infusate solution, NP may be driven to escape PVS and distribute into the ICS. We investigated the lateral striate artery (Figure 7.5A), a large blood vessel structure previously shown to significantly sequester NP [7], to determine the extent of NP escape from this major artery. When administered in water, both PS-PEG and PS-COOH were confined to PVS (Figure 7.5B); less than 10% of PS-PEG or PS-COOH fluorescence was detected at a distance of 20 μm from the blood vessel (Figure 7.5E). Similarly, when administered in 0.9% saline, only 20% of both PS-PEG and PS-COOH fluorescence was observed at a distance of 20 μm (Figure 7.5C, F), suggesting that even with non-adhesive coatings, NP fail to traverse the glia limitans into the ICS. But when particles were infused in hyperosmolar 3% saline, while PS-COOH were similarly sequestered in PVS, PS-PEG exhibited markedly improved escape from PVS (Figure 7.5D, G), indicating that a combination of a hyperosmolar solution with non-adhesive NP is necessary for PVS escape. In fact, 65% of PS-PEG fluorescence was observed at a distance of 20 μm with 20% of the fluorescence detectable even at 100 μm. In these same high-resolution lateral striate artery images, we further quantified the percent coverage of fluorescent NP outside the PVS and within the brain ICS. Fluorescence of PS-PEG administered in 3% saline was detected across 30% of the ICS in the image, a significantly higher coverage ($P < 0.05$) as compared to PS-PEG administered in 0.9% saline (8% coverage) and water (3% coverage) (Figure 7.5H).

The migration of non-adhesive NP from the PVS into the ICS following infusion in a hyperosmolar solution can likely be attributed to the disruption and enlargement of the 20 nm astrocytic intercellular clefts, similar to our prior modulation of the brain ECM pores. Thus, larger NP can then escape into the ICS, but only if the NP surface is rendered non-adhesive. Regardless of the infusate solution, conventional NP are unable to reenter the brain ICS due to their adhesive nature that confines them to the PVS. To date, only small molecules (i.e. water, alexafluor dyes, small dextrans) and 20 nm adeno-associated viruses (AAV) have been shown to partition from the PVS into the ICS [151, 153] but here, we detail a strategy that enables the delivery of NP therapeutics as large as 60 nm in diameter out of PVS, through the glia limitans, and into the ICS.

PVS have been shown to play an important role in numerous neurological diseases. In Alzheimer's disease, dysregulation of the PVS glymphatic system leads to widespread development of amyloid-β plaques [153, 170]. Similarly, PVS, as paths of least resistance, have been implicated in facilitating the migration of malignant gliomas throughout the brain [154, 171], thereby often leading to tumor recurrence. Hence, preferential NP trafficking through the PVS, followed by radial escape through the glia limitans and into the ICS, may be exploited to chase the propagation of neurological disease.

7.3.7. Applicable findings to therapeutically relevant PLGA-NP system

We sought to determine if our previous findings based on model NP probes can be translated to therapeutic NP derived from poly(lactic-co-glycolic acid) (PLGA), a commonly utilized FDA-approved polymer for delivering a variety of drugs [172]. We first characterized the sizes of PLGA-based NP in iso-osmolar and hyperosmolar saline solutions. Uncoated PLGA NP were 80 nm upon formulation, but were highly unstable and rapidly aggregated in 3% saline (Table 7.3). On the other hand, non-adhesive PLGA-PEG NP were 71 nm in diameter following formulation and remained stable in higher saline concentrations. Following *in vivo* CED administration, fluorescence based quantification of NP distribution yielded a statistically significant improvement in the distribution of PLGA-PEG NP as compared to its PLGA counterpart in both 0.9% saline and 3% saline (Figure 7.6A, B). Additionally, Vd of PLGA-PEG when administered in 3% saline was 2.7-fold than the Vd of PLGA-PEG administered in 0.9% saline (Figure 7.6C). Extensive PLGA-PEG distribution throughout the brain interstitium led to perivascular distribution along lateral striate arteries whereas unmodified PLGA NP remained localized to the point of administration (Figure 7.6D, E). In good agreement with our observations with probe particles (Figure 7.5D), we found that PLGA-PEG NP could escape PVS when administered in hyperosmolar 3% saline (Figure 7.6F). At a distance of 20 μm from the blood vessel, 52% and 12% of PLGA-PEG fluorescence was detected when administered in 3% saline and 0.9% saline, respectively (Figure 7.6F). Furthermore, the percent coverage of PLGA-PEG within the brain ICS following administration in 3% saline was significantly higher than PLGA-PEG administered in 0.9% saline (Figure 7.6G, $P < 0.05$). These results validate our findings with probe NP that the combined use of non-adhesive surface coatings and hyperosmolar infusate solution will maximize the distribution of NP as well as their drug payloads following CED. Therefore, we anticipate that administering a therapeutic, non-adhesive biodegradable NP using an appropriate hyperosmolar infusate solution may enhance therapeutic distribution and further improve therapeutic efficacy.

7.4. Conclusion

We have developed a delivery strategy that focuses on maximizing NP distribution in the brain. We overcome the hindrances of brain ECM components and preferable NP trafficking and sequestration within PVS by administering non-adhesive NP using CED in a hyperosmolar infusate solution. In doing so, this strategy addresses the major drawbacks currently associated with CED in both the preclinical and clinical settings for treatment of neurological diseases. The results of this mechanistic study provide an essential level of understanding for overcoming the hindrances of the brain ECM and NP accumulation in PVS, both of which must be carefully considered for CED of NP therapeutics as well as alternative CNS administration methods including systemic, intranasal or intrathecal delivery routes. We anticipate incorporating this delivery strategy with our developed nanoparticle systems including PLGA-PEG (Chapter 4), DNA-NP (Chapter 5), and CDDP-BPN (Chapter 6).

Table 7.1: Sizes of PSPEG and PSCOOH nanoparticles hypotonic, isotonic, or hypertonic saline solutions after 15 min incubation in respective solutions.

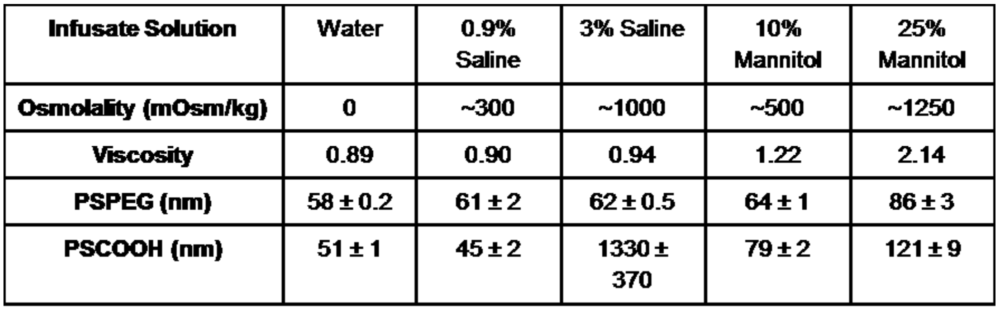

Infusate Solution	**Water**	**0.9% Saline**	**3% Saline**	**10% Mannitol**	**25% Mannitol**
Osmolality (mOsm/kg)	**0**	**~300**	**~1000**	**~500**	**~1250**
Viscosity	**0.89**	**0.90**	**0.94**	**1.22**	**2.14**
PSPEG (nm)	**58 ± 0.2**	**61 ± 2**	**62 ± 0.5**	**64 ± 1**	**86 ± 3**
PSCOOH (nm)	**51 ± 1**	**45 ± 2**	**1330 ± 370**	**79 ± 2**	**121 ± 9**

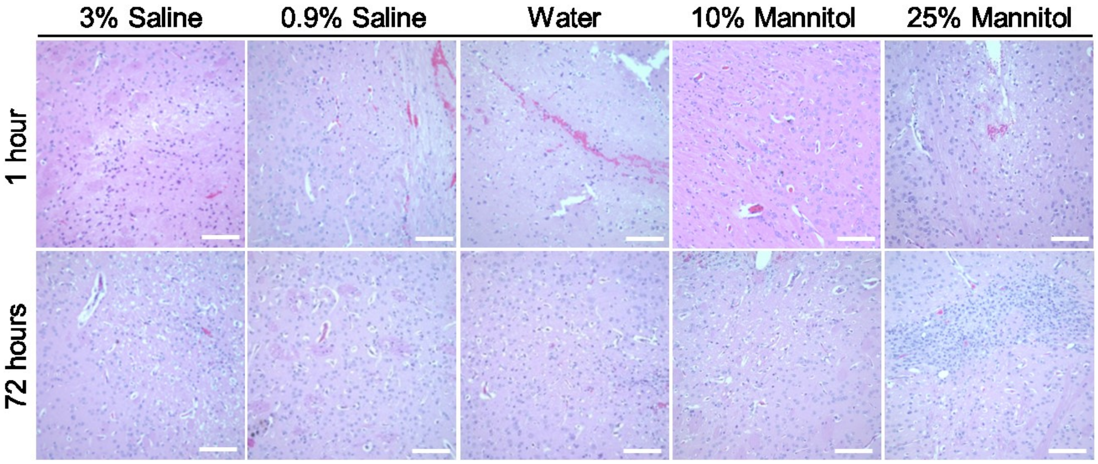

Figure 7.1: H&E images of rodent brains following administration of infusate solutions. Animals were sacrificed either 1 hour or 72 hours post-administration. Scale bar = 50um. No significant cellular toxicity or inflammation was observed in the vicinity of the implanted catheter at either timepoint indicating limited acute or chronic toxicities. All animals exhibited normal behavior up to 72 hours post administration. Scale bar = 100 microns.

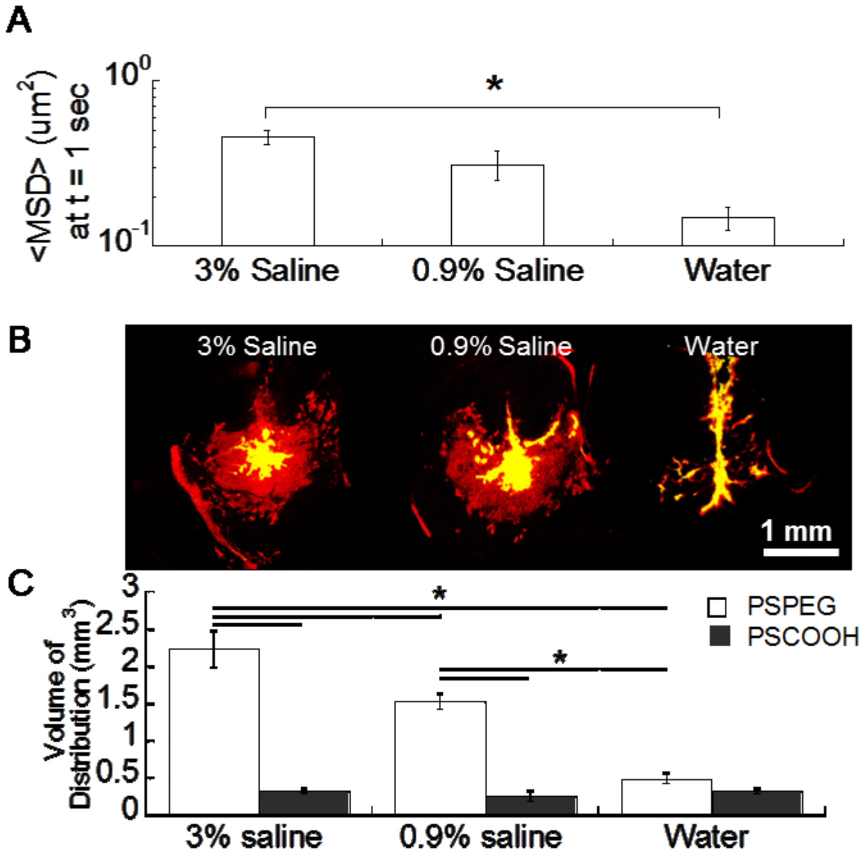

Figure 7.2: Characterization of nanoparticle diffusivity *ex vivo* and distribution *in vivo*. (A) Mean squared displacement of PS-PEG nanoparticles in rodent brain slices treated with varying solutions. N>100 nanoparticles tracked per sample, N=4 rodent samples. * $P<0.05$ denotes statistical significance. (B) Representative coronal slices depicting the injection site of PS-PEG (red) and PS-COOH (green) nanoparticles within rodent striatum. Yellow represents nanoparticle overlay. Scale bar = 1 mm. (C) Nanoparticle volume of distribution determined using image based MATLAB quantification methods. Statistical significance: * $P <0.05$ denoting statistical significance. (D) H&E images of rodent brains following administration of infusate solutions. Animals were sacrificed either 1 hour or 72 hours post-administration. Scale bar = 50um.

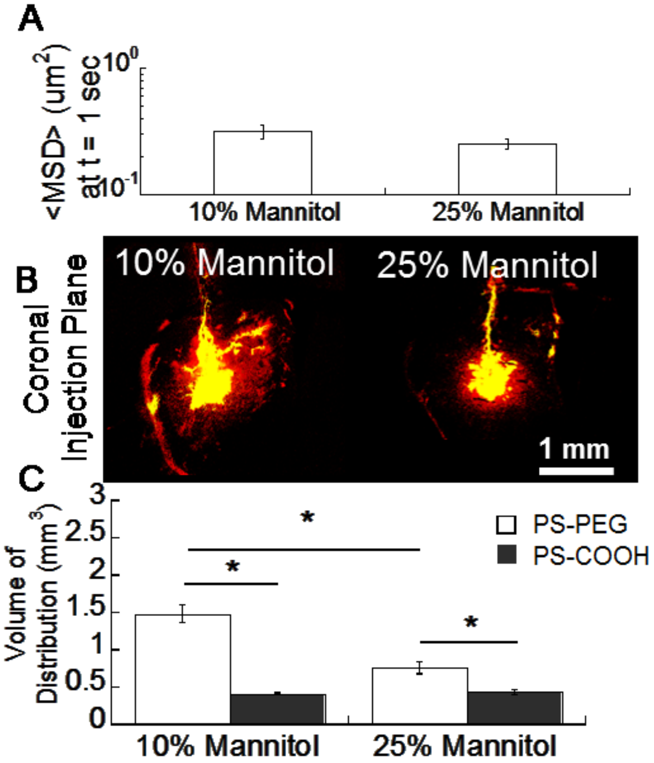

Figure 7.3: Nanoparticle diffusivity *ex vivo* and distribution *in vivo* in mannitol. (A) Mean squared displacement of PS-PEG nanoparticles in rodent brain slices treated with mannitol solutions. N>100 nanoparticles tracked per sample, N=4 rodent samples. **(**B) Representative coronal slices depicting the injection site of PS-PEG (red) and PS-COOH (green) nanoparticles within rodent striatum. Yellow represents nanoparticle overlay. Scale bar = 1 mm. (C) Nanoparticle volume of distribution determined using image based MATLAB quantification methods. Statistical significance: * $P < 0.05$ denoting statistical significance.

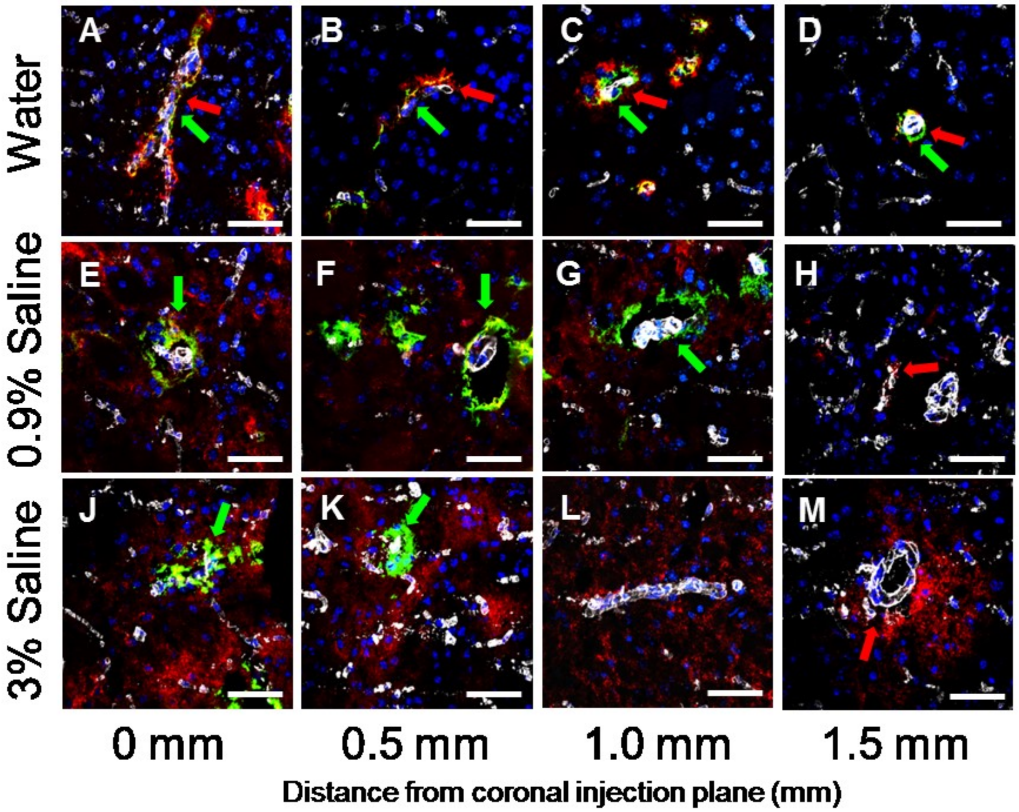

Figure 7.4: Nanoparticle-blood vessel association. Localization of PS-PEG (red) and PS-COOH (green) nanoparticles with collagen IV (white) stained blood vessels in the rodent brain is highly dependent on the tonicity of the solution the nanoparticles are infused in. Red and green arrows designates vessel of interest with PS-PEG and PS-COOH nanoparticles in the associated perivascular space, respectively. (A-D) Infusion in hypotonic water solution confines both nanoparticle types within perivascular spaces at all distances from the coronal plane of injection. (E, F, G) Up to 1.0 mm from the plane of injection, coinjection of nanoparticles in normal saline results in widespread distribution of PS-PEG in the parenchyma whereas the majority of PS-COOH line blood vessels. (H) At 1.5 mm, fewer PS-PEG nanoparticles are present and are mostly vessel-associated. (J-M) Following administration in hypertonic 3% saline, PS-PEG resides within the healthy tissue parenchyma up to 1.5 mm away from the plane of administration. PS-COOH distribution only extends out to 0.5 mm beyond the plane of injection with the majority associated with blood vessels. Scale bar = 50 um.

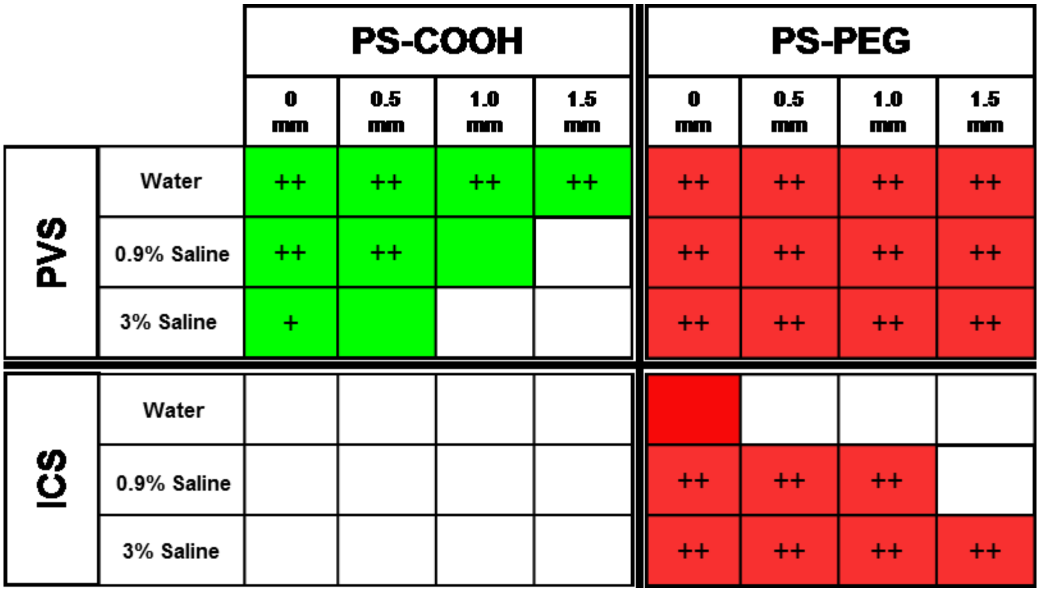

		PS-COOH				PS-PEG			
		0 mm	0.5 mm	1.0 mm	1.5 mm	0 mm	0.5 mm	1.0 mm	1.5 mm
PVS	Water	🟩 ++	🟩 ++	🟩 ++	🟩 ++	🟥 ++	🟥 ++	🟥 ++	🟥 ++
	0.9% Saline	🟩 ++	🟩 ++	🟩		🟥 ++	🟥 ++	🟥 ++	🟥 ++
	3% Saline	🟩 +	🟩			🟥 ++	🟥 ++	🟥 ++	🟥 ++
ICS	Water					🟥			
	0.9% Saline					🟥 ++	🟥 ++	🟥 ++	
	3% Saline					🟥 ++	🟥 ++	🟥 ++	🟥 ++

Table 7.2: Nanoparticle presence in perivascular or intercellular spaces. High resolution images from N=3 mice (Total of N ≥ 10 images) were analyzed for presence of PS-COOH and PS-PEG in PVS and ICS at specific distances from the plane of administration. Shaded boxes with "++" indicate that 90-100% of images depict the presence of NP. Shaded boxes with "+" indicate that NP were present in 80-89% of all images. Shaded boxes indicate presence of NP in between 20-80% of images. Blank boxes indicate NP presence in less than 20% of images.

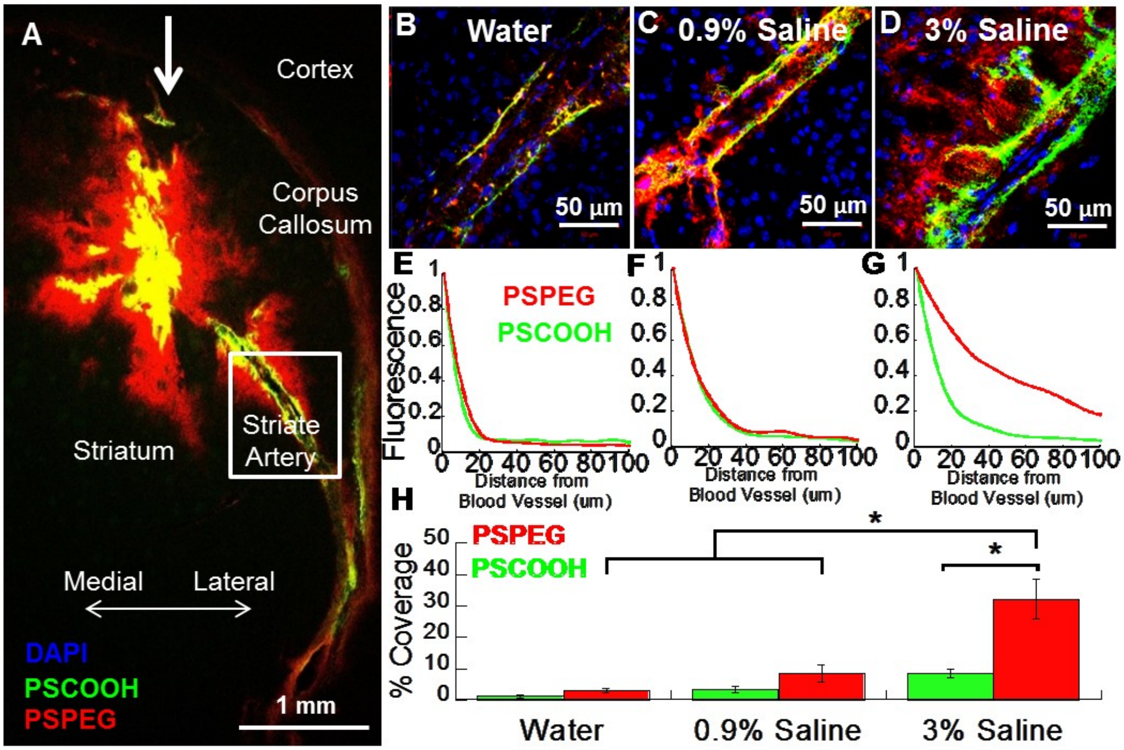

Figure 7.5: Perivascular distribution of nanoparticles following CED. (A) Presence of PS-PEG (red) and PS-COOH (green) nanoparticles one hour post-infusion into the striatum using CED. White arrow indicates direction of injection. Fluorescent nanoparticles were imaged in the striate arteries following administration in (B) 3% saline, (C) 0.9% saline, and (D) water. Blue = DAPI. Overlay of particles represented as yellow. Scale bar (A) = 1mm. Scale bar (B, C, D) = 50 um. (E) Presence of fluorescence corresponding to PS-PEG nanoparticles is seen up to 100um away from the perivascular space of the striate artery when delivered in hypertonic 3% saline solution. PS-COOH nanoparticles do not effectively escape from perivascular spaces regardless of tonicity of administration vehicle. At least N=3 striate vessels quantified for each condition. (F) Percent coverage of PS-PEG and PS-COOH nanoparticles calculated using image based MATLAB quantification.

Particle Type	PEG wt%	Size in 10mM NaCl (nm)	Size in 0.9% Saline (nm)	Size in 3% Saline (nm)
PLGA	0	80 ± 1	97 ± 13	1377 ± 224
PLGA-PEG	25	71 ± 1	75 ± 1	75 ± 3

Table 7.3: Sizes of PLGA and PLGA-PEG nanoparticles in isotonic, or hypertonic saline solutions after 15 min incubation in respective solutions.

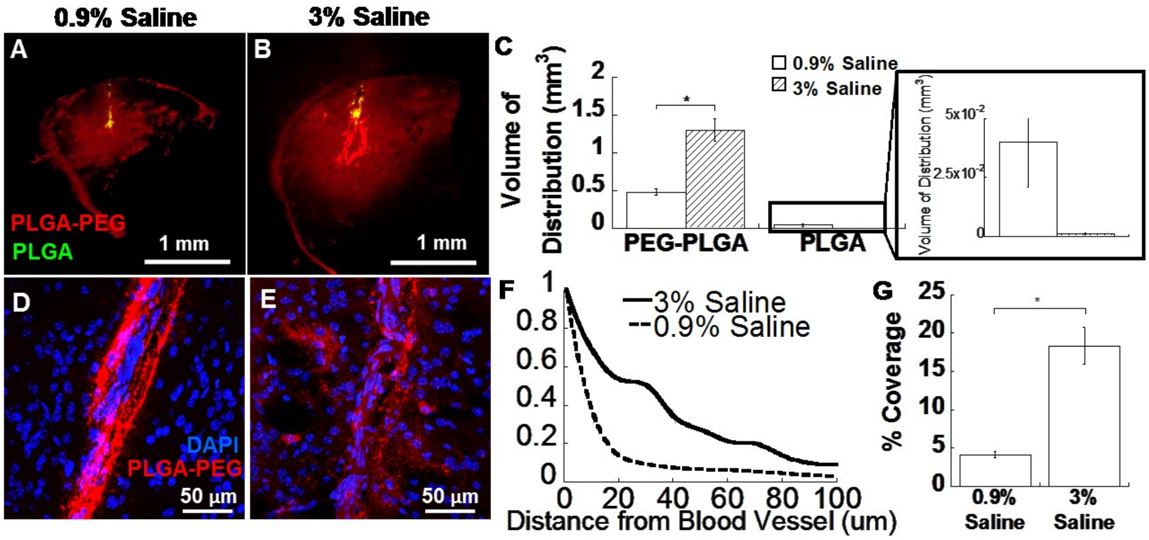

Figure 7.6: ***In vivo*** **distribution of therapeutic PLGA nanoparticles in mouse striatum administered via CED.** (A, B) Representative coronally sliced images of PLGA-PEG (red) and PLGA (green) nanoparticles infused in 0.9% saline and 3% saline. Data represent the average of $N \geq 3$ mouse brain specimen for each solution. (C) Quantified PLGA-PEG and PLGA volume of distributions in rodent striatum. Inset depicts the Vd of PLGA based nanoparticles. $^*P < 0.05$ denotes statistical significance. (D, E) High magnification of lateral striate arteries and PLGA-PEG nanoparticles following infusion in (D) 0.9% saline or (E) 3% saline. (F) Percent coverage of PLGA-PEG nanoparticles in varying saline solutions calculated using image based MATLAB quantification. $^*P < 0.05$ denotes statistical significance. G) Improved perivascular escape of PLGA-PEG nanoparticles occurs when administered in 3% saline as opposed to 0.9% saline. Note: Parts of Figure 7.6A and 7.6C are reproduced from earlier Figure 4.3

REFERENCES

1. Patel, M.A., et al., *The future of glioblastoma therapy: synergism of standard of care and immunotherapy.* Cancers (Basel), 2014. **6**(4): p. 1953-85.
2. Nance, E.A., et al., *A dense poly(ethylene glycol) coating improves penetration of large polymeric nanoparticles within brain tissue.* Sci Transl Med, 2012. **4**(149): p. 149ra119.
3. Makadia, H.K. and S.J. Siegel, *Poly Lactic-co-Glycolic Acid (PLGA) as Biodegradable Controlled Drug Delivery Carrier.* Polymers (Basel), 2011. **3**(3): p. 1377-1397.
4. Stupp, R., et al., *Radiotherapy plus concomitant and adjuvant temozolomide for glioblastoma.* N Engl J Med, 2005. **352**(10): p. 987-96.
5. Kunwar, S., et al., *Phase III randomized trial of CED of IL13-PE38QQR vs Gliadel wafers for recurrent glioblastoma.* Neuro Oncol, 2010. **12**(8): p. 871-81.
6. Sampson, J.H., et al., *Poor drug distribution as a possible explanation for the results of the PRECISE trial.* J Neurosurg, 2010. **113**(2): p. 301-9.
7. Krauze, M.T., et al., *Effects of the perivascular space on convection-enhanced delivery of liposomes in primate putamen.* Exp Neurol, 2005. **196**(1): p. 104-11.
8. Barua, N.U., et al., *Intrastriatal convection-enhanced delivery results in widespread perivascular distribution in a pre-clinical model.* Fluids Barriers CNS, 2012. **9**(1): p. 2.
9. Wang, Y. and T. Jiang, *Understanding high grade glioma: molecular mechanism, therapy and comprehensive management.* Cancer Lett, 2013. **331**(2): p. 139-46.
10. Giese, A., et al., *Cost of migration: invasion of malignant gliomas and implications for treatment.* J Clin Oncol, 2003. **21**(8): p. 1624-36.
11. Munson, J.M., et al., *Anti-invasive adjuvant therapy with imipramine blue enhances chemotherapeutic efficacy against glioma.* Sci Transl Med, 2012. **4**(127): p. 127ra36.
12. Siegal, T., *Which drug or drug delivery system can change clinical practice for brain tumor therapy?* Neuro Oncol, 2013. **15**(6): p. 656-69.
13. Zhang, J., M.F. Stevens, and T.D. Bradshaw, *Temozolomide: mechanisms of action, repair and resistance.* Curr Mol Pharmacol, 2012. **5**(1): p. 102-14.
14. Trinh, V.A., S.P. Patel, and W.J. Hwu, *The safety of temozolomide in the treatment of malignancies.* Expert Opin Drug Saf, 2009. **8**(4): p. 493-9.
15. Chamberlain, M.C., *Temozolomide: therapeutic limitations in the treatment of adult high-grade gliomas.* Expert Rev Neurother, 2010. **10**(10): p. 1537-44.
16. Ostermann, S., et al., *Plasma and cerebrospinal fluid population pharmacokinetics of temozolomide in malignant glioma patients.* Clin Cancer Res, 2004. **10**(11): p. 3728-36.
17. Abbott, N.J., L. Ronnback, and E. Hansson, *Astrocyte-endothelial interactions at the blood-brain barrier.* Nat Rev Neurosci, 2006. **7**(1): p. 41-53.
18. Pardridge, W.M., *Drug and gene delivery to the brain: the vascular route.* Neuron, 2002. **36**(4): p. 555-8.

19. Nance, E., et al., *Non-invasive delivery of stealth, brain-penetrating nanoparticles across the blood-brain barrier using MRI-guided focused ultrasound.* J Control Release, 2014. **189**: p. 123-32.
20. Allard, E., C. Passirani, and J.P. Benoit, *Convection-enhanced delivery of nanocarriers for the treatment of brain tumors.* Biomaterials, 2009. **30**(12): p. 2302-18.
21. Burgess, A. and K. Hynynen, *Noninvasive and targeted drug delivery to the brain using focused ultrasound.* ACS Chem Neurosci, 2013. **4**(4): p. 519-26.
22. Woodworth, G.F., et al., *Emerging insights into barriers to effective brain tumor therapeutics.* Front Oncol, 2014. **4**: p. 126.
23. Nance, E., et al., *Noninvasive delivery of stealth, brain-penetrating nanoparticles across the blood-brain barrier using MRI-guided focused ultrasound.* J Control Release, 2014.
24. Zamecnik, J., et al., *Extracellular matrix glycoproteins and diffusion barriers in human astrocytic tumours.* Neuropathol Appl Neurobiol, 2004. **30**(4): p. 338-50.
25. Voges, J., et al., *Imaging-guided convection-enhanced delivery and gene therapy of glioblastoma.* Ann Neurol, 2003. **54**(4): p. 479-87.
26. MacKay, J.A., D.F. Deen, and F.C. Szoka, Jr., *Distribution in brain of liposomes after convection enhanced delivery; modulation by particle charge, particle diameter, and presence of steric coating.* Brain Res, 2005. **1035**(2): p. 139-53.
27. Nance, E., et al., *Brain-penetrating nanoparticles improve paclitaxel efficacy in malignant glioma following local administration.* ACS Nano, 2014. **8**(10): p. 10655-64.
28. Zhou, J., et al., *Highly penetrative, drug-loaded nanocarriers improve treatment of glioblastoma.* Proc Natl Acad Sci U S A, 2013. **110**(29): p. 11751-6.
29. Yin, D., et al., *Convection-enhanced delivery improves distribution and efficacy of tumor-selective retroviral replicating vectors in a rodent brain tumor model.* Cancer Gene Ther, 2013. **20**(6): p. 336-41.
30. McGirt, M.J., et al., *Gliadel (BCNU) wafer plus concomitant temozolomide therapy after primary resection of glioblastoma multiforme.* J Neurosurg, 2009. **110**(3): p. 583-8.
31. Patel, T., et al., *Polymeric nanoparticles for drug delivery to the central nervous system.* Adv Drug Deliv Rev, 2012. **64**(7): p. 701-5.
32. Juratli, T.A., G. Schackert, and D. Krex, *Current status of local therapy in malignant gliomas--a clinical review of three selected approaches.* Pharmacol Ther, 2013. **139**(3): p. 341-58.
33. Zhou, J., et al., *Highly penetrative, drug-loaded nanocarriers improve treatment of glioblastoma.* Proc Natl Acad Sci U S A, 2013.
34. Slevin, J.T., et al., *Unilateral intraputaminal glial cell line-derived neurotrophic factor in patients with Parkinson disease: response to 1 year each of treatment and withdrawal.* Neurosurg Focus, 2006. **20**(5): p. E1.
35. Krauze, M.T., et al., *Real-time visualization and characterization of liposomal delivery into the monkey brain by magnetic resonance imaging.* Brain Res Brain Res Protoc, 2005. **16**(1-3): p. 20-6.
36. Bobo, R.H., et al., *Convection-enhanced delivery of macromolecules in the brain.* Proc Natl Acad Sci U S A, 1994. **91**(6): p. 2076-80.

37. Chen, M.Y., et al., *Variables affecting convection-enhanced delivery to the striatum: a systematic examination of rate of infusion, cannula size, infusate concentration, and tissue-cannula sealing time.* J Neurosurg, 1999. **90**(2): p. 315-20.
38. Barua, N.U., S.S. Gill, and S. Love, *Convection-Enhanced Drug Delivery to the Brain: Therapeutic Potential and Neuropathological Considerations.* Brain Pathol, 2013.
39. Saito, R., et al., *Tissue affinity of the infusate affects the distribution volume during convection-enhanced delivery into rodent brains: implications for local drug delivery.* J Neurosci Methods, 2006. **154**(1-2): p. 225-32.
40. Nance, E., et al., *Brain-Penetrating Nanoparticles Improve Paclitaxel Efficacy in Malignant Glioma Following Local Administration.* ACS Nano, 2014.
41. Saito, R., et al., *Gadolinium-loaded liposomes allow for real-time magnetic resonance imaging of convection-enhanced delivery in the primate brain.* Exp Neurol, 2005. **196**(2): p. 381-9.
42. Krauze, M.T., et al., *Reflux-free cannula for convection-enhanced high-speed delivery of therapeutic agents.* J Neurosurg, 2005. **103**(5): p. 923-9.
43. Kroll, R.A., et al., *Increasing volume of distribution to the brain with interstitial infusion: dose, rather than convection, might be the most important factor.* Neurosurgery, 1996. **38**(4): p. 746-52; discussion 752-4.
44. Goldmann, T. and M. Prinz, *Role of microglia in CNS autoimmunity.* Clin Dev Immunol, 2013. **2013**: p. 208093.
45. Panyam, J. and V. Labhasetwar, *Biodegradable nanoparticles for drug and gene delivery to cells and tissue.* Adv Drug Deliv Rev, 2003. **55**(3): p. 329-47.
46. Allen, T.M. and P.R. Cullis, *Drug delivery systems: entering the mainstream.* Science, 2004. **303**(5665): p. 1818-22.
47. Schneider, C.S., et al., *Minimizing the non-specific binding of nanoparticles to the brain enables active targeting of Fn14-positive glioblastoma cells.* Biomaterials, 2015. **42**: p. 42-51.
48. Wiley, D.T., et al., *Transcytosis and brain uptake of transferrin-containing nanoparticles by tuning avidity to transferrin receptor.* Proc Natl Acad Sci U S A, 2013. **110**(21): p. 8662-7.
49. Yan, F., et al., *Transferrin-conjugated, fluorescein-loaded magnetic nanoparticles for targeted delivery across the blood-brain barrier.* J Mater Sci Mater Med, 2013. **24**(10): p. 2371-9.
50. Ulbrich, K., et al., *Transferrin- and transferrin-receptor-antibody-modified nanoparticles enable drug delivery across the blood-brain barrier (BBB).* Eur J Pharm Biopharm, 2009. **71**(2): p. 251-6.
51. Ramge, P., et al., *Polysorbate-80 coating enhances uptake of polybutylcyanoacrylate (PBCA)-nanoparticles by human and bovine primary brain capillary endothelial cells.* Eur J Neurosci, 2000. **12**(6): p. 1931-40.
52. Kreuter, J., et al., *Direct evidence that polysorbate-80-coated poly(butylcyanoacrylate) nanoparticles deliver drugs to the CNS via specific mechanisms requiring prior binding of drug to the nanoparticles.* Pharm Res, 2003. **20**(3): p. 409-16.

53. Kreuter, J., et al., *Apolipoprotein-mediated transport of nanoparticle-bound drugs across the blood-brain barrier.* J Drug Target, 2002. **10**(4): p. 317-25.
54. Zensi, A., et al., *Albumin nanoparticles targeted with Apo E enter the CNS by transcytosis and are delivered to neurones.* J Control Release, 2009. **137**(1): p. 78-86.
55. Lutz, G.J., S.R. Sirsi, and J.H. Williams, *PEG-PEI copolymers for oligonucleotide delivery to cells and tissues.* Methods Mol Biol, 2008. **433**: p. 141-58.
56. Mora-Huertas, C.E., H. Fessi, and A. Elaissari, *Polymer-based nanocapsules for drug delivery.* Int J Pharm, 2010. **385**(1-2): p. 113-42.
57. O'Mahony, A.M., et al., *Non-viral nanosystems for gene and small interfering RNA delivery to the central nervous system: formulating the solution.* J Pharm Sci, 2013. **102**(10): p. 3469-84.
58. Lentz, T.B., S.J. Gray, and R.J. Samulski, *Viral vectors for gene delivery to the central nervous system.* Neurobiol Dis, 2012. **48**(2): p. 179-88.
59. Perez-Martinez, F.C., B. Carrion, and V. Cena, *The use of nanoparticles for gene therapy in the nervous system.* J Alzheimers Dis, 2012. **31**(4): p. 697-710.
60. Thomas, C.E., A. Ehrhardt, and M.A. Kay, *Progress and problems with the use of viral vectors for gene therapy.* Nat Rev Genet, 2003. **4**(5): p. 346-58.
61. Olsen, N.J. and C.M. Stein, *New drugs for rheumatoid arthritis.* N Engl J Med, 2004. **350**(21): p. 2167-79.
62. Xiao, X., J. Li, and R.J. Samulski, *Efficient long-term gene transfer into muscle tissue of immunocompetent mice by adeno-associated virus vector.* J Virol, 1996. **70**(11): p. 8098-108.
63. Chirmule, N., et al., *Humoral immunity to adeno-associated virus type 2 vectors following administration to murine and nonhuman primate muscle.* J Virol, 2000. **74**(5): p. 2420-5.
64. Lowenstein, P.R., et al., *Immune responses to adenovirus and adeno-associated vectors used for gene therapy of brain diseases: the role of immunological synapses in understanding the cell biology of neuroimmune interactions.* Curr Gene Ther, 2007. **7**(5): p. 347-60.
65. Lowenstein, P.R., K. Kroeger, and M.G. Castro, *Immunology of neurological gene therapy: how T cells modulate viral vector-mediated therapeutic transgene expression through immunological synapses.* Neurotherapeutics, 2007. **4**(4): p. 715-24.
66. Sun, X. and N. Zhang, *Cationic polymer optimization for efficient gene delivery.* Mini Rev Med Chem, 2010. **10**(2): p. 108-25.
67. Dunlap, D.D., et al., *Nanoscopic structure of DNA condensed for gene delivery.* Nucleic Acids Res, 1997. **25**(15): p. 3095-101.
68. Kukowska-Latallo, J.F., et al., *Intravascular and endobronchial DNA delivery to murine lung tissue using a novel, nonviral vector.* Hum Gene Ther, 2000. **11**(10): p. 1385-95.
69. Akinc, A., et al., *Exploring polyethylenimine-mediated DNA transfection and the proton sponge hypothesis.* J Gene Med, 2005. **7**(5): p. 657-63.
70. Mintzer, M.A. and E.E. Simanek, *Nonviral vectors for gene delivery.* Chem Rev, 2009. **109**(2): p. 259-302.

71. Pathak, A., S. Patnaik, and K.C. Gupta, *Recent trends in non-viral vector-mediated gene delivery.* Biotechnol J, 2009. **4**(11): p. 1559-72.
72. Jain, K.K., *Nanobiotechnology-based strategies for crossing the blood-brain barrier.* Nanomedicine (Lond), 2012. **7**(8): p. 1225-33.
73. Wohlfart, S., S. Gelperina, and J. Kreuter, *Transport of drugs across the blood-brain barrier by nanoparticles.* J Control Release, 2012. **161**(2): p. 264-73.
74. Patel, T., et al., *Polymeric nanoparticles for drug delivery to the central nervous system.* Advanced Drug Delivery Reviews, 2012. **64**(7): p. 701-705.
75. Vykhodtseva, N., N. McDannold, and K. Hynynen, *Progress and problems in the application of focused ultrasound for blood-brain barrier disruption.* Ultrasonics, 2008. **48**(4): p. 279-96.
76. Kroll, R.A. and E.A. Neuwelt, *Outwitting the blood-brain barrier for therapeutic purposes: osmotic opening and other means.* Neurosurgery, 1998. **42**(5): p. 1083-99; discussion 1099-100.
77. Sykova, E. and C. Nicholson, *Diffusion in brain extracellular space.* Physiol Rev, 2008. **88**(4): p. 1277-340.
78. Zamecnik, J., *The extracellular space and matrix of gliomas.* Acta Neuropathol, 2005. **110**(5): p. 435-42.
79. Zimmermann, D.R. and M.T. Dours-Zimmermann, *Extracellular matrix of the central nervous system: from neglect to challenge.* Histochem Cell Biol, 2008. **130**(4): p. 635-53.
80. Kenny, G.D., et al., *Multifunctional receptor-targeted nanocomplexes for the delivery of therapeutic nucleic acids to the Brain.* Biomaterials, 2013. **34**(36): p. 9190-200.
81. Writer, M.J., et al., *Lipid peptide nanocomplexes for gene delivery and magnetic resonance imaging in the brain.* J Control Release, 2012. **162**(2): p. 340-8.
82. Suk, J.S., et al., *Lung Gene Therapy with Highly Compacted DNA Nanoparticles that Overcome the Mucus Barrier.* J Control Release, 2014.
83. Kim, Y.K., et al., *Spermine-alt-poly(ethylene glycol) polyspermine as a safe and efficient aerosol gene carrier for lung cancer therapy.* J Biomed Mater Res A, 2013.
84. Kim, A.J., et al., *Non-degradative intracellular trafficking of highly compacted polymeric DNA nanoparticles.* J Control Release, 2012. **158**(1): p. 102-7.
85. Boylan, N.J., et al., *Enhancement of airway gene transfer by DNA nanoparticles using a pH-responsive block copolymer of polyethylene glycol and poly-L-lysine.* Biomaterials, 2012. **33**(7): p. 2361-71.
86. Schuster, B.S., et al., *Nanoparticle diffusion in respiratory mucus from humans without lung disease.* Biomaterials, 2013. **34**(13): p. 3439-46.
87. Martin, D.S., M.B. Forstner, and J.A. Kas, *Apparent subdiffusion inherent to single particle tracking.* Biophys J, 2002. **83**(4): p. 2109-17.
88. Savin, T. and P.S. Doyle, *Static and dynamic errors in particle tracking microrheology.* Biophys J, 2005. **88**(1): p. 623-38.
89. Elliott, S.L., et al., *EB1 is essential during Drosophila development and plays a crucial role in the integrity of chordotonal mechanosensory organs.* Mol Biol Cell, 2005. **16**(2): p. 891-901.

90. Petersen, H., et al., *Polyethylenimine-graft-poly(ethylene glycol) copolymers: influence of copolymer block structure on DNA complexation and biological activities as gene delivery system.* Bioconjug Chem, 2002. **13**(4): p. 845-54.
91. Malek, A., F. Czubayko, and A. Aigner, *PEG grafting of polyethylenimine (PEI) exerts different effects on DNA transfection and siRNA-induced gene targeting efficacy.* J Drug Target, 2008. **16**(2): p. 124-39.
92. Merkel, O.M., et al., *In vitro and in vivo complement activation and related anaphylactic effects associated with polyethylenimine and polyethylenimine-graft-poly(ethylene glycol) block copolymers.* Biomaterials, 2011. **32**(21): p. 4936-42.
93. Malek, A., et al., *In vivo pharmacokinetics, tissue distribution and underlying mechanisms of various PEI(-PEG)/siRNA complexes.* Toxicol Appl Pharmacol, 2009. **236**(1): p. 97-108.
94. MacKay, J.A., et al., *HIV TAT peptide modifies the distribution of DNA nanolipoparticles following convection-enhanced delivery.* Molecular Therapy, 2008. **16**(5): p. 893-900.
95. Stiles, D.K., et al., *Widespread suppression of huntingtin with convection-enhanced delivery of siRNA.* Exp Neurol, 2012. **233**(1): p. 463-71.
96. Fox, J.H., et al., *Cysteine Oxidation within N-terminal Mutant Huntingtin Promotes Oligomerization and Delays Clearance of Soluble Protein.* Journal of Biological Chemistry, 2011. **286**(20): p. 18320-18330.
97. Ruoslahti, E., *Brain extracellular matrix.* Glycobiology, 1996. **6**(5): p. 489-92.
98. Voges, J., et al., *Clinical protocol. Liposomal gene therapy with the herpes simplex thymidine kinase gene/ganciclovir system for the treatment of glioblastoma multiforme.* Hum Gene Ther, 2002. **13**(5): p. 675-85.
99. Amoozgar, Z. and Y. Yeo, *Recent advances in stealth coating of nanoparticle drug delivery systems.* Wiley Interdiscip Rev Nanomed Nanobiotechnol, 2012. **4**(2): p. 219-33.
100. Hatakeyama, H., H. Akita, and H. Harashima, *A multifunctional envelope type nano device (MEND) for gene delivery to tumours based on the EPR effect: a strategy for overcoming the PEG dilemma.* Adv Drug Deliv Rev, 2011. **63**(3): p. 152-60.
101. Pamujula, S., et al., *Cellular delivery of PEGylated PLGA nanoparticles.* J Pharm Pharmacol, 2012. **64**(1): p. 61-7.
102. Hu, Y., et al., *Effect of PEG conformation and particle size on the cellular uptake efficiency of nanoparticles with the HepG2 cells.* J Control Release, 2007. **118**(1): p. 7-17.
103. Mishra, S., P. Webster, and M.E. Davis, *PEGylation significantly affects cellular uptake and intracellular trafficking of non-viral gene delivery particles.* Eur J Cell Biol, 2004. **83**(3): p. 97-111.
104. Ogris, M., et al., *DNA/polyethylenimine transfection particles: influence of ligands, polymer size, and PEGylation on internalization and gene expression.* AAPS PharmSci, 2001. **3**(3): p. E21.
105. Sonawane, N.D., F.C. Szoka, Jr., and A.S. Verkman, *Chloride accumulation and swelling in endosomes enhances DNA transfer by polyamine-DNA polyplexes.* J Biol Chem, 2003. **278**(45): p. 44826-31.

106. Riely, G.J., et al., *Randomized phase II study of pulse erlotinib before or after carboplatin and paclitaxel in current or former smokers with advanced non-small-cell lung cancer.* J Clin Oncol, 2009. **27**(2): p. 264-70.
107. Davies, L.A., et al., *Enhanced lung gene expression after aerosol delivery of concentrated pDNA/PEI complexes.* Mol Ther, 2008. **16**(7): p. 1283-90.
108. Beyerle, A., et al., *PEGylation affects cytotoxicity and cell-compatibility of poly(ethylene imine) for lung application: structure-function relationships.* Toxicol Appl Pharmacol, 2010. **242**(2): p. 146-54.
109. Yurek, D.M., et al., *Compacted DNA nanoparticle gene transfer of GDNF to the rat striatum enhances the survival of grafted fetal dopamine neurons.* Cell Transplant, 2009. **18**(10): p. 1183-96.
110. Yurek, D.M., et al., *Long-term transgene expression in the central nervous system using DNA nanoparticles.* Mol Ther, 2009. **17**(4): p. 641-50.
111. Ziady, A.G., et al., *Minimal toxicity of stabilized compacted DNA nanoparticles in the murine lung.* Mol Ther, 2003. **8**(6): p. 948-56.
112. Ziady, A.G., et al., *Transfection of airway epithelium by stable PEGylated poly-L-lysine DNA nanoparticles in vivo.* Mol Ther, 2003. **8**(6): p. 936-47.
113. Konstan, M.W., et al., *Compacted DNA nanoparticles administered to the nasal mucosa of cystic fibrosis subjects are safe and demonstrate partial to complete cystic fibrosis transmembrane regulator reconstitution.* Hum Gene Ther, 2004. **15**(12): p. 1255-69.
114. Chan, I., et al., *Progression elevated gene-3 promoter (PEG-Prom) confers cancer cell selectivity to human polynucleotide phosphorylase (hPNPase(old-35))-mediated growth suppression.* J Cell Physiol, 2008. **215**(2): p. 401-9.
115. Hegi, M.E., et al., *MGMT gene silencing and benefit from temozolomide in glioblastoma.* N Engl J Med, 2005. **352**(10): p. 997-1003.
116. Palanichamy, K. and A. Chakravarti, *Combining drugs and radiotherapy: from the bench to the bedside.* Curr Opin Neurol, 2009. **22**(6): p. 625-32.
117. Oberoi, H.S., et al., *Nanocarriers for delivery of platinum anticancer drugs.* Adv Drug Deliv Rev, 2013.
118. Hargrave, D.R. and S. Zacharoulis, *Pediatric CNS tumors: current treatment and future directions.* Expert Rev Neurother, 2007. **7**(8): p. 1029-42.
119. Kim, I.H., et al., *Radiotherapy followed by adjuvant temozolomide with or without neoadjuvant ACNU-CDDP chemotherapy in newly diagnosed glioblastomas: a prospective randomized controlled multicenter phase III trial.* J Neurooncol, 2011. **103**(3): p. 595-602.
120. Silvani, A., et al., *Cisplatinum and BCNU chemotherapy in primary glioblastoma patients.* J Neurooncol, 2009. **94**(1): p. 57-62.
121. Grossman, S.A., et al., *Phase III study comparing three cycles of infusional carmustine and cisplatin followed by radiation therapy with radiation therapy and concurrent carmustine in patients with newly diagnosed supratentorial glioblastoma multiforme: Eastern Cooperative Oncology Group Trial 2394.* J Clin Oncol, 2003. **21**(8): p. 1485-91.
122. Cepeda, V., et al., *Biochemical mechanisms of cisplatin cytotoxicity.* Anticancer Agents Med Chem, 2007. **7**(1): p. 3-18.

123. de Groot, J.F., et al., *Phase II study of carboplatin and erlotinib (Tarceva, OSI-774) in patients with recurrent glioblastoma.* J Neurooncol, 2008. **90**(1): p. 89-97.
124. Sheleg, S.V., et al., *Local chemotherapy with cisplatin-depot for glioblastoma multiforme.* J Neurooncol, 2002. **60**(1): p. 53-9.
125. Bouvier, G., et al., *Intratumoral chemotherapy with multiple sources.* Ann N Y Acad Sci, 1988. **531**: p. 213-4.
126. Bouvier, G., et al., *Stereotactic administration of intratumoral chronic chemotherapy of recurrent malignant gliomas.* Appl Neurophysiol, 1987. **50**(1-6): p. 223-6.
127. Rousseau, J., et al., *Efficacy of intracerebral delivery of cisplatin in combination with photon irradiation for treatment of brain tumors.* J Neurooncol, 2010. **98**(3): p. 287-95.
128. Huo, T., et al., *Preparation, biodistribution and neurotoxicity of liposomal cisplatin following convection enhanced delivery in normal and F98 glioma bearing rats.* PLoS ONE, 2012. **7**(11): p. e48752.
129. Olivi, A., et al., *Direct delivery of platinum-based antineoplastics to the central nervous system: a toxicity and ultrastructural study.* Cancer Chemother Pharmacol, 1993. **31**(6): p. 449-54.
130. Chen, M.Y., et al., *Surface properties, more than size, limiting convective distribution of virus-sized particles and viruses in the central nervous system.* J Neurosurg, 2005. **103**(2): p. 311-9.
131. Mastorakos, P., Zhang, C., Berry, S., Oh, Y., Lee, S., Eberhart, C., Woodworth, G., Suk, J., Hanes, J., *Highly Compacted DNA Nanoparticles with Exceptionally Dense PEG Coatings Provide Uniform and Widespread Gene Transfer to the Central Nervous System.* ACS Nano, 2014. **Under Review**.
132. Mastorakos, P., et al., *Highly PEGylated DNA Nanoparticles Provide Uniform and Widespread Gene Transfer in the Brain.* Adv Healthc Mater, 2015.
133. Recinos, V.R., et al., *Combination of intracranial temozolomide with intracranial carmustine improves survival when compared with either treatment alone in a rodent glioma model.* Neurosurgery, 2010. **66**(3): p. 530-7; discussion 537.
134. Nishiyama, N., et al., *Preparation and characterization of self-assembled polymer-metal complex micelle from cis-dichlorodiammineplatinum(II) and poly(ethylene glycol)-poly(alpha,beta-aspartic acid) block copolymer in an aqueous medium.* Langmuir, 1999. **15**(2): p. 377-383.
135. Suk, J.S., et al., *Lung gene therapy with highly compacted DNA nanoparticles that overcome the mucus barrier.* J Control Release, 2014. **178C**: p. 8-17.
136. Uchino, H., et al., *Cisplatin-incorporating polymeric micelles (NC-6004) can reduce nephrotoxicity and neurotoxicity of cisplatin in rats.* British Journal of Cancer, 2005. **93**(6): p. 678-687.
137. Dhar, S., et al., *Targeted delivery of a cisplatin prodrug for safer and more effective prostate cancer therapy in vivo.* Proc Natl Acad Sci U S A, 2011. **108**(5): p. 1850-5.
138. Paraskar, A.S., et al., *Harnessing structure-activity relationship to engineer a cisplatin nanoparticle for enhanced antitumor efficacy.* Proc Natl Acad Sci U S A, 2010. **107**(28): p. 12435-40.

139. Plummer, R., et al., *A Phase I clinical study of cisplatin-incorporated polymeric micelles (NC-6004) in patients with solid tumours.* Br J Cancer, 2011. **104**(4): p. 593-8.
140. Dudev, T. and C. Lim, *Effect of carboxylate-binding mode on metal binding/selectivity and function in proteins.* Acc Chem Res, 2007. **40**(1): p. 85-93.
141. Buckner, J.C., et al., *Phase III trial of carmustine and cisplatin compared with carmustine alone and standard radiation therapy or accelerated radiation therapy in patients with glioblastoma multiforme: North Central Cancer Treatment Group 93-72-52 and Southwest Oncology Group 9503 Trials.* J Clin Oncol, 2006. **24**(24): p. 3871-9.
142. Westphal, M., et al., *A phase 3 trial of local chemotherapy with biodegradable carmustine (BCNU) wafers (Gliadel wafers) in patients with primary malignant glioma.* Neuro Oncol, 2003. **5**(2): p. 79-88.
143. Fung, L.K., et al., *Pharmacokinetics of interstitial delivery of carmustine, 4-hydroperoxycyclophosphamide, and paclitaxel from a biodegradable polymer implant in the monkey brain.* Cancer Res, 1998. **58**(4): p. 672-84.
144. Barth, R.F., et al., *Comparison of intracerebral delivery of carboplatin and photon irradiation with an optimized regimen for boron neutron capture therapy of the F98 rat glioma.* Appl Radiat Isot, 2011. **69**(12): p. 1813-6.
145. Vogelbaum, M.I.T., Inc. *Topotecan Using Convection-Enhanced Delivery (CED) in High Grade Glioma*. 2014 [cited 2015 April 14]; Available from: https://clinicaltrials.gov/ct2/show/NCT02278510.
146. Elder, J. *Carboplatin in Treating Patients with Recurrent High-Grade Gliomas*. 2012 [cited 2015 April 14]; Available from: https://clinicaltrials.gov/ct2/show/NCT01644955.
147. Inc, I.T. *The PRECISE Trial: Study of IL13-PE38QQR Compared to GLIADEL Wafer in Patients With Recurrent Glioblastoma Multiforme*. 2004 [cited 2015 April 14]; Available from: https://clinicaltrials.gov/ct2/show/NCT00076986.
148. Chaichana, K.L., L. Pinheiro, and H. Brem, *Delivery of local therapeutics to the brain: working toward advancing treatment for malignant gliomas.* Ther Deliv, 2015. **6**(3): p. 353-69.
149. Su, W., et al., *Phase I/Ii Study of Nc-6004, a Novel Micellar Formulation of Cisplatin, in Combination with Gemcitabine in Patients with Pancreatic Cancer in Asia - Results of Phase I.* Annals of Oncology, 2012. **23**: p. 247-247.
150. Saito, R. and T. Tominaga, *Convection-enhanced delivery: from mechanisms to clinical drug delivery for diseases of the central nervous system.* Neurol Med Chir (Tokyo), 2012. **52**(8): p. 531-8.
151. Salegio, E.A., et al., *Distribution of nanoparticles throughout the cerebral cortex of rodents and non-human primates: Implications for gene and drug therapy.* Front Neuroanat, 2014. **8**: p. 9.
152. Lang, A.E., et al., *Randomized controlled trial of intraputamenal glial cell line-derived neurotrophic factor infusion in Parkinson disease.* Ann Neurol, 2006. **59**(3): p. 459-66.
153. Iliff, J.J., et al., *A paravascular pathway facilitates CSF flow through the brain parenchyma and the clearance of interstitial solutes, including amyloid beta.* Sci Transl Med, 2012. **4**(147): p. 147ra111.

154. Cuddapah, V.A., et al., *A neurocentric perspective on glioma invasion.* Nat Rev Neurosci, 2014. **15**(7): p. 455-65.
155. Engelhardt, B. and C. Coisne, *Fluids and barriers of the CNS establish immune privilege by confining immune surveillance to a two-walled castle moat surrounding the CNS castle.* Fluids Barriers CNS, 2011. **8**(1): p. 4.
156. Foley, C.P., et al., *Real-time imaging of perivascular transport of nanoparticles during convection-enhanced delivery in the rat cortex.* Ann Biomed Eng, 2012. **40**(2): p. 292-303.
157. Lochhead, J.J. and R.G. Thorne, *Intranasal delivery of biologics to the central nervous system.* Adv Drug Deliv Rev, 2012. **64**(7): p. 614-28.
158. Neeves, K.B., et al., *Dilation and degradation of the brain extracellular matrix enhances penetration of infused polymer nanoparticles.* Brain Res, 2007. **1180**: p. 121-32.
159. Chen, K.C. and C. Nicholson, *Changes in brain cell shape create residual extracellular space volume and explain tortuosity behavior during osmotic challenge.* Proc Natl Acad Sci U S A, 2000. **97**(15): p. 8306-11.
160. Mastakov, M.Y., et al., *Combined injection of rAAV with mannitol enhances gene expression in the rat brain.* Mol Ther, 2001. **3**(2): p. 225-32.
161. Mamot, C., et al., *Extensive distribution of liposomes in rodent brains and brain tumors following convection-enhanced delivery.* J Neurooncol, 2004. **68**(1): p. 1-9.
162. Kume-Kick, J., et al., *Independence of extracellular tortuosity and volume fraction during osmotic challenge in rat neocortex.* J Physiol, 2002. **542**(Pt 2): p. 515-27.
163. Kamel, H., et al., *Hypertonic saline versus mannitol for the treatment of elevated intracranial pressure: a meta-analysis of randomized clinical trials.* Crit Care Med, 2011. **39**(3): p. 554-9.
164. Carty, N., et al., *Convection-enhanced delivery and systemic mannitol increase gene product distribution of AAV vectors 5, 8, and 9 and increase gene product in the adult mouse brain.* J Neurosci Methods, 2010. **194**(1): p. 144-53.
165. Pardridge, W.M., *Drug transport in brain via the cerebrospinal fluid.* Fluids Barriers CNS, 2011. **8**(1): p. 7.
166. Carare, R.O., et al., *Solutes, but not cells, drain from the brain parenchyma along basement membranes of capillaries and arteries: significance for cerebral amyloid angiopathy and neuroimmunology.* Neuropathol Appl Neurobiol, 2008. **34**(2): p. 131-44.
167. Patek, P., *The perivascular spaces of the mammalian brain.* Anat. Rec., 1944. **88**(1): p. 1-24.
168. Zhang, E.T., C.B. Inman, and R.O. Weller, *Interrelationships of the pia mater and the perivascular (Virchow-Robin) spaces in the human cerebrum.* J Anat, 1990. **170**: p. 111-23.
169. Papadopoulos, M.C., et al., *Aquaporin-4 facilitates reabsorption of excess fluid in vasogenic brain edema.* FASEB J, 2004. **18**(11): p. 1291-3.
170. Preston, S.D., et al., *Capillary and arterial cerebral amyloid angiopathy in Alzheimer's disease: defining the perivascular route for the elimination of amyloid beta from the human brain.* Neuropathol Appl Neurobiol, 2003. **29**(2): p. 106-17.

171. Baker, G.J., et al., *Mechanisms of glioma formation: iterative perivascular glioma growth and invasion leads to tumor progression, VEGF-independent vascularization, and resistance to antiangiogenic therapy.* Neoplasia, 2014. **16**(7): p. 543-61.
172. Bala, I., S. Hariharan, and M.N. Kumar, *PLGA nanoparticles in drug delivery: the state of the art.* Crit Rev Ther Drug Carrier Syst, 2004. **21**(5): p. 387-422.

CURRICULUM VITAE
Clark Zhang

400 N. Broadway Ave, Baltimore, MD 21231
Phone: (626) 417-3839, Email: czhang30@jhmi.edu

Date of Birth: August 4, 1988
Location of Birth: State College, PA

EDUCATION

Johns Hopkins University	Ph.D. in Biomedical Engineering, 2010-2015
Harvey Mudd College	B.S. in Engineering, 2010, GPA: 3.604/4.0

HONORS AND AWARDS

2014	Center for Nanomedicine Research Excellence Award
2010-2011	NIH NIBIB Neuroengineering T32 Training Fellowship
2010	Harvey Mudd Engineering Department Honors
2007-2010	Harvey Mudd College Dean of Students Honor Roll
2006-2010	National Merit Scholar
2006-2010	Harvey S. Mudd Merit Award

CERTIFICATIONS

2015	U.S. Patent and Trademark Office, Registration Number: 73,804

PROFESSIONAL EXPERIENCE

2011-Present **Ph.D. Candidate**, Center for Nanomedicine at the Wilmer Eye Institute, Johns Hopkins University School of Medicine, Baltimore MD

Dr. Justin Hanes' Advanced Drug and Gene Delivery Group

- Lead the "brain team" consisting of 10+ graduate, masters, and undergraduate students in developing therapeutic nanoparticles for optimal delivery and treatment of various neurological diseases
- Establish and maintain long-term collaborations with Johns Hopkins researchers and physicians from departments of Neurosurgery, Pathology, and Engineering
- Assist in raising over $2M for projects related to nanoparticle delivery to the brain through written proposals to federal research funding sources

2014-Present **Marketing Analyst**, Johns Hopkins Technology Ventures, Baltimore MD

- Develop informational pamphlets for new inventors regarding the roles of regulatory agencies (i.e. FDA) and JHTV in the technology commercialization process

- Generate marketing summaries of new invention disclosures and engage in push marketing with technology licensees
- File information disclosure statements for JHTV intellectual property cases

2010-Present **Head and Grandparent of Household**, Thread (Incentive Mentoring Program), Baltimore MD
Hopkins East Baltimore – Dunbar High School, Gajok Household

- Oversee and coordinate efforts of 15+ Hopkins affiliated mentors for academic tutoring and social guidance for underprivileged, inner city Baltimore high school students

PUBLICATIONS

Peer Reviewed

1. Nance, E., **Zhang, C.**, Shih, TY., Xu, Q., Schuster, B., Hanes, J., *Brain Penetrating Nanoparticles Improve Paclitaxel Efficacy In Malignant Glioma.* ACS Nano, 2014.
2. Schneider, C., Perez, J., Cheng, E., **Zhang, C.**, Mastorakos, P., Hanes, J., Winkles, J., Woodworth, G., Kim, A., *Minimizing the Non-specific Binding of Nanoparticles Enables Active Targeting of Remote Tumor Cells in the Brain*. Biomaterials, 2014.
3. Mastorakos, P., **Zhang, C.,** Berry, S., Oh, Y., Lee, S., Kim, A., Woodworth, G., Suk, J., Hanes, J., *Highly PEGylated DNA Nanoparticles Provide Uniform and Widespread Gene Transfer in the Brain*. Advanced Healthcare Materials, 2014.
4. Mastorakos, P., Song, E., **Zhang, C.,** Berry, S., Park, H., Kim, Y., Park, J., Lee, S., Suk, J., Hanes, J., *Polyethylene Glycol Coated Biodegradable DNA Nanoparticles for Widespread Gene Delivery in the Brain*. Small, 2015.

Under Review

5. Oh Y., Park, O., Swierczewska, M., Park, J., Kim, T., Lim, S., Eom, H., Jo, D., Lee, C., Kechrid, R., Mastorakos, P., **Zhang, C.**, Hahn, S., Jeon, O., Byun, Y., Kim, K., Hanes, J., Lee, K., Pomper, M., Gao, B., Lee, S., *PEGylated TRAIL treatment ameliorates liver cirrhosis in rats by targeting activated hepatic stellate cells*. Hepatology, 2015.
6. Berry, S., Mastorakos, P., **Zhang, C.**, Patel, H., Suk, J., Hanes, J., *Densely PEGylated Polypeptide-based Gene Vectors for Efficient Gene Delivery to the Brain*, Integrative Biology, 2015.

Papers in Preparation (Papers written, to be submitted)

7. **Zhang, C**., Nance, E., Mastorakos, P., Berry, S., Chisholm, J., Suk, J., Tyler, B., Brem, H., Hanes, J., *Local Administration of Cisplatin Nanoparticles for Treatment of Malignant Glioma*
8. **Zhang, C.,** Mastorakos, P., Sobral, M., Berry, S., Song., E., Nance, E., Eberhart, C., Suk, J., Hanes, J., *Strategies to Achieve Maximal Nanotherapeutic Distribution in the Brain*
9. Nance, E., **Zhang, C.**, Woodworth, G., Semenkow, S., Eberhart, C., Hanes, J., *Nanoparticle Diffusion in Glioblastomas*
10. Schneider, C.*, Chisholm, J.*, **Zhang, C.**, Peacock, C., Hanes, J., *Cisplatin Nanocomplexes for the local treatment of lung cancer*.

11. Mastorakos, P., **Zhang C.,** Song E., Suk J.S., Hanes J. *Gene therapy for glioblastoma using biodegradable tumor penetrating DNA nanoparticles.*

SELECT CONFERENCE ABSTRACTS AND PROCEEDINGS (TOP 20)

1. Mastorakos P., **Zhang C.**, Song E., Suk J.S., Hanes J. (2015). *Gene delivery using Brain Penetrating Gene vectors.* 42nd Annual Meeting & Exposition of the Controlled Release Society; Edinburgh, Scotland.
2. Mead B., Timbie K.F., Miller G.W., Mastorakos P., **Zhang C.,** Suk J.S., Song J., Hanes J., Price R.J. (2015). *Delivery of Brain-Penetrating Nanoparticles Across the Blood-Brain Barrier with Focused Ultrasound: Brain Tumor and Neurodegenerative Disease Applications.* 42nd Annual Meeting & Exposition of the Controlled Release Society; Edinburgh, Scotland.
3. **Zhang C.,** Nance, E., Mastorakos P., Berry, S., Suk J.S., Hanes J. (2015). *Cisplatin Nanoparticles for Malignant Glioma.* 9th Annual Nano-Bio Symposium, Institute of Biotechnology; Baltimore, MD.
4. Schneider, C., Perez, J., Cheng, E., **Zhang, C.**, Mastorakos, P., Hanes, J., Winkles, J., Woodworth, G., Kim, A. (2015), *Minimizing the Non-specific Binding of Nanoparticles in the Brain Enables Active Targeting of Fn14-Positive Brain Tumors*. AAPS, San Francisco, CA. Selected for **AAPS Innovation in Biotechnology Award**.
5. Mastorakos P., **Zhang, C.,** Mead B., Song E., Price R.J., Suk J.S., Hanes J. (2015). *Biodegradable Brain Penetrating DNA Nanoparticles for Gene Delivery to the Brain.* AANS Annual Meeting; Washington, DC.
6. **Zhang, C.,** Mastorakos, P., Sobral, M., Berry, S., Song, E., Nance, E., Suk, JS, Hanes, J. (2015), *Defining Essential Considerations to Achieve Optimal, Local Nanocarrier Delivery to the Brain*. NanoDDS; University of Washington, Seattle, WA.
7. Mastorakos P., **Zhang C.,** Song E., Berry S., Kim YE., Suk JS., Hanes J.. (2014). *Highly Compacted Biodegradable DNA Nanoparticles Capable of Rapidly Penetrating Brain Tissue Barrier for Treating Brain Tumors*. Oral Presentation presented at: Congress of Neurological Surgeons Annual Meeting 2014; Boston, MA.
8. **Zhang, C.,** Nance, E., Mastorakos, P., Chisholm, J., Berry, S., Hanes, J., (2014) *Nanotechnology strategies for Improving Cisplatin Treatment of Malignant Gliomas*. NanoDDS: University of North Carolina at Chapel Hill. **Poster selected for oral presentation**
9. Suk JS., Mastorakos P., **Zhang C.,** Berry S., Hanes J.. (2014). *Brain-penetrating DNA nanoparticles for brain gene therapy*. Poster presented at: NanoDDS; Chapel Hill, NC.
10. Mastorakos, P., **Zhang, C.**, Berry, S., Hanes, J., (2014) *Brain Penetrating non-viral gene vectors for efficient gene transfer to brain tumors*. Society for Neuro-Oncology: Miami, Fl.
11. Timbie, K., **Zhang, C.**, Nance, E., Song, Ji., Miller, W., Hanes, J., Price, R. (2014) *Ultrasound-mediated delivery of brain-penetrating nanoparticles across the blood-tumor barrier*. Focused Ultrasound 2014 – 4th International Symposium: Bethesda, MD.

12. **Zhang, C.**, Nance, E., Mastorakos, P., Chisholm, J., Berry, S., Suk, J., Hanes, J. (2014) *Improving the Therapeutic Relevancy of Cisplatin for Malignant Gliomas Using Nanotechnology.* Biomedical Engineering Society: San Antonio, TX. **Oral Presentation.**
13. Mastorakos, P., da Silva, A., **Zhang, C.**, Chisholm, J., et al. (2014) *Biodegradable DNA Nanoparticles for Efficient in vivo Gene Delivery*. Biomedical Engineering Society: San Antonio, TX.
14. **Zhang, C.**, Nance, E., Mastorakos, P., Chisholm, J., Berry, S., Hanes, J. (2014) *Densely PEG Coated Cisplatin Nanoparticles for Treatment of Malignant Gliomas*. Controlled Release Society: Chicago, IL.
15. Mastorakos, P., Berry, S., **Zhang, C.,** Kim, A. et al. (2014) *Brain Penetrating Nanoparticles for Brain Gene Therapy*. Controlled Release Society: Chicago, IL.
16. Mastorakos, P., **Zhang, C.**, Berry, S., Kim, A. et al. (2014) *Brain Penetrating Gene Vectors for Efficient Gene Transfer to the Central Nervous System*. ASGCT: Washington DC.
17. Timbie, K., Nance, E., **Zhang, C.**, Miller, M., Song, J., Hanes, J., Price., R.. (2014) *Ultrasound-Mediated Nanoparticle Delivery Across the Blood-Brain Barrier*. International Society of Therapeutic Ultrasound: Las Vegas, NV.
18. Nance, E., **Zhang, C.**, Shih, TY, Hanes, J. (2013) *Brain Penetrating Nanoparticles Improve Efficacy Against Gliosarcomas*. Biomedical Engineering Society: Seattle, Washington
19. Timbie, K. Nance, E., **Zhang, C.**, Hanes, J., Price, R. (2013) *Controlling nanoparticle delivery across the blood-brain barrier using MR guided focused ultrasound*. Biomedical Engineering Society: Seattle, Washington.
20. Nance, E., Shih, TY, **Zhang, C.**, Woodworth G., Xu, Q., Hanes, J. (2012) *Biodegradable Brain-Tissue Penetrating Nanoparticles*. Biomedical Engineering Society: Atlanta, GA.

RESEARCH FUNDING

Training Grants:

1. NIH T32EB003383 (Thakor, JHU) 08/2010 – 08/2011
   Neuroengineering Training Initiative

Significant written and experimental contributions towards the following successfully funded grants:

1. Focused Ultrasound Foundation (Price & Hanes) - $100,000 06/2014 – 06/2015
   Delivery of Brain Penetrating Gene Vectors with MR-Guided Focused Ultrasound
2. NIH 1R24MH106083 - (Wong, JHU) - $497,799 09/2014 – 06/2017
   Imaging in vivo neurotransmitter modulation of brain network activity in realtime
3. NIH 1R01EB020147 - (Price & Hanes) - $626,441 05/2015 – 02/2019
   MRI-Guided miRNA nanoparticle delivery to Glioblastoma with focused ultrasound
4. NIH 1R01CA197111 - (Price & Hanes) - $537,316/year 06/2015 – 05/2020
   Immunotherapeutic Nanoparticle Delivery to Melanoma with MR-Guided Focused Ultrasound

5. NIH 1R01CA204968 – (Price & Hanes) – 1 percentile 04/2016-05/2021
Targeted delivery of brain penetrating DNA nanoparticles to brain tumors

PATENTS

1. Mastorakos, P., Suk, J., **Zhang, C.,** Woodworth, G., Hanes., J. *Engineering Synthetic Brain Penetrating Gene Vectors*. PCT application: 61/991,898, 61/991,920, 61/001,994
2. **Zhang, C.,** Mastorakos, P., Suk, J. Hanes, J. *A Method to Improve Nanoparticle Distribution by Enabling their Escape from Perivascular Spaces*. 62/217,194

LEADERSHIP EXPERIENCE

2011-Present	Thread (Incentive Mentoring Program), Baltimore, MD, *Volunteer, Head of Household, Grandparent of Household*
2011-2012	NIBIB T32 Neuroengineering Training, *Community Outreach Chair*

TEACHING EXPERIENCE

Spring 2013	Teacher Assistant, *Biomechanics*, Johns Hopkins University
Fall 2012	Teacher Assistant, *Systems Bioengineering Lab*, Johns Hopkins University
2009-2010	Teacher Assistant, *Digital Computer Architecture*, Harvey Mudd College